

Mechanics of motion and propagation in a binate frame

Samuel H. Talbert

22 Taunton Place, Ottawa, Ontario K1J 7J6, Canada

email: talbert.samy@primus.ca

Abstract. Since clocks are not needed to observe many physical phenomena where light propagates among moving bodies, it should be possible to explain these observations without clock synchronization considerations. The paper provides such explanations from a modern perspective. It uses a new type of reference system, a *binate frame* where all four coordinates of an event are physical distances. In a binate frame, familiar relativistic notions such as ‘speed of light’, ‘time dilation’, and ‘Lorentz transformations’ are not needed. We show that light’s ability to propagate without material support endows the manifold of events with a non-diagonal metric of Lorentz signature. All our kinematical analyses of familiar phenomena then yield the results expected from Special Relativity. For dynamical analyses, we use a second form of Hamilton’s principle, which obtains the usual canonical equations for the phase variables. Electrodynamics applications employ the covariant form of Maxwell’s equations, which are presented in binate-frame coordinatization.

Contents

1	Introduction	2
2	Considerations restricted to one physical-space dimension ...	5
2.1	The relation between near-events along the path of a light signal	6
2.2	A system with three rulers in collinear motion	8
2.3	Kinematical considerations	10
2.4	Exploring the local geometry of a world of one physical-space dimension	11
2.5	Dynamical considerations	15
2.6	A first comparison with the spacetime approach	19
3	Considerations involving two physical-space dimensions ...	20
3.1	The quadric of a propagating light signal	21
3.2	A system with three bodies in coplanar motion	23
3.3	Further kinematical considerations	27
3.4	Further geometric and dynamical considerations	30
3.5	A second comparison with the spacetime approach	34
4	Considerations involving all physical-space dimensions	36
4.1	Electrodynamics	37
4.2	Dynamics of a charged particle in a given electromagnetic field	38
4.3	Foliations	41
5	Conclusion: <i>observer-frame</i> or <i>binate-frame</i> , which is more valuable?	42

Appendices

A	Relativistic phenomena: one physical-space dimension	44
A1	Longitudinal optical Doppler effect	44
A2	Lorentz-Fitzgerald contraction	45
A3	The decay of cosmic-ray mesons	46
A4	Fully inelastic collisions	48
A5	Of moving clocks and light signals	49
B	Relativistic phenomena: two physical-space dimensions	52
B1	Transverse optical Doppler effect	52
B2	Bradley’s annual stellar-aberration	54
B3	Michelson-Morley null-effect	55
B4	The Sagnac effect	57
B5	Elastic Scattering	61
C	Relativistic phenomena: three physical-space dimensions	63
C1	The Sagnac effect revisited	63
C2	Plane electromagnetic waves	65
C3	The field of a charged particle	65
	References	66

“To understand a subject, one must tear it apart and reconstruct it in a form intellectually satisfying to oneself, and that (in view of the differences between individual minds) is likely to be different from the original form.”

J. L. Synge [1]

1 Introduction

The reviews of Special Relativity at its Centenary Anniversary [2-4] bear witness to their authors' confidence that phenomena where light propagates among moving bodies are well understood today. Their confidence rests on the strength of the geometric character of the calculations involved and the successful testing of the predictions so arrived at [5]. Yet, no matter how successful, a physical theory is inevitably accompanied by disputes, open questions, controversies, and conceptual reformulations like the one we propose to present here. Their cumulative effect, over the centuries, is to advance the science.

Einstein's Special Theory of Relativity emerged from considerations based on the equivalence of inertial frames, the constancy of the speed of light, the relativity of time, and the procedure for synchronizing distant clocks. Among these basic concepts, only the equivalence of inertial frames, a classical mechanics notion that he postulated to apply to all physical processes, remained undisputed over the past century.

The debate over the constancy of the velocity of light [6,7] is about its one-way speed: Is it measurable or not? A related debate is over the isotropy of the speed of light in one-way propagation. This isotropy was experimentally verified on a theoretical basis that relied on a “preferred inertial frame of reference” [8], some ether so to speak, where light propagates with the same speed in all the directions of the physical space. But since it was understood as early as the 1920th that “All experimental methods of measuring the velocity of light determine only an average to-and-fro velocity” [9], the constant speed of light principle is now taken to refer to the round-trip (averaged) speed of a light signal, rather than to its one-way speed. Thus the debates over the speed of light are today only marginally relevant to the foundations of Special Relativity.

In contrast, the dispute over the ‘relativity of time’ and the controversy over the ‘conventionality’ of any clock-synchronization procedure, which are also at the root of the debate about the one-way speed of light [10], feed the perception of weaknesses in the foundation of Special Relativity. This perception is reinforced when considering that no clocks are needed to measure the observed effects of light propagating among moving bodies. It is also noticeable when occasionally some authors feel it necessary to remind the readers that only those experimental outcomes that do not depend on the stipulated clock synchronization procedure are physically significant, and to advise them on how to set experiments that allow for changing this procedure (see for example [3]).

In view of the above perception, it seems desirable to reformulate the mechanics of motion and propagation in a manner that dispenses with the time-coordinate, and thus also with the clock synchronization procedure, while retaining the logico-mathematical clarity of the covariant four-dimensional presentation. But then, could relativistic effects be predicted without ‘time’ as a fourth coordinate, thus without Lorentz transformations? The purpose of this paper is to show that this is indeed possible.

To overcome the prevalent view that physical events are ‘naturally’ endowed with one ‘time’ and three ‘space’ coordinates, it might seem enough to find, like we do here, operational means of attaching other types of coordinates to physical events. But this is far from being the case. Difficulties arise not from the mathematics, but from the need to provide physical interpretations that are likely to withstand strict scrutiny by those who might wish to pursue the logical implications of the new coordinatization. (Quantum Mechanics reliance on the Hamiltonian rather than the Newtonian mechanics shows that alternative parameterizations eventually, over the years, could possibly lead to startling new insights!)

Given the importance of the interpretation issue, we understood that the paper had to be more than trivial mathematical manipulations of changing coordinates – it had also to be phenomenological in the manner that it introduces a new type of reference system, the *binate frame*. We diligently avoided generalizations and excessive formalism so as to remain faithful to the purpose of the paper. And for the same reason, we listed only a minimum of references, usually one of the oldest and one of the more recent we were aware of, not to comment on their content, but to guide the interested reader to some of the relevant literature.

Our presentation pursues the logical consequences of the simple observation that light signals propagate without material support. This is a qualitative characteristic of the entire spectrum of electromagnetic waves, but is not one possessed by mechanical waves, such as those emitted by shocks or sounds. Thus while a mechanical wave has a natural rest-reference for its group velocity, namely, the material through which it propagates, no such reference is available for the electromagnetic wave. This deficiency is irrelevant in electrodynamics since Maxwell’s equations provide a physically measurable constant with the appropriate dimensions of speed and with the attribute of group velocity. But it is critical in classical mechanics: its predictions are contradicted by observed phenomena, and in the laboratory, whenever the group velocity of a light-pulse is used as the ‘speed’ of light and compounded classically with other velocities. By revising the classical law for the addition of collinear velocities, Special Relativity enabled the consistent use of the constant of the electromagnetic waves as the speed of a light pulse.

For our alternative approach, we attempted to find a quantitative description of a propagating light pulse that endows it with neither a classical nor a relativistic speed. The null geodesics of a metric with Lorentz signature are known to provide a frame-invariant description of the path of a light signal. It is not necessary to parameterize the geodesics so as to attach a physical attribute to light that could be taken as its ‘speed’. With this in mind, we looked for a system of reference that naturally has other than the familiar one-time and three-space coordinates and furthermore, provides also the material support for physical measurements. The *binate frame*, which we define and use here as our reference system, meets these two conditions.

Having identified the binate frame as our new reference system, we could have just postulated the form of an appropriate line-element for the manifold of events. Then we could have shown that it yields the same predictions as those of Special Relativity, for observed phenomena and for experiments describable in terms that do not depend on the clock synchronization stipulation. We rejected the axiomatic approach and instead, derive *ab initio* the required line-element, step-by-step, progressively in physical spaces of one, two and three dimensions, from considerations that we summarize below.

We view a material body as geometrically extended in all the dimensions of the physical space. The particles of the body occupy a finite region of this extended physical space, which is the body's own *relative space*. This is the classic notion of relative space; it is distinct from the usual relativistic view of 'space' as being a constant-time slice of spacetime, and also differs from the alternative view whereby the term 'relative space' refers to the manifold of the timelike curves traced by the physical locations [11].

As we see it, the physical world is a continuously changing configuration of fields and material bodies. A body is imbedded and moves in the relative spaces of all the other bodies of the world. An event always happens at a well-defined place in the relative space of each body. These places coincide at the event. The set of place-coincidences provides a tangible, physical background where particles and light-rays could leave traces, the relevant events could be located, and the attributes of various fields could be measured. In a physical space of one dimension, the set of place-coincidences is two-dimensional; it is three-dimensional in a physical space of two dimensions; and is four-dimensional in a physical space of three dimensions.

We identify an event with the coinciding places from the relative spaces of two selected bodies in uniform relative motion, neither rotating nor changing the direction of their movement. (We explain in Sec. 2.1 the measurements needed for such judgment to be made.) We use the paired bodies as a reference system: they form what we call here a *binate frame*. Distances between places on the relative spaces of the reference bodies are measurable (for example, by triangulation) and thus a network of space-coordinates could (in principle) be laid on each body and its relative space.

We probe with light signals the geometric structure of the place-coincidences manifold. The unique character of these signals is that they propagate without material support. Considerations based on this, and on the fact that the propagation is neither instantaneous nor dependent on the motion of the source, lead to the conclusion that, in a binate frame, the equation of the propagating light pulse is determined by a null-valued, quadratic differential-form with a symmetric, non-diagonal matrix of Lorentz signature. But then the manifold of place-coincidences has at least a conformal structure [12,13] and thus three families of curves exist, distinguished by the null-, positive-, or negative-value of this form applied to vectors tangent to the curves. Subsequent analysis of how particles (point-wise bodies) move in a binate frame shows that the matrix of the quadratic form also provides a physically meaningful, locally flat metric for the manifold. This entitles us to use on this manifold the appropriate tensor calculus.

All that we need is now available for the kinematical and dynamical analyses of situations where light signals propagate among bodies in arbitrary motion. But only if we continue to avoid notions, such as 'velocity', that require synchronized clocks, which we do not employ here. This means that the usual Lagrangian dynamics cannot be used in a binate frame, but many other, quite equivalent and well-known approaches are available [14,15]. We adopt here the covariant formalism that Synge calls "the *second form* of Hamilton's *principle*" [16]. With this choice, the parameter along the path of a particle is determined by the canonical equations, and could always be related back to the separation between the events along the particle's path and thus also to the relativistic 'proper time.'

We found no reference in the literature to the binate-frame approach of this paper. The novel elements that most distinguish it from the observer-frame approach of Special Relativity are: i) our logical considerations start here from some qualitative rather than

quantitative aspects of light propagation; ii) we employ a manifold of identifiable place-coincidences rather than a spacetime; iii) the event-coordinates are measured as physical distances and thus no clocks are needed. In later sections, we expand on these and some other major differences between the binate frame and the observer frame. The paper ends with a comprehensive comparison between these two types of frames.

2 Considerations restricted to one physical-space dimension

Say two rulers are strapped to carts that slide as in Fig. 1, in opposite directions along a track. (Figure 1 shows only the rulers; it omits the carts and the track.) A spark emits a light signal and this event marks on each ruler the place where it happened (the little blot in Fig. 1a). A sensor on one of the rulers detects the signal and this event marks on the other ruler the place of the detection (the photo-camera icon in Fig. 1b).

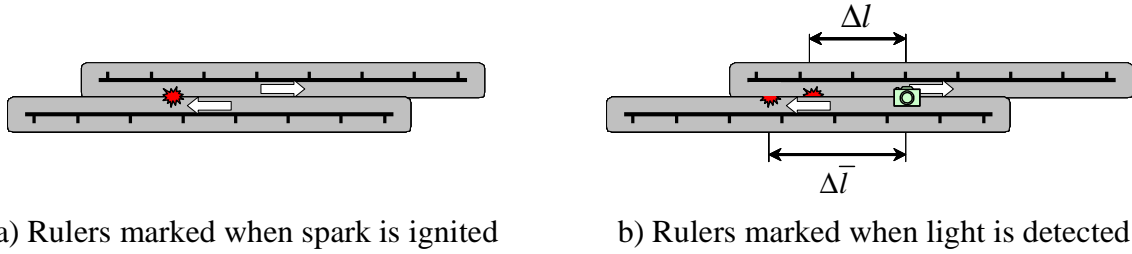


Fig. 1 The emission and detection of a light signal along two rulers in relative motion.

The diagrams in Fig. 1 are sketched after the experiment, to summarize its outcome, in principle rather than at scale: The rulers are first brought to rest, then removed from their carts and positioned as shown, side by side, with either the emission marks coinciding (Fig. 1a), or with the detection marks coinciding (Fig. 1b). The illustrated distances are then measured. On the ruler with the detector, Δl denotes the distance from the detector to the place marked by the emitting event. On the other ruler, $\Delta \bar{l}$ denotes the distance between the places marked by the emission and the detection events.

Since no signal propagates instantaneously, the qualitative assessment is that the measured distances Δl and $\Delta \bar{l}$ cannot be of equal length, even though it is unlikely that today's instruments are capable of detecting the minute length differences expected in a lab-based experiment. The shorter distance would always be on the ruler whose motion is in the propagation direction of the detected signal. That is, we get $\Delta l < \Delta \bar{l}$ when the detector is placed as in Fig. 1, on the right-hand side of the mark left by the emission event, and thus detects the signal propagating in the direction of the top ruler's motion. In contrast, we get $\Delta \bar{l} < \Delta l$ when the detector is placed on the other side of the mark, and thus detects the signal propagating in the direction of the bottom ruler's motion. In each case, let k be the ratio of the shorter to the longer of the distances Δl and $\Delta \bar{l}$.

For comparing the results of our analyses with those of Special Relativity, we need to know what the latter predicts for the outcome of the above experiment. For the relativistic calculations, the rulers are two inertial frames in their standard configuration.

Say the top ruler is the ‘moving’ (t', x') -frame and the bottom ruler is the ‘stationary’ (t, x) -frame. Let $\beta = v/c$ refer to the relative motion between the frames.

A light signal is emitted as illustrated in Fig. 1a, when the origins of the two frames meet. It would be detected at the events with coordinates $(t = \frac{\Delta \bar{l}}{c}, x = \Delta \bar{l})$ and $(t' = \frac{\Delta l}{c}, x' = \Delta l)$, respectively. Lorentz transformations then yield $x' = (x - vt)/\sqrt{1 - \beta^2}$, and thus the predicted outcome of the experiment is that $\frac{\Delta l}{\Delta \bar{l}} = \sqrt{\frac{1 - \beta}{1 + \beta}}$. But then the following relation between k and β holds true since k was defined as just the above ratio of the two distances:

$$0 < k = \sqrt{(1 - \beta)/(1 + \beta)} < 1 \quad (2.1)$$

The relation between k and β is presented here solely for the purpose of comparing our results with those of Special Relativity. In our approach, (2.1) serves no other purposes.

2.1 The relation between near-events along the path of a light signal

Each ruler in Fig. 1 is now endowed with a linear coordinate, as in Fig. 2. The A-ruler carries the x_A coordinate; the \aleph -ruler carries the x_{\aleph} coordinate. (The subscripts $_A$ and $_{\aleph}$ are not covariant indices, but rather labels that associate a coordinate with its ruler.) Our choice of notation emphasizes the symmetry between the two rulers: the ‘aleph’ symbol, \aleph , is the first letter of the Hebrew alphabet and thus the counterpart of A, the first letter of the Latin alphabet. (To facilitate the handwriting of the rulers’ names, it would have been better perhaps to employ other labels. But the A- and B-letters are not appropriate since they imply a precedence relation between the rulers, and calling them the L- and the R-rulers, is not advisable since what is ‘Left’ and ‘Right’ for the reader gets reversed when looking at the same pairs of rulers but facing the reader rather than the page.)

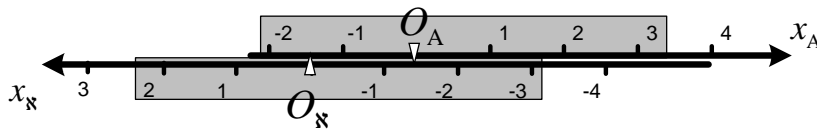


Fig. 2 The coordinates carried by the two rulers.

Events are assumed to mark on each ruler the place where they occur. Thus an event is identified with a pair of coordinates, (x_A, x_{\aleph}) . We now look for the relation between the coordinate differentials at two near-events along the path of a propagating light signal.

The light signal from the spark in Fig. 1 is emitted as O_A passes over O_{\aleph} , that is, at the event \mathcal{O} with the coordinates $(0, 0)$. Two light-points propagate from this emission

in opposite directions along the $x_A x_K$ -line. A sensor located at $dx_A = \Delta l > 0$ detects one of the light-points just as it passes over the place at $dx_K = -\Delta \bar{l} < 0$. The coordinates of this detection are $(\Delta l, -\Delta \bar{l})$. By definition, we have $k = \frac{\Delta l}{\Delta \bar{l}}$, and thus $dx_A + k dx_K = 0$ for this light-point. Similarly, as it passes over $dx_K = \Delta \bar{l} > 0$, a sensor at $dx_A = -\Delta l < 0$ detects the other light-point. The coordinates of this other detection are $(-\Delta l, \Delta \bar{l})$, and now $k = \frac{\Delta \bar{l}}{\Delta l}$; it yields $k dx_A + dx_K = 0$ for this light-point. Thus when a light signal is detected near an emission event, the coordinate differentials, dx_A and dx_K , are related either by $dx_A = -k dx_K > 0$ or by $dx_K = -k dx_A > 0$.

The experimental set-up might allow for the motion of the rulers to be controlled and changed between the runs. The same relations would then obtain, but the k -values in any one run need not be the same as the k -values in any other run. Furthermore, in each run, the experiment could be repeated with the origins of the coordinates at different locations. The coordinate differentials of any detection near the emission event would be related as before, but the k -values need not remain unchanged.

When the motion of the rulers is such that it yields the same value of k for all the pairs of emission-detection events of the respective run, regardless of where the origins of the coordinates are places on the rulers, we view their relative motion as *uniform* and say that the experimental set-up is *calibrated* to the measured k -value.

A pair of rulers whose motion is calibrated to some k -value is our choice of a reference system for the events. We call it a *binate frame*, to highlight the fact that it consists of two parts in relative motion. A label such as the ' k_{AK} -frame' identifies the two rulers of the frame as well as its calibration constant.

In a k_{AK} -frame, every detection event that does not stop the light signal could be viewed as re-emitting the light. Thus in this frame, the above mentioned relations hold between the coordinate differentials of any two events near each other along the path of a light signal, not just between an emission and a detection event:

$$dx_A + k_{AK} dx_K = 0 \text{ if } dx_A > 0 \text{ and } k_{AK} dx_A + dx_K = 0 \text{ if } dx_K > 0. \quad (2.2)$$

These relations are *locally* valid even when the rulers' motion is not calibrated, but then (2.2) could not be integrated unless we know how k_{AK} depends on the coordinates.

The physical possibility of calibration to a desired k -value is an assumption that we make: it is like the assumption of Special Relativity that free particles could be used to verify that an observer's frame is inertial. In the spirit of Synge's Neo-Cartesianism, and aware of his advice that it could turn someone into "a machine with all brakes and no horsepower" [17], we hasten to add that the presentation so far contains all that we need to analyze the outcome of longitudinal optical-Doppler experiments in weak gravitational fields. The experiments could be used to operationally achieve the desired calibration for the binate frame. In appendix A1, we consider the set-up of Fig. 2, with light signals emitted when O_K passes first over O_A and then over a series of triggers located at equal

distances Δl_e along the x_A -axis. A sensor at $x_A = -L$ detects all the emitted signals; the detections mark the $x_{\mathfrak{N}}$ -axis. The prediction derived from (2.2) is that the motion between the two rulers is calibrated to the desired $k_{A\mathfrak{N}}$ when the measured distance Δl_d between two successive detection marks is unchanged: $\Delta l_d = k_{A\mathfrak{N}} \Delta l_e$.

With $k_{A\mathfrak{N}} = \sqrt{(1 - \beta_{A\mathfrak{N}})/(1 + \beta_{A\mathfrak{N}})}$, from (2.1), substituted in the above prediction for the longitudinal optical Doppler effect, we get the usual relativistic relation between the wavelengths of the emitted and detected optical signals. But only our prediction is manifestly synchrony-independent since: (i) it is expressed in terms of the calibration constant $k_{A\mathfrak{N}}$ rather than the speed factor $\beta_{A\mathfrak{N}}$, and (ii) it is derived without any notion of ‘synchronized’ clocks.

2.2 A system with three rulers in collinear motion

Our further considerations refer not only to the two rulers of Fig. 2, but also to the track that guides the carts with the rulers. The motion of each ruler is independently calibrated with respect to the track so as to form with it a binate frame. Figure 3 shows the A-ruler, represented by its x_A -coordinate, and the \mathfrak{N} -ruler, represented by its $x_{\mathfrak{N}}$ -coordinate. The line in the middle represents the track, which is like a third ruler. We call it the \mathfrak{S} -ruler when paired with the A-ruler to form the $k_{A\mathfrak{S}}$ -frame, and call it the T-ruler when paired with the \mathfrak{N} -ruler to form the $k_{T\mathfrak{N}}$ -frame. Two related coordinates, $x_{\mathfrak{S}} = -x_{\mathfrak{T}}$, are used on the track so that, in each of these frames, it has a coordinate in the opposite direction of the paired ruler’s x -coordinate. (As before, the subscripts \mathfrak{S} and \mathfrak{T} are not covariant indices but labels that distinguish between the two x -coordinates of the track.)

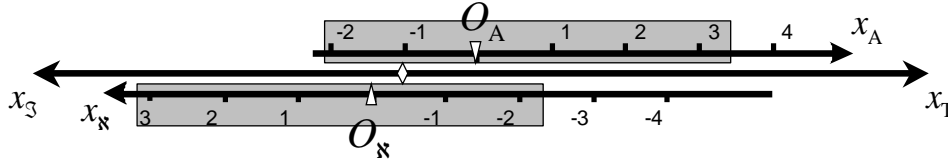


Fig. 3 Two rulers sliding on a track represented by the middle line; the small rhomb on the track is the origin $O_{\mathfrak{S}} \equiv O_{\mathfrak{T}}$ of its two x -coordinates.

Say the set-up is such that O_A and $O_{\mathfrak{N}}$ meet when they pass over $O_{\mathfrak{S}} \equiv O_{\mathfrak{T}}$. Denote \mathcal{O} the encounter of these origins; a light signal is emitted at this event. Not shown in Fig. 3, a device on the track, at $x_{\mathfrak{T}} = -x_{\mathfrak{S}} = \hat{l} > 0$, detects the signal and marks the rulers. Say the marks are placed at $x_A = l > 0$ and $x_{\mathfrak{N}} = -\bar{l} < 0$. The calibration of the motion of the rulers with respect to the track ensures that (2.2) is met all along the path of the light signal and could be integrated to yield $x_A + k_{A\mathfrak{S}}x_{\mathfrak{S}} = 0$ and $x_{\mathfrak{T}} + k_{T\mathfrak{N}}x_{\mathfrak{N}} = 0$ at the detection event. The last two relations lead to $x_A + k_{A\mathfrak{N}}x_{\mathfrak{N}} = 0$, where we put

$$k_{A\aleph} = k_{A\Im} k_{T\aleph}. \quad (2.3)$$

This shows that the A - and \aleph -rulers form a third binate frame, the $k_{A\aleph}$ -frame.

For the reader who at this early stage in the presentation would like to verify that (2.3) is indeed correct, we digress for a moment to note that the three rulers are in relative collinear motion. For relativistic calculations, one would attribute to these motions the following β -values: $\beta_{A\aleph}$, $\beta_{A\Im}$, and $\beta_{T\aleph}$. When $k = \sqrt{(1-\beta)/(1+\beta)}$, from (2.1), is substituted with the respective subscripts in (2.3), it obtains the rule for the addition of collinear velocities in Special Relativity. Our approach does not use such a relation since the notion of ‘velocity’ is undefined in a binate frame.

We derive next a relation between differential displacements. In Fig. 3, an event differentially close to \mathcal{O} is identifiable with any one of the following pairs of coordinates: (dx_A, dx_{\Im}) , or (dx_T, dx_{\aleph}) , or (dx_A, dx_{\aleph}) . This means that the differentials involved: dx_A , $dx_T = -dx_{\Im}$, and dx_{\aleph} , are linearly related. Say we express dx_T in terms of the other two differentials and two constant factors. Since the relation must hold at all events, it should be true in particular along the path of a light signal. Thus when $dx_A = -k_{A\aleph} dx_{\aleph}$ on such a path, we must have $dx_T = -k_{T\aleph} dx_{\aleph}$ regardless of the value of dx_{\aleph} . And similarly, when $dx_{\aleph} = -k_{A\aleph} dx_A$, we must have $dx_T \equiv -dx_{\Im} = k_{T\aleph} dx_A$ regardless of the value of dx_A . These two conditions suffice to obtain the values of the constant factors. Calculations yield

$$(k_{A\aleph}^{-1} - k_{A\aleph}) dx_T = (k_{T\aleph}^{-1} - k_{T\aleph}) dx_A - (k_{A\Im}^{-1} - k_{A\Im}) dx_{\aleph}. \quad (2.4)$$

In a physical situation where three linear bodies (viewed as rulers) are in relative motion, there could be no three-way symmetry. At any event whatsoever, just one of the bodies would be such that an observer on it and present at the event would see the other two bodies moving away in opposite directions along of their line of relative motion. The asymmetry of the situation is well reflected in (2.4). To apply (2.4) in unchanged form, one should designate the distinct body as the ‘track’. Thus $dx_T = -dx_{\Im}$ in (2.4) refers to the coordinate differential along the body that distinguishes itself, at all the events near the considered event, in the manner just indicated. When this convention is followed, $k_{A\aleph}$ is the lowest of the three k ’s involved: $k_{A\aleph} = \text{Min}(k_{A\aleph}, k_{A\Im}, k_{T\aleph}) = \sqrt{k_{A\aleph} k_{A\Im} k_{T\aleph}}$, which is just another form of (2.3).

In appendix A2, we analyze an experiment involving two rods sliding uniformly along each other. The reader would recall that Einstein envisaged such an experiment to explain how the length contraction effect could be measured without using synchronized clocks [18]. Our analysis shows that in fact clocks are not needed even for predicting the outcome of the experiment: the effect is a direct consequence of (2.4). Though it is well known that the length contraction is insensitive to the stipulated clock synchronization procedure, we did not find in the literature any ‘clock-less’ derivation of this effect.

2.3 Kinematical considerations

We proceed next to discuss some particular types of motion. Refer to Fig. 3 and the three binate frames formed when pairing the two rulers together, and each ruler with the track. A point-wise body located at some place on the A-ruler and denoted the A-body moves with respect to the other ruler and to the track. Between near-events attended by this body, we have $dx_A = 0$, since its x_A -coordinate is unchanged. At two such near-events, let the body mark both the track and the \mathfrak{N} -ruler. We would then get $dx_{\mathfrak{S}} = -dx_T < 0$ between the marks on the track and $dx_{\mathfrak{N}} < 0$ between the marks on the ruler. From (2.4),

$$\text{we would also obtain } \frac{dx_{\mathfrak{S}}}{k_{A\mathfrak{S}}^{-1} - k_{A\mathfrak{S}}} = \frac{dx_{\mathfrak{N}}}{k_{A\mathfrak{N}}^{-1} - k_{A\mathfrak{N}}}.$$

The fractions on the two sides of the above relation have the same form, but $k_{A\mathfrak{S}}$ and $dx_{\mathfrak{S}}$ relate to A-body's motion with respect to the track whereas $k_{A\mathfrak{N}}$ and $dx_{\mathfrak{N}}$ relate to the motion of the same body with respect to the \mathfrak{N} -ruler. Thus we have on each side of the equal sign a differential quantity related to the A-body's motion relative to the track and the \mathfrak{N} -ruler, respectively: $ds_A = -\frac{2k_{A\mathfrak{S}}}{1-k_{A\mathfrak{S}}^2} dx_{\mathfrak{S}} = -\frac{2k_{A\mathfrak{N}}}{1-k_{A\mathfrak{N}}^2} dx_{\mathfrak{N}}$. (The factor 2 was

introduced here for consistency with what follows whereas the minus sign makes ds_A a positive quantity.) We call ds_A the (*differential*) *separation* of near-events on the path of A-body's motion. The so defined separation ds_A is physically meaningful: it is the scaled distance traveled by the A-body along some other body, here the track or the \mathfrak{N} -ruler. The scaling factor is the same function of the considered relative motion, which is specified in terms of the respective calibration constant.

Similarly, a point-wise body located on the \mathfrak{N} -ruler moves uniformly with respect to the other ruler and the track. Now we have $dx_{\mathfrak{N}} = 0$, $dx_T = -dx_{\mathfrak{S}} < 0$, and $dx_A < 0$. This leads to the separation $ds_{\mathfrak{N}} = -\frac{2k_{T\mathfrak{N}}}{1-k_{T\mathfrak{N}}^2} dx_T = -\frac{2k_{A\mathfrak{N}}}{1-k_{A\mathfrak{N}}^2} dx_A$ between near events attended by this \mathfrak{N} -body.

Finally, we have $dx_{\mathfrak{S}} = dx_T = 0$, $dx_A < 0$ and $dx_{\mathfrak{N}} < 0$ at near-events attended by a body on the track. The separation ds along the path of this body is:

$$ds = -\frac{2k_{A\mathfrak{S}}}{1-k_{A\mathfrak{S}}^2} dx_A = -\frac{2k_{T\mathfrak{N}}}{1-k_{T\mathfrak{N}}^2} dx_{\mathfrak{N}}. \quad (2.5)$$

From (2.5), we get $k_{A\mathfrak{S}}$ in terms of ds and dx_A , as well as $k_{T\mathfrak{N}}$ in terms of ds and $dx_{\mathfrak{N}}$. We further substitute $k_{A\mathfrak{S}}$ and $k_{T\mathfrak{N}}$ in (2.3) and rearrange the new relation to read:

$$ds^2 = \left(\frac{2k_{A\mathfrak{N}}}{1-k_{A\mathfrak{N}}^2} \right)^2 \left[dx_A^2 + \frac{1+k_{A\mathfrak{N}}^2}{k_{A\mathfrak{N}}} dx_A dx_{\mathfrak{N}} + dx_{\mathfrak{N}}^2 \right] > 0. \quad (2.6)$$

Similar calculations show that with the appropriate change of subscripts, (2.6) applies to the A-body's motion with respect to the $k_{T\aleph}$ -frame, and to the \aleph -body's motion with respect to the $k_{A\aleph}$ -frame.

Moreover, (2.6) applies even in the case of a material particle moving arbitrarily in the $k_{A\aleph}$ -frame. In the neighborhood of an event attended by the particle, its relative space (like a third ruler) would form momentarily a binate frame with each ruler of the reference frame. But then the mere presence of a particle at near-events separated by (dx_A, dx_{\aleph}) in a $k_{A\aleph}$ -frame suffices to define its motion in the neighborhood. First, when the coordinate differentials are substituted in (2.6), we get the separation ds between the events. Then, we get the k -value of the body's motion with respect to each ruler of the $k_{A\aleph}$ -frame when ds and (dx_A, dx_{\aleph}) are substituted in (2.5). If the particle's motion is not uniform, the so obtained k -values change along the path of the particle as it travels through different event-neighborhoods.

More familiar is the parametric form of the equations of motion. In a $k_{A\aleph}$ -frame, these are given by: $x_A = x_A(\zeta)$ and $x_{\aleph} = x_{\aleph}(\zeta)$, with ζ the *parameter* along the path of the particle. Substitutions in (2.6) yield $ds(\zeta)$, and this in turn is used to obtain $k_{A\aleph}(\zeta)$ and $k_{T\aleph}(\zeta)$, as just explained. From (2.6), integration of $ds(\zeta)$ between two events \mathcal{E}_1 and \mathcal{E}_2 along the particle's path yields the finite separation between these events. This separation reflects the properties of the path: it attains its largest value for the straightest path between the specified events, when the motion of the particle is uniform.

Special Relativity interprets the finite separation as the duration of an elapsed time interval of the particle's 'proper time' between the considered pair of events. Even though we need not adopt this view here, our analysis of decaying mesons (appendix A3) does indeed show that the finite separation between a meson's birth and decay correlates well with its experimentally measured lifespan.

2.4 Exploring the local geometry of a world of one physical-space dimension

With what we learned so far, we are now able to explore the geometry of a world where all the action takes place in one physical-space dimension. The relative space of each body is a line, with the body located somewhere on it. Distances between places are well defined on each of these lines since all physical lengths are measurable. The lines move along each other. When a physical event occurs, this happens at one place on each line (relative spaces) of all the bodies involved; these places coincide at the event. Some events would emit rays of light that propagate along these lines, in both directions. The rays might be detected by still other events.

It is immaterial whether an event occurs at some identifiable place-coincidence, or nothing of physical interest happens there. A place-coincidence by itself is an event, and we do not distinguish between this 'place-coincidence *cum* event' and any other event that might happen at the coinciding places, except when needed to resolve ambiguities. (For example in Sec. 2.2, an event in a three-rulers system was identified with coinciding places from three different pairs of lines.) The place-coincidences form a set whose *local*

geometry we wish to explore next. The term ‘local’ refers as usual to the geometry in a ‘small neighborhood’ of a given event (pair of coinciding places). Operationally, we assume that the events in this neighborhood leave marks on the lines that represent the relative spaces of each body of the considered system, and furthermore, that all the marks on any one line are contained in an open interval of a differential length. It is the relations between such marks that we analyze and describe next, in geometric terms.

As our reference system for the events, we use a binate frame formed with the relative spaces (the A - and \aleph -lines) of a selected pair of bodies whose motion just happens to be, or is purposefully calibrated to some $k_{A\aleph}$, at least in the neighborhood of the selected event. Say an event marks the A - and \aleph -lines and the places so marked are selected as the origins O_A and O_\aleph of the respective x -coordinates. Thus at this event, denoted \mathcal{O} , the two origins pass by each other. With the x_A - and x_\aleph -axes selected as in Fig. 2, we could then use all our results so far.

The neighborhood of \mathcal{O} is a set of coinciding places, one from a small interval around O_A and one from a similar small interval around O_\aleph . This set of coincidences is a two-dimensional differential manifold. To find a physically meaningful metric for this manifold, we focus on an event \mathcal{R} with coordinates (dx_A, dx_\aleph) ; \mathcal{R} is the coincidence of the place at $dx_A|_{\mathcal{R}}$ on the A - line with the place at $dx_\aleph|_{\mathcal{R}}$ on the \aleph -line.

We observe that (2.6) could be viewed as the line-element of a Riemannian manifold: $ds^2 = \eta_{\mu\nu} dz^\mu dz^\nu$, where we put:

$$\eta_{\mu\nu} = \left(\frac{2k_{A\aleph}}{1 - k_{A\aleph}^2} \right)^2 \begin{bmatrix} 1 & \frac{1 + k_{A\aleph}^2}{2k_{A\aleph}} \\ \frac{1 + k_{A\aleph}^2}{2k_{A\aleph}} & 1 \end{bmatrix} \text{ and } dz^\mu = \begin{bmatrix} dx_A \\ dx_\aleph \end{bmatrix}. \quad (2.7)$$

The metric has evidently the $(+, -)$ signature since with a simple change of variables:

$z^1 = \xi^1 + \xi^2$ and $z^2 = \xi^1 - \xi^2$, the matrix of the metric components realizes one of its

diagonal forms: $diag \left(\frac{4k_{A\aleph}}{(1 - k_{A\aleph}^2)^2}, \frac{-4k_{A\aleph}}{(1 + k_{A\aleph}^2)^2} \right)$.

The above line-element is physically meaningful when $ds^2 > 0$, since then (2.6) applies and thus ds is the differential separation between two near events along the path of a particle. The line-element is also clearly meaningful when $ds^2 = 0$ since then (2.2) and (2.6) are both equivalent to:

$$ds^2 = \frac{4k_{A\aleph}}{(1 - k_{A\aleph}^2)^2} (k_{A\aleph} dx_A + dx_\aleph) (dx_A + k_{A\aleph} dx_\aleph) = 0. \quad (2.8)$$

This shows that in this case, ds is the null separation between near events along the rays of a light signal. What remains to be done is to find a physical interpretation for the case

when $ds^2 < 0$. For this, we recall how Synge proposed to “physicise the geometrical element ds of separation between two adjacent events” [19], and perform the required calculations in our binate-frame.

Say a device at O_A emits a light signal at some event \mathcal{E} that is slightly prior to \mathcal{O} , when O_A meets O_R . A near event \mathcal{R} detects the light and reflects it back to the emitting device. The event \mathcal{R} is so selected that the device at O_A detects the reflected signal at an event \mathcal{D} that is slightly after \mathcal{O} . This is a *round-trip* (or *two-way*) propagation of a light signal: from the emission event \mathcal{E} attended by O_A , to a selected event \mathcal{R} , and back to the detection event \mathcal{D} attended by O_A . Since O_A is present at both \mathcal{E} and \mathcal{D} , each of these two events has one null coordinate: $dx_A|_{\mathcal{E}} = dx_A|_{\mathcal{D}} = 0$. We now apply (2.2) to the forward and backward rays of light. This yields the second coordinate of \mathcal{E} and \mathcal{D} in terms of the coordinates of \mathcal{R} :

$$dx_R|_{\mathcal{E}} = (dx_R + k_{AR}^{-1} dx_A)|_{\mathcal{R}} > 0, \text{ and } dx_R|_{\mathcal{D}} = (dx_R + k_{AR} dx_A)|_{\mathcal{R}} < 0. \quad (2.9)$$

We have shown in Sec. 2.3 that the separation between two near-events along the path of a body located on the A -ruler of a k_{AR} -frame is $ds_A = -\frac{2k_{AR}}{1-k_{AR}^2} dx_R$. When considering

the path of the device at O_A , this yields $ds_A|_{\mathcal{EO}} = \frac{2k_{AR} dx_R|_{\mathcal{E}}}{1-k_{AR}^2}$ for the separation between

\mathcal{E} and \mathcal{O} , and $ds_A|_{\mathcal{OD}} = -\frac{2k_{AR} dx_R|_{\mathcal{D}}}{1-k_{AR}^2}$ for the separation between \mathcal{O} and \mathcal{D} . With the

coordinates of \mathcal{E} and \mathcal{D} replaced from (2.9) in terms of the coordinates of \mathcal{R} , we calculate the product $ds_A|_{\mathcal{EO}} ds_A|_{\mathcal{OD}}$ and compare it to the separation $ds^2|_{\mathcal{OR}}$ between the \mathcal{R} and \mathcal{O} , as obtained from (2.6):

$$0 < ds_A|_{\mathcal{EO}} ds_A|_{\mathcal{OD}} = -\left(\frac{2k_{AR}}{1-k_{AR}^2}\right)^2 \left(dx_A^2 + \frac{1+k_{AR}^2}{k_{AR}} dx_A dx_R + dx_R^2\right)|_{\mathcal{R}} = -ds^2|_{\mathcal{OR}}. \quad (2.10)$$

Notably, the same result obtains also when O_R rather than O_A initiates the round-trip of the light signal to \mathcal{R} and back. Even more remarkable, we also arrive at the same result when considering the round-trip of a light signal emitted by a third body, provided it is also present at \mathcal{O} . To prove this, one just recalculates (2.10) with the coordinates of the appropriate emission and detections events along the path of the third body. These events should meet the equations of the respective light rays to and from \mathcal{R} .

We conclude that in a binate frame, when $ds^2 < 0$ between \mathcal{O} and a near-event \mathcal{R} , the differential separation is physically meaningful since $\sqrt{-ds^2|_{\mathcal{OR}}} = \sqrt{ds|_{\mathcal{EO}} ds|_{\mathcal{OD}}}$ and the right-hand side is the geometric average of the separations between some events

along the path of a body that initiated a light signal at \mathcal{E} , was present at \mathcal{O} , and then detected at \mathcal{D} the signal reflected back from \mathcal{R} . Our conclusions thus mirror those arrived at by Synge in the above quoted reference.

Having shown that the set of place-coincidences in a binate frame is a metric manifold, we now have at our disposal the usual calculus associated with tensors on this kind of manifold. This enables us to consider in the next section some dynamical aspects of motion in a binate frame.

Diagonal forms of the line element: The relation between the binate-frame and the observer-frame parameterizations is one-to-many, rather than one-to-one. The time and space coordinates that diagonalize the metric of (2.6) are observer-dependent. Consider, for example, an observer located on the A-ruler in Fig. 2. When present at an event, this observer uses $dx = dx_A$ to measure the distances to near events. The measurement is along his/her own relative space, the geometric extension of the A-ruler. When dx_A is set apart in (2.6), we obtain the diagonal metric form adapted to the observer's frame:

$$ds^2 = \left(\frac{1+k_{A\aleph}^2}{1-k_{A\aleph}^2} dx_A + \frac{2k_{A\aleph}}{1-k_{A\aleph}^2} dx_{\aleph} \right)^2 - dx_A^2. \quad (2.6a)$$

This singles out the time-coordinate: $cdt_A = -\frac{1+k_{A\aleph}^2}{1-k_{A\aleph}^2} dx_A - \frac{2k_{A\aleph}}{1-k_{A\aleph}^2} dx_{\aleph}$, in units of length. In contrast, an observer located on the \aleph -ruler in Fig. 2 and attending the same event would use $dx = -dx_{\aleph}$ and obtain $cdt_{\aleph} = -\frac{2k_{A\aleph}}{1-k_{A\aleph}^2} dx_A - \frac{1+k_{A\aleph}^2}{1-k_{A\aleph}^2} dx_{\aleph}$. Simple algebra then shows that the space and time coordinates of the two observers are related by a Lorentz transformation with $\beta_{A\aleph} = (1-k_{A\aleph}^2)/(1+k_{A\aleph}^2)$. This last relation is the inverse of (2.1).

Also of some interest is the diagonal form of (2.6) as adapted to an observer that views the two rulers in Fig. 2 as moving with equal speeds in opposite directions. For this observer, both the time- and the space-component of the metric has to be symmetric in x_A and x_{\aleph} . This is realized with the following expression for the line element (2.6):

$$ds^2 = \frac{k_{A\aleph}}{(1-k_{A\aleph})^2} (dx_A + dx_{\aleph})^2 - \frac{k_{A\aleph}}{(1+k_{A\aleph})^2} (dx_A - dx_{\aleph})^2 \quad (2.6b)$$

In general, we use a technique from General Relativity to obtain the space and time adapted to the motion $z^\mu = z^\mu(s)$ of an observer: we construct a *projection operator*, that is, the tensor $\delta_\mu^\nu - \eta_{\mu\sigma} \dot{z}^\sigma \dot{z}^\nu$, where $\dot{z}^\mu \equiv dz^\mu/ds$. A displacement $d\bar{z}^\mu$ between two near events attended by this observer then projects in his/her relative space as the vector $(\delta_\mu^\nu - \eta_{\mu\sigma} \dot{z}^\sigma \dot{z}^\nu) d\bar{z}^\mu$, and projects parallel to the observer's motion as $\eta_{\mu\sigma} \dot{z}^\sigma \dot{z}^\nu d\bar{z}^\mu$. The two vectors are $\eta_{\mu\nu}$ -orthogonal and add up to the given displacement.

2.5 Dynamical considerations

The metric nature of the place-coincidences manifold enables us to associate physical quantities with geometric objects, here denoted in time-honored tradition, through their (binate-frame) components. Of primary interest are vectors defined along the path of a particle's motion: $\dot{z}^\mu = dz^\mu/ds$ is the *unit-tangent* to the path since $\dot{\mathbf{z}} \equiv \sqrt{\eta_{\mu\nu} \dot{z}^\mu \dot{z}^\nu} = 1$; $\ddot{z}^\mu = d\dot{z}^\mu/ds$ is *normal* to \dot{z}^μ , since $\eta_{\mu\nu} \dot{z}^\mu \ddot{z}^\nu = 0$, and its magnitude $\ddot{\mathbf{z}} = \sqrt{\eta_{\mu\nu} \ddot{z}^\mu \ddot{z}^\nu}$ gives the path *curvature*. The tangent to the arbitrarily parameterized path $z^\mu = z^\mu(\zeta)$ of a particle is the vector $z'^\mu = dz^\mu/d\zeta$ whose magnitude is $\mathbf{z}' \equiv \sqrt{\eta_{\mu\nu} z'^\mu z'^\nu} = ds/d\zeta \equiv s'$.

With a particle's motion, we associated a (*generalized*) *momentum* vector, usually presented in terms of its covariant components, p_μ . This vector is the foundation of all our dynamical considerations, though it could not be defined here in terms of 'velocity,' as in Newtonian mechanics and Special Relativity, since there is no notion of 'time' in a binate frame. For the same reason, we cannot obtain from a Lagrangian the 'canonical' momentum. But although the Lagrangian dynamics is not available to us, many others, quite-equivalent approaches are well known [14-16]. Each defines its own notion of (generalized) momentum, by virtue of the equations used in calculations.

Our preference is to employ what Synge calls "the *second form* of Hamilton's *principle*" [16]. When adopted for our purpose, it reads as follows: The path of a particle in a binate frame is the stationary curve of the *Hamiltonian action* $\int_{\mathcal{E}_1}^{\mathcal{E}_2} p_\mu z'^\mu d\zeta$ with fixed ends at the events \mathcal{E}_1 and \mathcal{E}_2 , and constrained by an *energy equation* of the form $Q(z^\mu, p_\mu) = 0$, where Q is a (scalar) function of the listed *phase* variables. The principle yields the canonical form of Hamilton's *equations of motion*: $z'^\mu = \frac{\partial Q}{\partial p_\mu}$ and $p'_\mu = -\frac{\partial Q}{\partial z^\mu}$.

These yield the particle's path $z^\mu(\zeta)$ and its momentum vector $p_\mu(\zeta)$ as defined here. Furthermore, the equations also determine the finite separation $s(\zeta)$ between the events along the particle's path. The stipulated form of $Q(z^\mu, p_\mu)$ controls the dynamics since it obtains the coordinates of the events attended by the particle as well as the momentum components conjugate to these coordinates. The label 'energy equation' was adopted by Synge to reflect the fact that $Q(z^\mu, p_\mu)$, just like a Hamiltonian $H(z^\mu, p_\mu)$ in classical mechanics, produces canonical equations of motion.

Free particles: In a $k_{\text{A}\text{N}}$ -frame, consider a particle whose momentum vector p_μ is unchanged throughout the motion. This suggests an energy equation $Q(z^\mu, p_\mu) = 0$ of the form: $\frac{1}{2m}(p_\mu p^\mu - \mathbf{p}_0^2) = 0$, where $\mathbf{p}_0 \equiv \sqrt{p_\mu p^\mu} \Big|_{\zeta=0}$ is the magnitude of the particle's initial momentum and m is its mass, as understood and measured in classical mechanics.

The factor $\frac{1}{2}$ and the contravariant components $p^\mu = \eta^{\mu\nu} p_\nu$ of the momentum vector merely simplify the writing; $\eta^{\mu\nu}$ denotes the inverse of $\eta_{\mu\nu}$ in (2.7):

$$\eta^{\mu\nu} = \begin{bmatrix} -1 & \frac{1+k_{\text{A}\text{N}}^2}{2k_{\text{A}\text{N}}} \\ \frac{1+k_{\text{A}\text{N}}^2}{2k_{\text{A}\text{N}}} & -1 \end{bmatrix}. \quad (2.11)$$

Say the particle's motion starts at $z^1 \equiv x_{\text{A}} = 0$ and $z^2 \equiv x_{\text{N}} = 0$, with an initial momentum $p_\mu|_{\zeta=0} = [p_{\text{A}} \quad p_{\text{N}}]$ where the two covariant components are specified so as to meet:

$$-p_{\text{A}}^2 + \frac{1+k_{\text{A}\text{N}}^2}{k_{\text{A}\text{N}}} p_{\text{A}} p_{\text{N}} - p_{\text{N}}^2 = \mathbf{p}_0^2. \quad (2.12)$$

(Recall that the subscripts $_{\text{A}}$ and $_{\text{N}}$ are always used as labels, not covariant indices.)

Hamilton's equations of motion are derived from the energy specification. This yields: $mz'^\mu = p^\mu$ and $p'_\mu = 0$. The latter equations are met when $p_\mu = [p_{\text{A}} \quad p_{\text{N}}]$; the contravariant components are $p^1 = -p_{\text{A}} + \frac{1+k_{\text{A}\text{N}}^2}{2k_{\text{A}\text{N}}} p_{\text{N}}$ and $p^2 = \frac{1+k_{\text{A}\text{N}}^2}{2k_{\text{A}\text{N}}} p_{\text{A}} - p_{\text{N}}$. The tangent to the path has the constant direction: $z'^\mu = p^\mu/m$ and the separation of near events along the particle's path obtains as $ds = \mathbf{z}' d\zeta = (\mathbf{p}_0/m) d\zeta$. Substitutions yield the particle's path: $z^\mu = (p^\mu/\mathbf{p}_0)s$. The dynamics so specified is that of a uniform motion, typical of a *free* particle.

For the experimental verification, one needs the technical means for calibrating a binate frame and for locating the particle at various events. Say the free particle is present at an event \mathcal{E} with measured coordinates $dx^\mu = (dx_{\text{A}}, dx_{\text{N}})$, near the start of its motion. The solution to Hamilton's equations yields the path of the particle:

$$dx_{\text{A}} = \left(-\frac{p_{\text{A}}}{\mathbf{p}_0} + \frac{1+k_{\text{A}\text{N}}^2}{2k_{\text{A}\text{N}}} \frac{p_{\text{N}}}{\mathbf{p}_0} \right) ds \quad \text{and} \quad dx_{\text{N}} = \left(\frac{1+k_{\text{A}\text{N}}^2}{2k_{\text{A}\text{N}}} \frac{p_{\text{A}}}{\mathbf{p}_0} - \frac{p_{\text{N}}}{\mathbf{p}_0} \right) ds. \quad (2.13)$$

With the measured values of dx_{A} and dx_{N} , (2.6) obtains the separation ds from the start of the motion to the specified near-event event \mathcal{E} , and then (2.13) yields the covariant momentum components at this event, evidently in units of \mathbf{p}_0 . The constancy of these components is experimentally verifiable by collecting data at other near-events along the particle's path, and repeating the above calculations. Note that the magnitude of the particle's constant momentum remains undetermined — the experiment yields only the ratio between the components of the free particle's momentum.

In Sec. 2.3, we showed that a particle located at O_A in the $k_{A\aleph}$ -frame moves according to: $dx_A = 0$ and $dx_{\aleph} = -\frac{1-k_{A\aleph}^2}{2k_{A\aleph}}ds$. To show that such a motion is dynamically possible, we first note that $dz^1 = 0$ and $dz^2 = -\frac{1-k_{A\aleph}^2}{2k_{A\aleph}}\frac{\mathbf{p}_0}{m}d\zeta$ is a solution of Hamilton's equations for a free particle with: $p_1 \equiv p_A = -\frac{1+k_{A\aleph}^2}{1-k_{A\aleph}^2}\mathbf{p}_0$ and $p_2 \equiv p_{\aleph} = -\frac{2k_{A\aleph}}{1-k_{A\aleph}^2}\mathbf{p}_0$. (The contravariant components are: $p^1 = 0$ and $p^2 = -\frac{1-k_{A\aleph}^2}{2k_{A\aleph}}\mathbf{p}_0$.) The separation between events along the particle's path being $ds = (\mathbf{p}_0/m)d\zeta$, substitutions show that this solution is indeed the motion whose kinematics was discussed in Sec. 2.3.

The above selected form of $Q(z^\mu, p_\mu)$ for the free particle is not unique, and thus the resulting relation between ds and $d\zeta$ is also not unique. Non-uniqueness is typical of the Hamiltonian approach, but although a different Q function leads to a solution with a different path parameter ζ , the predicted motion is uniquely determined by the initial conditions. That is, when the Q -dependent parameter ζ is replaced in terms of the separation s , we always arrive at the same solution: $dx_A = 0$ and $dx_{\aleph} = -\frac{1-k_{A\aleph}^2}{2k_{A\aleph}}ds$ for the motion of the free particle described in Sec. 2.3.

The particle's momentum vector is a geometrical object. Projected in the frame of an inertial observer, it yields the relativistic energy-momentum vector, as measured by the observer. An observer at O_A , for example, would use the coordinates that obtain the diagonal form (2.6a) of the line element. In the frame $x^\alpha = (ct_A, x_A)$ of this observer, the momentum vector is $p^\alpha = \frac{\partial x^\alpha}{\partial z^\mu} p^\mu = \begin{bmatrix} 1 \\ 0 \end{bmatrix} \mathbf{p}_0$. The relativistic interpretation then assigns to the free particle the 'energy' $\mathbf{p}_0 c$ and no momentum, as expected since the particle is at rest in this frame. In contrast, $p^\alpha = \frac{1+k_{A\aleph}^2}{2k_{A\aleph}} \begin{bmatrix} 1 \\ \frac{1-k_{A\aleph}^2}{1+k_{A\aleph}^2} \end{bmatrix} \mathbf{p}_0$ in the frame $x^\alpha = (ct_{\aleph}, -x_{\aleph})$ of

an observer at O_{\aleph} , who then assigns to the particle a different 'energy': $\frac{1+k_{A\aleph}^2}{2k_{A\aleph}}\mathbf{p}_0 c$, and a non-zero momentum: $\frac{1-k_{A\aleph}^2}{2k_{A\aleph}}\mathbf{p}_0$. Thus the particle moves uniformly in the frame of this observer.

Special Relativity defines the energy-momentum vector as $p^\mu = mc \dot{z}^\mu$, and this yields the relation $\mathbf{p} \equiv \sqrt{p_\mu p^\mu} = mc$, where m is often called the particle's 'rest mass'.

Both observers obtain the same value, $m = \mathbf{p}_o/c$, for the particle's 'rest mass,' which is invariant under a change of frame. We use no such designation for the mass m , since the notion of 'rest' is foreign to the binate-frame approach. Furthermore, our analysis of the dynamics of a free particle does not yield any fundamental relation between mass m and the magnitude \mathbf{p} of the here defined (generalized) momentum vector. Notwithstanding, for the purpose of comparing our results with relativistic predictions, and solely for such purpose, we would use here the relation $\mathbf{p} = mc$.

In appendix A4 we analyze the dynamics of two free particles that collide and coalesce to form a new free particle. The analysis uses the k_{AN} -frame formed with the relative spaces of the two particles just prior to the collision. It yields the usual prediction that the momentum-magnitude of the coalesced particle $\hat{\mathbf{p}}$ is always larger than the sum $\bar{\mathbf{p}} + \bar{\bar{\mathbf{p}}}$ of the momentum-magnitudes of the colliding particles:

$$\hat{\mathbf{p}}^2 = (\bar{\mathbf{p}} + \bar{\bar{\mathbf{p}}})^2 + \left(\sqrt{k_{\text{AN}}^{-1}} - \sqrt{k_{\text{AN}}} \right)^2 \bar{\mathbf{p}} \bar{\bar{\mathbf{p}}}. \quad (2.14)$$

With $k_{\text{AN}} = \sqrt{(1 - \beta_{\text{AN}})/(1 + \beta_{\text{AN}})}$, from (2.1), and β_{AN} the relative speed between the particles prior to the collision, our result matches the relativistic prediction when $\mathbf{p} = mc$ is used for the comparison.

Forced particles: A particle is not free when its momentum changes along the path. We expect the energy equation to reflect that. For example, the momentum of a particle that moves from \mathcal{O} to a near event \mathcal{E} could be changing because of the *work*, $F_\mu z^\mu \Big|_{\mathcal{E}}$, of what could be classically termed a *force* $F^\mu = \eta^{\mu\nu} F_\nu$. But then an energy

equation of the form: $\frac{1}{2m}(p_\mu p^\mu - \mathbf{p}_o^2) - F_\mu z^\mu = 0$ is worth exploring since when the work of the given force is the only reason for the energy of the particle to be changing, work and energy should balance.

With a constant F^μ , we get from Hamilton's equations: $m\dot{z}'^\mu = p^\mu$ and $p'_\mu = F_\mu$. Thus $p_\mu = F_\mu \zeta + p_\mu \Big|_{\zeta=0}$ and the separation is $ds = \mathbf{z}' d\zeta = (\mathbf{p}/m)d\zeta$. Substitutions yield the covariant equations: $\dot{z}^\mu = p^\mu/\mathbf{p}$ and $\dot{p}_\mu = mF_\mu/\mathbf{p}$. Remarkably, calculations then show that $\dot{\mathbf{p}} = m\mathbf{F}/\mathbf{p} \rightarrow 0$ as $s \rightarrow \infty$. Thus a constant force is less and less effective in increasing the momentum of the forced particle as it moves along its path. (This is what is expected from the usual relativistic considerations and experiments with charged particles that are accelerated by electromagnetic fields.) Finally, integration yields

$$\frac{1}{2m}(\mathbf{p}^2 - \mathbf{p}_o^2) = \mathbf{F}s, \text{ which reflects the expected balance of work and energy.}$$

Since we could always view the particle's motion between near events as being uniform, like that of a free particle, experimental verification of the solution is addressed as before. With the means to locate the particle at various events along its path, we get the components of the force and the initial momentum from the coordinates of a few of such events. Then the coordinates of still other near-events also attended by the particle

could be used to verify that when the force remains constant, the particle's momentum indeed changes as presented by the solution.

Path of constant curvature: Special Relativity focuses on the consequences of Lorentz transformations of coordinates between inertial observers. Even then, the motion of an observer who measures his/her own acceleration and finds it of constant magnitude receives particular attention. Such motion is usually called 'hyperbolic,' and its covariant specification has the form: $\ddot{z}^\mu = \lambda^2 \dot{z}^\mu$, that is, the proper-time rate of change of each acceleration component is proportional to the respective velocity component, with the coefficient of proportionality being the square of the acceleration-magnitude. Simple calculations then show that the particle's motion is along a path of constant curvature: $\ddot{z}_\mu \ddot{z}^\mu = -\lambda^2$.

A constant force does not move a particle along a path of constant curvature, but we show in Sec. 4.2 that the dynamics of such motion is realized when a constant electric field acts on a charged particle.

2.6 A first comparison with the spacetime approach

We are now ready to compare the spacetime approach of Special Relativity with ours. The comparison is limited to the mechanics of motion and light propagation in the world of one physical-space dimension that we have examined so far. We undertake further comparisons later in the presentation.

An event occurs at a definite place on the extended physical space of each body involved in any phenomena or experiment under consideration. These places coincide at the event. So much the spacetime approach and ours have in common. Differences emerge when considering the reference systems used by the two approaches. At least for computational purposes, the spacetime approach identifies an event with the place and time of its occurrence, as measured by a selected observer present at, or near the event. The place is identified from its distance to the observer, while the time is identified from the reading of the clock located where the event happened and initially synchronized with the observer's clock, in accordance with a stipulated procedure. In contrast, we identify an event by the places where it occurs in the relative spaces of a pair of bodies in relative motion. These were selected to form our reference system. We use no clocks, and thus need no synchronization procedure.

As already noted, our reference system uses a pair of bodies rather than just one observer. This is not an added complication when considering that even the principle of relativity uses two observers in relative motion. In fact, the binate frame simplifies the presentation: We use one pair of coordinates to analyze phenomena and experiments. For the same purpose, Special Relativity needs two pairs of coordinates, and then constrains them with two relations, the Lorentz transformations between two observer-frames!

With the spacetime approach, the relative motion between any two bodies that attend an event is specified in terms of the measured relative speeds, usually presented in units of the speed of light, that is, as fractional speeds β . Here, for the same purpose, we use the dimensionless k -value. The two approaches are equivalent since (2.1) relates the β - and k -values. However, the speed of light (one-way experiments) is in principle not

measurable. Instead, one measures the average round-trip speed — Einstein’s postulated constancy of the speed of light had to be reinterpreted over the years to reflect this. Our approach dispenses entirely with the notion of a time coordinate and thus also with the concept of ‘speed,’ being that of a light signal or of a particle. This did not hinder any of our analyses.

When the event-coordinates are changed back and forth between (cdt, dx) and (dx_A, dx_K) , this involves a change between the corresponding parameterizations in two frames that belong to different families of reference systems, namely, an observer frame and a binate frame, each with its own conceptual elements and their respective physical interpretations. Thus, for example, (i) The dichotomy between ‘rest’ and ‘motion’ is evident with the spacetime approach. The frame of a selected observer, not necessarily inertial, provides a standard of ‘rest’ for observers and particles: they are said to be at rest when they retain with time their location in the frame of the selected observer, otherwise, they are moving. The dichotomy is absent in a binate frame, since a particle cannot be at ‘rest’ in a binate frame. Even when it retains its location on one ruler of the frame, the particle is still moving with respect to the other ruler. (ii) Special Relativity stipulates the same standard of motion for all observer-frames when it attaches a numerical value to the speed of light and then uses it to construct the dimensionless factor β . In contrast, the calibration of the binate frame to a selected k -value provides a measurable standard of motion that could be adapted to the physical situation under consideration.

The conceptual differences just illustrated do not lead to different predictions. We note however that over the years, synchronization-dependent definitions and predictions made by Special Relativity have not always been recognized as being devoid of fundamental importance [3]. A binate-frame approach inevitably leads to definitions and predictions free of synchronization effects. Furthermore, calculations are simpler in a binate frame. And even more importantly, also the physical interpretations are simpler. This is because all observer-dependent notions so prevalent in Special Relativity are absent in our binate-frame approach.

In appendix A5, we analyze an envisaged situation where light signals propagate back and forth among moving clocks. It serves to illustrate the simplifications brought about by our approach. The binate-frame analysis is preceded by an analysis typical of Special Relativity. The discussion brings forward some fine details of both approaches.

3 Considerations involving two physical-space dimensions

In two physical-space dimensions, the relative space of each material body is an infinite plane. The plane could slide and rotate in the planes of the relative spaces of all the other bodies. Figure 4 shows two such planes in translational motion. The planes are visualized as flat, transparent sheets firmly attached to the A - and K -rulers of Fig. 2 and equipped with Cartesian coordinates. For clarity, Fig. 4 omits the y_A -axis, which runs upward from O_A , and the y_K -axis, which runs downward from O_K .

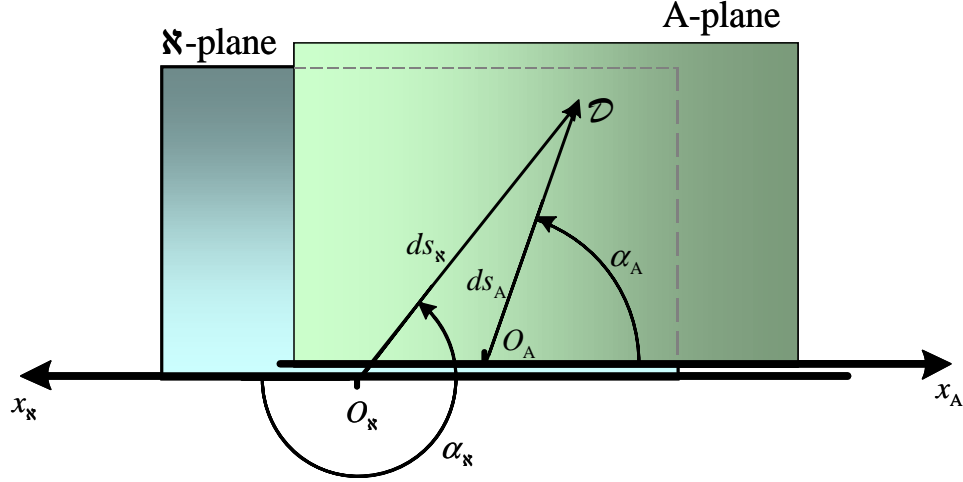


Fig. 4 The diagram of the two planes at the event \mathcal{D} .

Events could mark on each plane the place where they occur. Then a diagram like that of Fig. 4, which relates to an experiment involving some event \mathcal{D} , is obtained as follows: The A- and K-planes that were in relative motion during the experiment are stopped at its completion. Then the planes are superposed with their x -axes aligned and the mark left by \mathcal{D} on one plane positioned on top of the mark left on the other plane. All the desired measurements are made with the planes so positioned. Granted that the geometry of each plane is Euclidean, the measured coordinate differentials of any pair of near events meet: $dy_A = -dy_K$, $ds_A^2 = dx_A^2 + dy_A^2$, and $ds_K^2 = dx_K^2 + dy_K^2$.

3.1 The quadric of a propagating light signal

Consider experiments with the above system of two planes attached to rulers whose motion was calibrated to k_{AK} . Say a light signal is emitted at the event \mathcal{O} , when O_A passes over O_K . Say further that the diagram of Fig. 4 shows the event \mathcal{D} when a detector near O_A in the A-plane detects the light from \mathcal{O} and marks the place of detection on the K-plane. (A similar diagram for the emission event \mathcal{O} would have shown O_A coinciding with O_K .) The coordinates (dx_A, dy_A) of the detector and the coordinate dx_K of the location where the detector marked the K-plane suffice to draw the illustrated detection event. We read from the diagram that $(-dx_A - dx_K)|_{\mathcal{D}} = |O_A O_K|$. This relation holds when the two planes are brought to rest and positioned as shown. (We know nothing about the situation that existed when the detection occurred, with the planes in relative motion; all our information comes from the coordinates on the two planes when at relative rest, and from the marks left by the detection event.)

Suppose other detectors are also near O_A . They too would detect the emitted light signal and mark the place of detection. But only those detections \mathcal{D} whose coordinates

meet the relation $(-dx_A - dx_{\mathfrak{K}})_{\mathcal{D}} = |\overline{O_A O_{\mathfrak{K}}}|$ for the same distance between O_A and $O_{\mathfrak{K}}$ could be placed on one and the same diagram. This raises the question of finding the locus of all such detections. We address this question next.

Because a propagating light signal needs no material support, it privileges none of the two planes. Thus a line tangent to the desired locus, at any event \mathcal{D} on it, is equally inclined to $\overline{O_A \mathcal{D}}$ and $\overline{O_{\mathfrak{K}} \mathcal{D}}$. This is only possible when the locus is an ellipse with O_A and $O_{\mathfrak{K}}$ as its foci. (Recall that for the same symmetry reason, light from one focus of an elliptic mirror always reflects to the other focus of the mirror.)

We proceed now to find the equation of the ellipse. According to (2.2), a light signal that propagates from \mathcal{O} along the $x_A x_{\mathfrak{K}}$ -axis could be detected at an event \mathcal{D}_0 with coordinates $dy_A = -dy_{\mathfrak{K}} = 0$ only when either $dx_A + k_{A\mathfrak{K}} dx_{\mathfrak{K}} = 0$ or $k_{A\mathfrak{K}} dx_A + dx_{\mathfrak{K}} = 0$. If in addition, $(-dx_A - dx_{\mathfrak{K}})|_{\mathcal{D}_0} = |\overline{O_A O_{\mathfrak{K}}}|$, then \mathcal{D}_0 is on the desired ellipse and furthermore:

$$\begin{aligned} dx_A|_{\mathcal{D}_0} &= \frac{k_{A\mathfrak{K}}}{1-k_{A\mathfrak{K}}} |\overline{O_A O_{\mathfrak{K}}}| \quad \text{and} \quad dx_{\mathfrak{K}}|_{\mathcal{D}_0} = \frac{-1}{1-k_{A\mathfrak{K}}} |\overline{O_A O_{\mathfrak{K}}}|, \quad \text{or} \\ dx_A|_{\mathcal{D}_0} &= \frac{-1}{1-k_{A\mathfrak{K}}} |\overline{O_A O_{\mathfrak{K}}}| \quad \text{and} \quad dx_{\mathfrak{K}}|_{\mathcal{D}_0} = \frac{k_{A\mathfrak{K}}}{1-k_{A\mathfrak{K}}} |\overline{O_A O_{\mathfrak{K}}}|. \end{aligned} \quad (3.1)$$

The first pair of equations (3.1) relates to the detection of the signal that propagates in the positive direction of the x_A -axis, whereas the second relates to the detection of the signal that propagates in the positive direction of the $x_{\mathfrak{K}}$ -axis.

For the two detections \mathcal{D}_0 that meet (3.1) to be on the ellipse, its semi-major and semi-minor axis should be: $\frac{1}{2}(dx_A - dx_{\mathfrak{K}})|_{\mathcal{D}_0}$ and $\sqrt{-dx_A dx_{\mathfrak{K}}}|_{\mathcal{D}_0}$, respectively. The ellipse

$$\left[\frac{(dx_A - dx_{\mathfrak{K}})|_{\mathcal{D}}}{(dx_A - dx_{\mathfrak{K}})|_{\mathcal{D}_0}} \right]^2 + \left[\frac{dy_A|_{\mathcal{D}}}{\sqrt{-dx_A dx_{\mathfrak{K}}}|_{\mathcal{D}_0}} \right]^2 = 1 \quad \text{meets the specifications. The distance between}$$

its foci is $(-dx_A - dx_{\mathfrak{K}})|_{\mathcal{D}_0}$, and furthermore $(-dx_A - dx_{\mathfrak{K}})|_{\mathcal{D}} = |\overline{O_A O_{\mathfrak{K}}}| = (-dx_A - dx_{\mathfrak{K}})|_{\mathcal{D}_0}$ at all points on the ellipse. But then, from (3.1), we get $dx_A|_{\mathcal{D}_0}$ and $dx_{\mathfrak{K}}|_{\mathcal{D}_0}$ in terms of $dx_A|_{\mathcal{D}}$ and $dx_{\mathfrak{K}}|_{\mathcal{D}}$, which we substitute in the equation of the ellipse so that all the differentials there are now calculated at the same event \mathcal{D} . This yields:

$$\left(\frac{2k_{A\mathfrak{K}}}{1-k_{A\mathfrak{K}}^2} \right)^2 (dx_A^2 + \frac{1+k_{A\mathfrak{K}}^2}{k_{A\mathfrak{K}}} dx_{\mathfrak{K}} dx_A + dx_{\mathfrak{K}}^2) + dy_A dy_{\mathfrak{K}} = 0. \quad (3.2)$$

(The last term is always negative since $dy_A dy_{\mathfrak{K}} = -dy_A^2 = -dy_{\mathfrak{K}}^2$.)

We conclude that one could view (3.2) as relating the coordinate differentials of either an event that emits a light signal and a near event that subsequently detects it, or two events near each other along the ray of a light signal. A simple restructuring obtains from (3.2) the counterparts of the diagonal forms (2.6a) and (2.6b), which were adapted to observers whose motions we described in Sec. 2.6:

$$\left(\frac{1+k_{\text{A}\text{N}}^2}{1-k_{\text{A}\text{N}}^2} dx_{\text{A}} + \frac{2k_{\text{A}\text{N}}}{1-k_{\text{A}\text{N}}^2} dx_{\text{N}} \right)^2 - dx_{\text{A}}^2 - dy_{\text{A}}^2 = 0 \quad (3.2a)$$

$$\frac{k_{\text{A}\text{N}}}{(1-k_{\text{A}\text{N}})^2} (dx_{\text{A}} + dx_{\text{N}})^2 - \frac{k_{\text{A}\text{N}}}{(1+k_{\text{A}\text{N}})^2} (dx_{\text{A}} - dx_{\text{N}})^2 + dy_{\text{A}} dy_{\text{N}} = 0 \quad (3.2b)$$

A light signal traces, respectively, the lines $dx_{\text{A}} = dy_{\text{A}} \cot \alpha_{\text{A}}$ and $dx_{\text{N}} = dy_{\text{N}} \cot \alpha_{\text{N}}$ in the A - and N -planes. (The angular elevations α_{A} and α_{N} are measured counter-clockwise from the positive direction of the respective x -axis, as in Fig. 4.) When the equations of the lines are substituted in (3.2), we get:

$$k_{\text{A}\text{N}} + \cot(\tfrac{1}{2}\alpha_{\text{A}}) \cot(\tfrac{1}{2}\alpha_{\text{N}}) = 0. \quad (3.3)$$

The transverse optical-Doppler effect (appendix B1), Bradley's annual stellar aberration (appendix B2), and Michelson-Morley null-effect (appendix B3) are direct consequences of this last relation between the angular elevations of the traces projected by the light ray in the two planes of the binate frame.

3.2 A system with three bodies in coplanar motion

We wish to undertake, in two physical-space dimensions, the counterpart of the earlier analysis (Sec. 2.2) of the three rulers in collinear motion. For this, we join a third plane to the planes of the $k_{\text{A}\text{N}}$ -frame in Fig. 4. The new situation is illustrated in Fig. 5. The third plane is denoted the \mathfrak{S} -plane when considering its motion with respect to the A - plane, and the T-plane when considering its motion with respect to the N - plane. The relative motion between the \mathfrak{S} - and A - planes is along a line inclined at an angle α_{A} to the x_{A} - axis, and is calibrated to $k_{\text{A}\mathfrak{S}}$. Since the A -plane participates in two reference systems (the $k_{\text{A}\text{N}}$ - and $k_{\text{A}\mathfrak{S}}$ -frames), it has two pairs of coordinates related by:

$$d\bar{x}_{\text{A}} = dx_{\text{A}} \cos \alpha_{\text{A}} + dy_{\text{A}} \sin \alpha_{\text{A}} \quad \text{and} \quad d\bar{y}_{\text{A}} = -dx_{\text{A}} \sin \alpha_{\text{A}} + dy_{\text{A}} \cos \alpha_{\text{A}}. \quad (3.4)$$

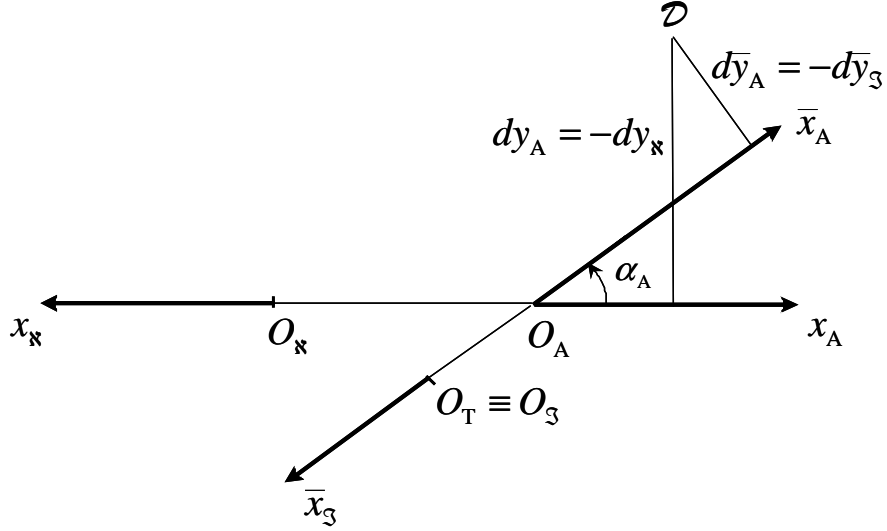


Fig. 5 The geometry of the situation when recorded on the A -plane at the event \mathcal{D} .

Say a light signal is emitted at the event \mathcal{O} , when the origins of the three planes meet, and is detected at some near-event \mathcal{D} . Either $(dx_A, dx_K, dy_A = -dy_K)$ in the k_{AK} -frame or $(d\bar{x}_A, d\bar{x}_S, d\bar{y}_A = -d\bar{y}_S)$ in the k_{AS} -frame could be used to identify the detection event.

The segment $\overline{O_A \mathcal{D}}$ in Fig. 5 belongs to the A -plane common to both frames. Its length $ds_A^2 = dx_A^2 + dy_A^2$ in the k_{AK} -frame is the same as its length $d\bar{s}_A^2 = d\bar{x}_A^2 + d\bar{y}_A^2$ in the k_{AS} -frame. We calculate the former from (3.2a) and the latter from the appropriately subscripted counterpart of (3.2a). Then we equate the two expressions:

$$\frac{1+k_{AK}^2}{1-k_{AK}^2}dx_A + \frac{2k_{AK}}{1-k_{AK}^2}dx_K = \frac{1+k_{AS}^2}{1-k_{AS}^2}d\bar{x}_A + \frac{2k_{AS}}{1-k_{AS}^2}d\bar{x}_S. \quad (3.5)$$

Consider now some other event \mathcal{P} , near \mathcal{O} , that might or might not detect the light signal emitted at \mathcal{O} . As before, either $(dx_A, dx_K, dy_A = -dy_K)$ or $(d\bar{x}_A, d\bar{x}_S, d\bar{y}_A = -d\bar{y}_S)$ could be used as \mathcal{P} 's coordinates. From (3.4), dy_A and $d\bar{y}_A$ could be expressed in terms of dx_A and $d\bar{x}_A$. The remaining four differentials involved are linearly related since there are only three independent ones. To find this relation, recall that (3.5) was obtained from an analysis of events \mathcal{D} that detect a light signal from \mathcal{O} . Since (3.5) is a linear relation and since no other such relation for the same differentials could be independent of (3.5), we conclude that (3.5) is valid at all the events \mathcal{P} near \mathcal{O} , regardless whether they could, or could not detect the light signal from \mathcal{O} . When $\alpha_A = 0$, we could substitute $dx_A = d\bar{x}_A$ in (3.5) and thus obtain (2.4), which applies in one physical-space dimension.

By pairing the K -plane with the T-plane (the relabeled S -plane), we get a third reference system, the k_{KT} -frame. Here α_K is the inclination of the T-plane's direction of motion with respect to x_K -axis. The coordinates for the k_{KT} -frame cannot be shown in Fig. 5 since the angle α_K is measured in the K -plane whereas the illustration shows the

geometry of the situation as recorded in the A -plane. But the geometry in the \aleph -plane is very similar to the one illustrated in Fig. 5. The \aleph -plane participates in both the $k_{A\aleph}$ - and $k_{\aleph T}$ -frames, and thus its two pairs of coordinates are related by:

$$d\bar{x}_{\aleph} = dx_{\aleph} \cos \alpha_{\aleph} + dy_{\aleph} \sin \alpha_{\aleph} \quad \text{and} \quad d\bar{y}_{\aleph} = -dx_{\aleph} \sin \alpha_{\aleph} + dy_{\aleph} \cos \alpha_{\aleph}. \quad (3.6)$$

Calculations similar to the ones earlier performed for (3.5) then yield:

$$\frac{2k_{A\aleph}}{1-k_{A\aleph}^2} dx_A + \frac{1+k_{A\aleph}^2}{1-k_{A\aleph}^2} dx_{\aleph} = \frac{1+k_{\aleph T}^2}{1-k_{\aleph T}^2} d\bar{x}_{\aleph} + \frac{2k_{\aleph T}}{1-k_{\aleph T}^2} d\bar{x}_T. \quad (3.7)$$

From (3.5) and (3.7), we get a third relation with the same structure:

$$\frac{2k_{A\Im}}{1-k_{A\Im}^2} d\bar{x}_A + \frac{1+k_{A\Im}^2}{1-k_{A\Im}^2} d\bar{x}_{\Im} = \frac{2k_{\aleph T}}{1-k_{\aleph T}^2} d\bar{x}_{\aleph} + \frac{1+k_{\aleph T}^2}{1-k_{\aleph T}^2} d\bar{x}_T. \quad (3.8)$$

The motion of O_{\Im} traces the line $dx_A = dy_A \cot \alpha_A$ in the A -plane of the $k_{A\aleph}$ - and $k_{A\Im}$ -frames. Since the coordinates of O_{\Im} meet: $d\bar{x}_{\Im} = 0$, $d\bar{y}_{\Im} = -d\bar{y}_A = 0$ and $dy_{\aleph} = -dy_A$, we get $d\bar{x}_A = dy_A / \sin \alpha_A$ from (3.4), and then $\frac{1+k_{A\aleph}^2}{1-k_{A\aleph}^2} \frac{dy_{\aleph}}{\tan \alpha_A} - \frac{2k_{A\aleph}}{1-k_{A\aleph}^2} dx_{\aleph} = \frac{1+k_{A\Im}^2}{1-k_{A\Im}^2} \frac{dy_{\aleph}}{\sin \alpha_A}$ from (3.5). The latter we solve for $\frac{dy_{\aleph}}{dx_{\aleph}}$. This obtains the angle α_{\aleph} in the \aleph -plane that

the trace of O_{\Im} 's motion makes with the x_{\aleph} -axis, since $\tan \alpha_{\aleph} = \frac{dy_{\aleph}}{dx_{\aleph}}$. Finally, we get

$d\bar{x}_{\aleph}$ from (3.6) and $k_{\aleph T}$ from either (3.7) or (3.8), since $d\bar{x}_T = 0$. We conclude that the initially specified $k_{A\aleph}$, $k_{A\Im}$, and α_A completely define not only the diagram of Fig. 5, for the events recorded in the A -plane, but also the similar diagrams for events recorded in the other two planes.

Projected angular elevations: The O_{\aleph} 's motion traces the line $d\bar{x}_A = -d\bar{y}_A \cot \alpha_A$ in the A -plane of the $k_{A\aleph}$ - and $k_{A\Im}$ -frames. Since the coordinates of O_{\aleph} meet: $dx_{\aleph} = 0$, $dy_{\aleph} = -dy_A = 0$ and $d\bar{y}_{\Im} = -d\bar{y}_A$, we get $dx_A = -d\bar{y}_A / \sin \alpha_A$ from (3.4), and as before, a further relation, $\frac{1+k_{A\Im}^2}{1-k_{A\Im}^2} \frac{d\bar{y}_{\Im}}{\tan \alpha_A} + \frac{2k_{A\Im}}{1-k_{A\Im}^2} d\bar{x}_{\Im} = \frac{1+k_{A\aleph}^2}{1-k_{A\aleph}^2} \frac{d\bar{y}_{\Im}}{\sin \alpha_A}$, from (3.5). We solve the latter for $\frac{d\bar{y}_{\Im}}{d\bar{x}_{\Im}}$. This obtains the angle α_{\Im} in the \Im -plane that the trace of O_{\aleph} 's motion makes with the x_{\Im} -axis, since $\tan \alpha_{\Im} = \frac{d\bar{y}_{\Im}}{d\bar{x}_{\Im}}$.

The interesting aspect of the just obtained $\tan \alpha_{\mathfrak{N}}$ and $\tan \alpha_{\mathfrak{S}}$ is that their relation to $\tan \alpha_A$ does not depend on the differential displacements used for the calculations:

$$\tan \alpha_A \frac{1+k_{A\mathfrak{N}}^2}{2k_{A\mathfrak{N}}} \tan \alpha_{\mathfrak{N}} \frac{1+k_{A\mathfrak{S}}^2}{2k_{A\mathfrak{S}}} \tan \alpha_{\mathfrak{S}} = \tan \alpha_A + \frac{1+k_{A\mathfrak{N}}^2}{2k_{A\mathfrak{N}}} \tan \alpha_{\mathfrak{N}} + \frac{1+k_{A\mathfrak{S}}^2}{2k_{A\mathfrak{S}}} \tan \alpha_{\mathfrak{S}}. \quad (3.9)$$

The above is easily recognized as a relation between the angles of a triangle. The first angle of the triangle, α_A , is exactly that shown in Fig. 5, since this is the geometry as recorded in the A-plane. Complementing α_A and forming with it a triangle are the two angles $\widehat{O_A O_{\mathfrak{N}} O_T}$ and $\widehat{O_{\mathfrak{N}} O_T O_A}$ (centered at $O_{\mathfrak{N}}$ and O_T , respectively). These angles are the *projections* in the A-plane of the angles $\alpha_{\mathfrak{N}}$ and $\alpha_{\mathfrak{S}}$, which are measured in the \mathfrak{N} - and \mathfrak{S} -planes, respectively. From (3.9), we then get $\tan \widehat{O_A O_{\mathfrak{N}} O_T} = \frac{1+k_{A\mathfrak{N}}^2}{2k_{A\mathfrak{N}}} \tan \alpha_{\mathfrak{N}}$ and

$$\tan \widehat{O_{\mathfrak{N}} O_T O_A} = \frac{1+k_{A\mathfrak{S}}^2}{2k_{A\mathfrak{S}}} \tan \alpha_{\mathfrak{S}}.$$

Two other relations similar to (3.9) obtain first with α_A and α_T projected in the \mathfrak{N} -plane, and then with α_A and $\alpha_{\mathfrak{N}}$ projected in the T-plane:

$$\tan \alpha_{\mathfrak{N}} \frac{1+k_{A\mathfrak{N}}^2}{2k_{A\mathfrak{N}}} \tan \alpha_A \frac{1+k_{\mathfrak{N}T}^2}{2k_{\mathfrak{N}T}} \tan \alpha_T = \tan \alpha_{\mathfrak{N}} + \frac{1+k_{A\mathfrak{N}}^2}{2k_{A\mathfrak{N}}} \tan \alpha_A + \frac{1+k_{\mathfrak{N}T}^2}{2k_{\mathfrak{N}T}} \tan \alpha_T, \quad (3.10)$$

$$\tan \alpha_{\mathfrak{S}} \frac{1+k_{A\mathfrak{S}}^2}{2k_{A\mathfrak{S}}} \tan \alpha_A \frac{1+k_{\mathfrak{N}T}^2}{2k_{\mathfrak{N}T}} \tan \alpha_{\mathfrak{N}} = \tan \alpha_{\mathfrak{S}} + \frac{1+k_{A\mathfrak{S}}^2}{2k_{A\mathfrak{S}}} \tan \alpha_A + \frac{1+k_{\mathfrak{N}T}^2}{2k_{\mathfrak{N}T}} \tan \alpha_{\mathfrak{N}}. \quad (3.11)$$

Evidently, only two of the three relations (3.9) – (3.11) are independent.

There are further relations that do not involve the differential displacements. Such is, for example,

$$\frac{2k_{A\mathfrak{N}}}{1-k_{A\mathfrak{N}}^2} \sin \alpha_T = \frac{2k_{\mathfrak{N}T}}{1-k_{\mathfrak{N}T}^2} \sin \alpha_A = \frac{2k_{A\mathfrak{S}}}{1-k_{A\mathfrak{S}}^2} \sin \alpha_{\mathfrak{N}}. \quad (3.12)$$

Incidentally, since $k_{A\mathfrak{N}}$, $k_{A\mathfrak{S}}$ and α_A are known, one could obtain $\alpha_{\mathfrak{N}}$, $\alpha_{\mathfrak{S}}$ and $k_{\mathfrak{N}T}$ either from a pair of the *tangent*-relations and one of the above two *sinus*-relations, or from one of the *tangent*-relations and both *sinus*-relations. None of these involve the coordinate differentials; hence, $\alpha_{\mathfrak{N}}$, $\alpha_{\mathfrak{S}}$ and $k_{\mathfrak{N}T}$ are indeed constant in the neighborhood of \mathcal{O} , as expected. (Earlier, we took for granted that the calibration required for the $k_{A\mathfrak{N}}$ - and $k_{A\mathfrak{S}}$ -frames ensured that the relative motion between the \mathfrak{N} - and T-planes at the near events under consideration is automatically calibrated to form the $k_{\mathfrak{N}T}$ -frame.)

Our results here would not surprise the reader familiar with Special Relativity and thus with how angles get distorted when measured by an observer in motion with respect to the frame where the considered angle is at rest. An observer could only measure in its own frame the projection of an angle from a moving frame, not the angle itself. Lorentz transformations yield the usual relativistic relation between the angle and its projection, in terms of the respective relative speeds between the frames. Our results, (3.9) – (3.12), reflect the same reality when considering that, in a binate frame, (2.1) yields $\frac{1+k^2}{2k} = \gamma$ and $\frac{1-k^2}{2k} = \beta\gamma$, where as usual γ stands for $1/\sqrt{1-\beta^2}$.

3.3 Further kinematical considerations

In some $k_{A\aleph}$ -frame, consider a particle present when O_A meets O_\aleph . The relative space of the particle is a third plane that moves like the particle itself, without rotating around it. The particle's plane is denoted either the T-plane or the \Im -plane, as explained in Sec. 3.2. The particle is at the origin $O_T \equiv O_\Im$ of this plane's pair of x -axes: \bar{x}_\Im is in the direction of the particle's motion relative to the A-plane, and \bar{x}_T is in the direction of the particle's motion relative to the \aleph -plane (see Fig. 6). With each of these two reference planes, the particle's plane forms a binate frame, the $k_{A\Im}$ - and $k_{\aleph T}$ -frames.

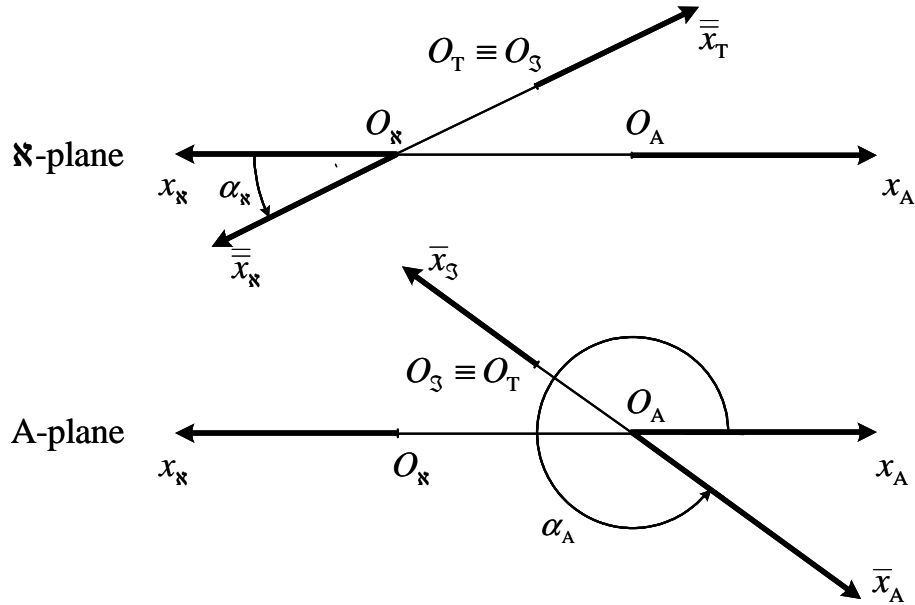


Fig. 6 The geometry of the situation in the A - and \aleph -planes of the $k_{A\aleph}$ -frame.

Figure 6 shows that the particle traces a line in the A-plane, at an angle α_A with respect to the x_A -axis, and a line in the \aleph -plane, at α_\aleph relative to the x_\aleph -axis. Two near events

attended by the particle are separated by a displacement whose components in the $k_{A\aleph}$ -frame are $(dx_A, dx_{\aleph}, dy_A = -dy_{\aleph})$. The non-null component of this displacement is $d\bar{x}_A = -\left|\overline{O_A O_{\aleph}}\right|$ in the $k_{A\aleph}$ -frame and $d\bar{x}_{\aleph} = -\left|\overline{O_{\aleph} O_T}\right|$ in the $k_{\aleph T}$ -frame.

When $d\bar{x}_{\aleph} = d\bar{x}_T = 0$ are substituted in (3.8), on each side of the equal sign there is a differential quantity related to the particle's motion in the $k_{A\aleph}$ - and $k_{A\aleph}$ -frames, respectively., which applies when $\alpha_A = 0$. We conclude (consistent with Sec. 2.3) that the separation along the particle's path is $ds = -\frac{2k_{A\aleph}}{1-k_{A\aleph}^2} d\bar{x}_A = -\frac{2k_{\aleph T}}{1-k_{\aleph T}^2} d\bar{x}_{\aleph}$. This obtains either $k_{A\aleph}$ in terms of ds , which we substitute in (3.5) with $d\bar{x}_A^2 = dx_A^2 + dy_A^2$, or $k_{\aleph T}$ in terms of ds , which we substitute in (3.7) with $d\bar{x}_{\aleph}^2 = dx_{\aleph}^2 + dy_{\aleph}^2$. In each case, we obtain an expression for ds^2 that is symmetric in the coordinates of the $k_{A\aleph}$ -frame:

$$ds^2 = \left(\frac{2k_{A\aleph}}{1-k_{A\aleph}^2}\right)^2 \left(dx_A^2 + \frac{1+k_{A\aleph}^2}{k_{A\aleph}} dx_A dx_{\aleph} + dx_{\aleph}^2\right) + dy_A dy_{\aleph}. \quad (3.13)$$

We are now ready to examine next some circular motions of particular interest.

Particle in uniform circular motion: Say a particle moves along a circular track with radius ρ and centered at O_A in the A-plane of a $k_{A\aleph}$ -frame. The equations of this particle's motion are: $x_A = \rho \cos \theta$, $x_{\aleph} = x_{\aleph}(\theta)$, and $y_A = -y_{\aleph} = \rho \sin \theta$, where the angle of rotation, θ , is measured counter-clockwise from the positive direction of x_A -axis. From (3.13), by differentiation and substitution, we get:

$$\left(\frac{ds}{d\theta}\right)^2 = \left(\frac{2k_{A\aleph}}{1-k_{A\aleph}^2}\right)^2 \left[\rho^2 \sin^2 \theta - \frac{1+k_{A\aleph}^2}{k_{A\aleph}} \rho \sin \theta \frac{dx_{\aleph}}{d\theta} + \left(\frac{dx_{\aleph}}{d\theta}\right)^2\right] - \rho^2 \cos^2 \theta. \quad (3.14)$$

We now wish to determine $x_{\aleph}(\theta)$ so that $\frac{ds}{d\theta}$ is independent of the angle θ , since in such case, we view the particle's motion as being a *uniform* rotation. We derive next the required restriction on $x_{\aleph}(\theta)$.

A binate frame is said here to be *adapted* to the particle's rotation when it is so calibrated that $\left.\frac{dx_{\aleph}}{d\theta}\right|_{\theta=\pi/2} = 0$. Then at $\theta = \pi/2$, the particle moves like any other particle

of the \aleph -plane. In the adapted frame, (3.14) shows that $\left.\frac{ds}{d\theta}\right|_{\theta=\pi/2} = \frac{2k_{A\aleph}}{1-k_{A\aleph}^2} \rho$, and this

rate is unchanged when $\frac{dx_{\aleph}}{d\theta} = -\frac{1+k_{A\aleph}^2}{2k_{A\aleph}} (1 - \sin \theta) \rho$. Thus this is the condition under which the particle's rotation is uniform.

Suppose the particle is present at the event $(\rho, 0, 0)$. Then by integration, the above equation produces the missing function for $x_{\mathfrak{N}}(\theta)$. We obtain the following parametric description of the particle's wavy-like trace in the \mathfrak{N} -plane:

$$x_{\mathfrak{N}} = -\frac{1+k_{\mathfrak{A}\mathfrak{N}}^2}{2k_{\mathfrak{A}\mathfrak{N}}}(\theta + \cos\theta - 1)\rho \quad \text{and} \quad y_{\mathfrak{N}} = -\rho \sin\theta. \quad (3.15)$$

The particle returns to its start place in the A-plane when θ is an integer multiple of 2π . Thus $\lambda = -x_{\mathfrak{N}}|_{2\pi} + x_{\mathfrak{N}}|_0$ is the *wavelength* of the particle's trace in the \mathfrak{N} -plane. From (3.15), this wavelength obtains as

$$\lambda = \frac{1+k_{\mathfrak{A}\mathfrak{N}}^2}{2k_{\mathfrak{A}\mathfrak{N}}} 2\pi\rho. \quad (3.16)$$

Thus λ is greater than the length of the particle's circular track in the A-plane. Since the selected binate frame is not arbitrary but uniquely adapted to the particle's motion, the wavelength so defined is an intrinsic property of this particle's rotation.

The relation (3.16) is verifiable with a gyroscopic detector placed at the end of a rotating arm of nominal length ρ_o . Each time the detector senses a full rotation of the arm, it places a mark to record in the A- and \mathfrak{N} -planes the place where the detection occurred. The measured distance ρ from the marked place to O_A is the effective length of the arm; $\rho > \rho_o$ because the arm extends when submitted to centrifugal forces. The measured distance between successive marks in the \mathfrak{N} -plane is the wavelength λ .

Ring rotating uniformly: We expand our analysis of circular motions to the case of a ring of radius ρ centred at O_A and rotating in the A-plane. All ring particles are labeled by their angular displacement α from a selected reference particle on the ring, to which we assign the label $\alpha = 0$. When this reference particle is in uniform rotation, its equations of motion with respect to the adapted binate frame are just as earlier calculated. Furthermore, considerations similar to those already made show that it is kinematically possible for all ring particles to move like the reference particle; that is, the α -labeled particle would move according to: $x_A = \rho \cos(\alpha + \theta)$, $y_A = \rho \sin(\alpha + \theta)$ and

$$x_{\mathfrak{N}} = -\frac{1+k_{\mathfrak{A}\mathfrak{N}}^2}{2k_{\mathfrak{A}\mathfrak{N}}}[\theta + \cos(\alpha + \theta) - 1]\rho. \quad (3.17)$$

For a particularly simple application of (3.17), consider a light ray that is emitted by $O_{\mathfrak{N}}$ when it meets the reference particle at the event with coordinates $(\rho, 0, 0)$. The light ray is emitted along the x_A -axis and toward O_A . The light is detected by the ring particle that happens to be present at the place $(x_A = -\rho, y_A = 0)$ in the A-plane when the ray arrives at this location. Thus only two coordinates of this detection event are known: $(-\rho, ?, 0)$.

The missing third coordinate, $x_{\mathbb{K}}$, should meet both, the equation of the light ray and the equations of motion of the ring particle that detects this light signal. We do next the required calculations.

Since the ray is in the $x_{\mathbb{K}} > 0$ direction, (2.2) tells us that it would reach $x_A = -\rho$ when $-k_{\mathbb{A}\mathbb{K}}\rho + x_{\mathbb{K}} = 0$. A ring particle would detect the light at $(x_A = -\rho, y_A = 0)$ when its α label is such that $\alpha + \theta|_{\mathcal{D}} = \pi$, where $\theta|_{\mathcal{D}}$, the ring's angle of rotation at this event, has yet to be found. With $x_{\mathbb{K}} = k_{\mathbb{A}\mathbb{K}}\rho$ and $\alpha = \pi - \theta|_{\mathcal{D}}$ substituted in (3.17), we solve it to get $\theta|_{\mathcal{D}} = 2 \frac{1 - k_{\mathbb{A}\mathbb{K}}^2}{1 + k_{\mathbb{A}\mathbb{K}}^2}$. Thus the particle at $\alpha = \pi - 2 \frac{1 - k_{\mathbb{A}\mathbb{K}}^2}{1 + k_{\mathbb{A}\mathbb{K}}^2}$ detects the emitted light.

The prediction is in principle verifiable: a device at $O_{\mathbb{K}}$ could mark the ring when it reaches $x_A = \rho$ and could emit a light ray at this event. Then a detector in the A-plane, at $(x_A = -\rho, y_A = 0)$, could mark the ring when it detects the light signal. The measured arc between the two marks on the ring should match the value of α as predicted from our calculations with the $k_{\mathbb{A}\mathbb{K}}$ -frame adapted to the ring's rotation.

Needless to say, the same prediction obtains from the joint consideration of (i) the classical mechanics description of how the ring particles move: $x = \rho \cos(\alpha + \omega t)$ and $y = \rho \sin(\alpha + \omega t)$, and (ii) the time it takes for light ray to cross the diameter of the ring: $t = 2\rho/c$. Thus the α -labeled particle that meets $\alpha + 2\omega \rho/c = \pi$ would detect the light signal. This is just our prediction, since $\omega\rho = v_{\theta} = \beta_{\mathbb{A}\mathbb{K}}c$ is the peripheral speed of ring particles and $\beta_{\mathbb{A}\mathbb{K}} = \frac{1 - k_{\mathbb{A}\mathbb{K}}^2}{1 + k_{\mathbb{A}\mathbb{K}}^2}$ from (2.1).

In appendix B4 we use the analysis of the rotating ring to predict the magnitude of the Sagnac effect.

3.4 Further geometric and dynamical considerations

From a geometric point of view, (3.2) and (3.13) are the clearest indication that the set of events in a world of two physical-space dimensions could be identified with the set of place-coincidences from a binate frame and, furthermore, we could attribute to the latter set the structure of a metric manifold with a line-element of the form $ds^2 = \eta_{\mu\nu} dz^{\mu} dz^{\nu}$. In the $k_{\mathbb{A}\mathbb{K}}$ -frame, $z^{\mu} = (x_A, x_{\mathbb{K}}, y_A = -y_{\mathbb{K}})$, the matrix of the metric tensor obtains as usual, from the coefficients of the quadratic form (3.13):

$$\eta_{\mu\nu} = \begin{bmatrix} \left(\frac{2k_{\mathcal{A}\mathcal{R}}}{1-k_{\mathcal{A}\mathcal{R}}^2}\right)^2 & \left(\frac{2k_{\mathcal{A}\mathcal{R}}}{1-k_{\mathcal{A}\mathcal{R}}^2}\right)^2 \frac{1+k_{\mathcal{A}\mathcal{R}}^2}{2k_{\mathcal{A}\mathcal{R}}} & 0 \\ \left(\frac{2k_{\mathcal{A}\mathcal{R}}}{1-k_{\mathcal{A}\mathcal{R}}^2}\right)^2 \frac{1+k_{\mathcal{A}\mathcal{R}}^2}{2k_{\mathcal{A}\mathcal{R}}} & \left(\frac{2k_{\mathcal{A}\mathcal{R}}}{1-k_{\mathcal{A}\mathcal{R}}^2}\right)^2 & 0 \\ 0 & 0 & -1 \end{bmatrix}. \quad (3.18)$$

The inverse matrix is much simpler:

$$\eta^{\mu\nu} = \begin{bmatrix} -1 & \frac{1+k_{\mathcal{A}\mathcal{R}}^2}{2k_{\mathcal{A}\mathcal{R}}} & 0 \\ \frac{1+k_{\mathcal{A}\mathcal{R}}^2}{2k_{\mathcal{A}\mathcal{R}}} & -1 & 0 \\ 0 & 0 & -1 \end{bmatrix}. \quad (3.19)$$

From our earlier calculations, we could assign to this line element an immediate physical meaning only when $ds^2 \geq 0$: it is the separation either along the ray of a propagating light, when $ds^2 = 0$, as shown in Sec. 3.1, or along the path of a particle, when $ds^2 > 0$, as shown in Sec. 3.3. But when $ds^2 < 0$ between \mathcal{O} and some near-event \mathcal{R} , we still have to show that the relation $\sqrt{-ds^2}|_{\mathcal{O}\mathcal{R}} = \sqrt{ds|_{\mathcal{E}\mathcal{O}} ds|_{\mathcal{O}\mathcal{D}}}$ of Sec. 2.4 applies, and thus also its physically meaningful interpretation that such ds is related to the separation between near-events along the path of a body that initiated a light signal at \mathcal{E} , was present at \mathcal{O} , and detected at \mathcal{D} the signal reflected from \mathcal{R} . The proof next follows step-by-step the approach of Sec. 2.4.

A light signal is emitted at \mathcal{E} by a device at $O_{\mathcal{A}}$ and is reflected at a near-event \mathcal{R} so as to be detected at \mathcal{D} by the device that emitted the signal. The three events are near each other. Furthermore, the event \mathcal{O} , when $O_{\mathcal{A}}$ meets $O_{\mathcal{R}}$, is somewhere between the events \mathcal{E} and \mathcal{D} along the path of the device's motion. The event \mathcal{R} is off this path and separated from \mathcal{O} by $ds^2|_{\mathcal{O}\mathcal{R}} < 0$. From (3.2), the emitted and reflected rays meet:

$$\begin{aligned} (dy_{\mathcal{A}}|_{\mathcal{R}})^2 &= \left(\frac{2k_{\mathcal{A}\mathcal{R}}}{1-k_{\mathcal{A}\mathcal{R}}^2}\right)^2 \left[(dx_{\mathcal{A}}|_{\mathcal{R}})^2 + \frac{1+k_{\mathcal{A}\mathcal{R}}^2}{k_{\mathcal{A}\mathcal{R}}} dx_{\mathcal{A}}|_{\mathcal{R}} dx_{\mathcal{R}}|_{\mathcal{E}} + (dx_{\mathcal{R}}|_{\mathcal{E}})^2 \right], \text{ and} \\ (-dy_{\mathcal{A}}|_{\mathcal{R}})^2 &= \left(\frac{2k_{\mathcal{A}\mathcal{R}}}{1-k_{\mathcal{A}\mathcal{R}}^2}\right)^2 \left[(-dx_{\mathcal{A}}|_{\mathcal{R}})^2 + \frac{1+k_{\mathcal{A}\mathcal{R}}^2}{k_{\mathcal{A}\mathcal{R}}} (-dx_{\mathcal{A}}|_{\mathcal{R}}) dx_{\mathcal{R}}|_{\mathcal{D}} + (dx_{\mathcal{R}}|_{\mathcal{D}})^2 \right]. \end{aligned} \quad (3.20)$$

Here $dx_{\mathbf{x}}|_{\mathcal{E}}^{\mathcal{R}} \equiv dx_{\mathbf{x}}|_{\mathcal{R}} - dx_{\mathbf{x}}|_{\mathcal{E}}$ and $dx_{\mathbf{x}}|_{\mathcal{R}}^{\mathcal{D}} \equiv dx_{\mathbf{x}}|_{\mathcal{D}} - dx_{\mathbf{x}}|_{\mathcal{R}}$, for short. The two equations (3.20) have the same quadratic form while $dx_{\mathbf{x}}|_{\mathcal{E}}$ is the unknown in the first and $dx_{\mathbf{x}}|_{\mathcal{D}}$ in the second. Thus the pair of solutions to any one of (3.20) yields both $dx_{\mathbf{x}}|_{\mathcal{E}}$ and $dx_{\mathbf{x}}|_{\mathcal{D}}$.

As explained in Sec. 2.3, the motion of O_A is such that along its path, we have $ds|_{\mathcal{E}0} = \frac{2k_{A\mathbf{x}} dx_{\mathbf{x}}|_{\mathcal{E}}}{1 - k_{A\mathbf{x}}^2}$ and $ds|_{\mathcal{D}0} = -\frac{2k_{A\mathbf{x}} dx_{\mathbf{x}}|_{\mathcal{D}}}{1 - k_{A\mathbf{x}}^2}$. We substitute the solutions for $dx_{\mathbf{x}}|_{\mathcal{E}}$ and $dx_{\mathbf{x}}|_{\mathcal{D}}$ in the equations for $ds|_{\mathcal{E}0}$ and $ds|_{\mathcal{D}0}$. Subsequent calculations show that indeed: $ds^2|_{\mathcal{O}\mathcal{R}} = -ds|_{\mathcal{D}0} ds|_{\mathcal{D}\mathcal{R}}$, and this completes the proof.

The availability of a physically meaningful line element allows us to extend to the world of planar motions the dynamical considerations presented in Sec. 2.5. For example, we analyze the scattering of colliding particles in appendix B5 and obtain the results expected from Special Relativity. But collision problems are particularly simple: they involve only the balance of momentum for the incoming and outgoing free particles. A more interesting case is that of a uniform rotation. The kinematics of this motion was presented in Sec. 3.3; we are now ready to look at its dynamics. The second form of Hamilton's principle (see Sec. 2.5) applies since it is not dimensionally bound.

Dynamics of circular motion: A particle constrained to remain on a circular track but otherwise free from external influences is expected to be at a permanent location on the track, or in uniform motion around the track. In the latter case, the magnitude of the particle's momentum is expected to retain its initial value while the components vary so as to affect the continuous change of the particle's direction of motion.

In a $k_{A\mathbf{x}}$ -frame adapted to the particle's motion, the track is in the A -plane and thus the constraint reads $x_A^2 + y_A^2 = \rho^2$; it would affect the momentum of the particle when the particle's energy equation contains a scalar field, $\varphi(z^\mu) = (z^1)^2 + (z^3)^2 - \rho^2$, that vanishes on the track. (The field could be specified in covariant fashion, but it is not needed since the physical plane of motion is known and the given form is applied in this plane only.) As specified, the particle is free except for the constraint imposed by the track. Hence, it seems appropriate to explore the dynamics based on the free particle's energy equation adjusted for the contribution of the track:

$$\frac{1}{2m}(p_\mu p^\mu - \mathbf{p}_0^2) - \frac{1}{2}\lambda\varphi(z^\mu) = 0. \quad (3.21)$$

Hamilton's equations are: $m z'^\mu = p^\mu$ and $p'_\mu = \frac{\lambda}{2} \frac{\partial \varphi}{\partial z^\mu}$, where λ is a yet undetermined constant. We differentiate the former set of equations and eliminate the momentum components using the latter set, since $p'^\mu = \eta^{\mu\nu} p'_\nu$. This yields: $m z''^\mu = \frac{\lambda}{2} \eta^{\mu\nu} \frac{\partial \varphi}{\partial z^\nu}$, where $\varphi(z^\mu)$ is as earlier specified. To this set of differential equations, we attach the specification of the initial event along the path of the particle:

$$\begin{cases} m x_A'' = -\lambda x_A \\ m x_N'' = \frac{1+k_{AN}^2}{2k_{AN}} \lambda x_A, \text{ with } \begin{cases} x_A = \rho \\ x_N = 0 \\ y_A = 0 \end{cases} \text{ at } \zeta = 0. \\ m y_A'' = -\lambda y_A \end{cases} \quad (3.22)$$

The equations admit a periodic solution, the circular motion with $\theta = \sqrt{\frac{\lambda}{m}} \zeta$ whose kinematics was presented in Sec. 3.3:

$$\begin{cases} x_A = \rho \cos \theta \\ x_N = -\frac{1+k_{AN}^2}{2k_{AN}} \rho (\theta + \cos \theta - 1) \\ y_A = \rho \sin \theta \end{cases} \quad (3.23)$$

The momentum components conjugated to these coordinates are:

$$\begin{cases} p_1 = -\sqrt{m\lambda} \rho \left[\left(\frac{1+k_{AN}^2}{1-k_{AN}^2} \right)^2 - \sin \theta \right] \\ p_2 = -\sqrt{m\lambda} \rho \left(\frac{2k_{AN}}{1-k_{AN}^2} \right) \left(\frac{1+k_{AN}^2}{1-k_{AN}^2} \right) \\ p_3 = -\sqrt{m\lambda} \rho \cos \theta \end{cases} \quad (3.24)$$

Calculations yield $p_\mu p^\mu = \left(\frac{2k_{AN}}{1-k_{AN}^2} \right)^2 m \lambda \rho^2$, which shows that this momentum vector

retains constant its magnitude. The energy constraint is met for $\lambda = \left(\frac{1-k_{AN}^2}{2k_{AN}} \right)^2 \frac{\mathbf{p}_0^2}{m \rho^2}$.

This in turn yields $\sqrt{m\lambda} \rho = \frac{1-k_{AN}^2}{2k_{AN}} \mathbf{p}_0$ and $s = \frac{2k_{AN}}{1-k_{AN}^2} \rho \theta$.

Were the particle be allowed to leave the track at $\theta = \pi/2$, it would remain at the place in the \mathbf{N} -plane where it was released, since the frame is adapted to the particle's rotation. Indeed, when liberated from the effect of the track's constraint, the particle's momentum would be: $p_1 = -\frac{2k_{AN}}{1-k_{AN}^2} \mathbf{p}_0$, $p_2 = -\frac{1+k_{AN}^2}{1-k_{AN}^2} \mathbf{p}_0$ and $p_3 = 0$, like any other free particle of the \mathbf{N} -plane (see Sec. 2.5). Conversely, a particle located at $y_N = -\rho$ somewhere in the \mathbf{N} -plane could smoothly enter the track at $\theta = \pi/2$: the momentum of the entering particle would match the momentum of a particle already on the track.

3.5 A second comparison with the spacetime approach

The binate frames used here and the observer frames used for relativistic calculations differ in at least three fundamental ways: (i) A binate frame requires the calibration of the motion of its planes. In principle, this is a simple kinematical procedure, aided by a light signal. In contrast, to establish that an observer frame is inertial requires a procedure that invokes the dynamical notion of a ‘free’ particle. (ii) In a binate frame, there is no natural notion of ‘distant simultaneity,’ and moreover, such a notion is not necessary. In contrast, an observer frame uses ‘time’ as the fourth coordinate, and thus needs to stipulate a clock synchronization procedure. This endows the frame with a notion of distant simultaneity: same time at different places. But this notion is relative, not frame invariant, and thus it is devoid of physical significance. (iii) Relative to a binate frame, not only light but also material particles are never at ‘rest.’ A particle moves incessantly with respect to one or the other or both reference planes. This motion is either uniform or accelerated. The binate frame then provides a standard of *uniform motion*: a particle is in uniform motion when its relative space forms a new binate frame with each plane of the original frame. In contrast, an observer frame provides a standard of *rest*: the particle is at rest in the frame when its place does not change in time.

Further differences emerge when considering how Special Relativity describes motion and propagation with respect to the frame of an inertial observer. The space and time distinction between the frame coordinates is needed for the physical interpretation of the concepts involved. This restricts the coordinate transformations to those prescribing how new space and time coordinates obtain from previous space and time coordinates: Galilean transformations suffice at low speeds but Lorentz transformations are needed at high speeds. To maintain a ‘space and time’ view, the line element of the events manifold is almost exclusively shown in its diagonal form, which Special Relativity regards as ‘canonical.’ The postulated existence of an inertial family of coordinates that realizes this canonical form endows the form with a physical meaning and further enhances its status.

But other forms of a line element with Lorentz signature $(+, -, -)$, like our form (3.13) for a two-dimensional physical space, also induce the same hyperbolic geometry. A family of coordinates is associated with each particular form of the line element. Each family is distinct from each other, and all are a faithful representation of the same Lorentz group. The line element (3.13), which is in non-diagonal form, defines here the family of coordinates used with the binate frames; it is distinct from the usual family of spacetime coordinates that realizes the diagonal form of the metric.

The binate-frame approach explains the observed kinematics of some inherently relativistic phenomena, the same ones that have so far being analyzed with the observer-frame approach of Special Relativity. Our analyses provide explanations that do not rely of any notion of temporal order between distant events, neither universal (Newtonian) nor frame-dependent (relativistic). Though mathematically equivalent, the familiar spacetime approach and our approach are nevertheless distinct in their interpretation of the concepts involved. The binate-frame approach seems to have overcome the well-known difficulties of relativistic interpretations that over the past century lead to disputes that generated an

enormous amount of literature. To support this conjecture, we advance the following symmetry considerations.

Symmetry between inertial frames: Inertial reference frames are essential for both classical and relativistic analyses. They are postulated to exist and, in principle at least, this is verifiable in experiments with free particles. The complexity of conceptualizing and identifying an inertial frame is still the subject of intense scrutiny [20-22].

An inertial frame provides a ‘standard of rest’, that is, a body is said to be at rest when its location in the frame is unchanged. The dichotomy of *rest* versus *motion* applies with respect to a selected frame of reference, viewed (in some physical sense not usually specified) as being ‘stationary.’ But singling out as stationary one inertial frame among all other equivalent ones gives it a privileged status (at least for the purpose of spacetime calculations) and breaks the natural symmetry between these frames. Is it really necessary to do so, to break this symmetry, right from the start of the chain of logic considerations that eventually explain the nature of physical phenomena where motion and propagation are jointly involved? Often a simpler picture emerges when the conceptual model reflects the natural symmetry of the physical circumstances.

We recognize that the stationary privilege could be transferred indifferently from one frame to another, but would this restore the natural symmetry? We do not think so. What obtains through the possibility of this transfer is a conceptual symmetry, between two distinct views of one and the same physical situation, which remains nevertheless asymmetrically modeled. A pair of inertial frames has a symmetry that is physical. This natural symmetry is broken when distinct roles are assigned to the frames of the pair: one frame is ‘stationary,’ the other is ‘moving.’ Interchanging these roles does not restore the physical symmetry but rather transfers from one frame to the other frame the asymmetry that the spacetime conceptual model has from the start assigned to the circumstances that are being analyzed. The binate-frame approach respects the physical symmetry of paired inertial frames.

Symmetry between moving clocks: It is generally accepted that all asymmetric experimental outcomes and predictions of Special Relativity emerge necessarily from some asymmetry in the set-up of the considered physical situation. Thus in situations that respect the symmetry between clocks in relative motion, we expect the calculations to yield symmetric predictions.

We recognize that two inertial observers that move with different velocities with respect to a clock that they both watch should indeed consider in their calculations the difference between the time intervals measured with their own clocks and those obtained with the readings of the watched clock. From the point of view of each observer, it is true that the watched clock is moving while the observer itself is stationary. Yet, we do not think that any of the two observers should conclude that the rhythm of the ‘moving’ clock differs from that of their own clocks. Such a view would attribute to the watched clock the physical impossibility of adapting its rhythm differently to accommodate different observers. The correct interpretation is that the asymmetry between clocks in relative motion is due to the way ‘time’ is measured: “For two frames in uniform relative motion, it is always a proper time interval, recorded by a single clock at rest in one frame, that is compared with an improper time interval obtained from spatially separated clocks in the other frame.” [23] The binate-frame approach uses no time-coordinate and thus makes no claim as to the nature of the flow of time.

4 Considerations involving all physical-space dimensions

We are now ready to consider our actual physical world. Each material body is embedded and moves in the three-dimensional physical-spaces of the geometric extensions of all other bodies of this world (of course, occasionally provoking collisions). When an event happens, it always does so at a definite place in the (extended) physical space of each body. All these places coincide where the event occurs. Any two bodies that, in some considered circumstances, are in mutual translation without joint rotation around a axis could form a binate frame whose coordinates could be used to identify the considered events, as we have seen in previous sections, for physical spaces of lower dimensions.

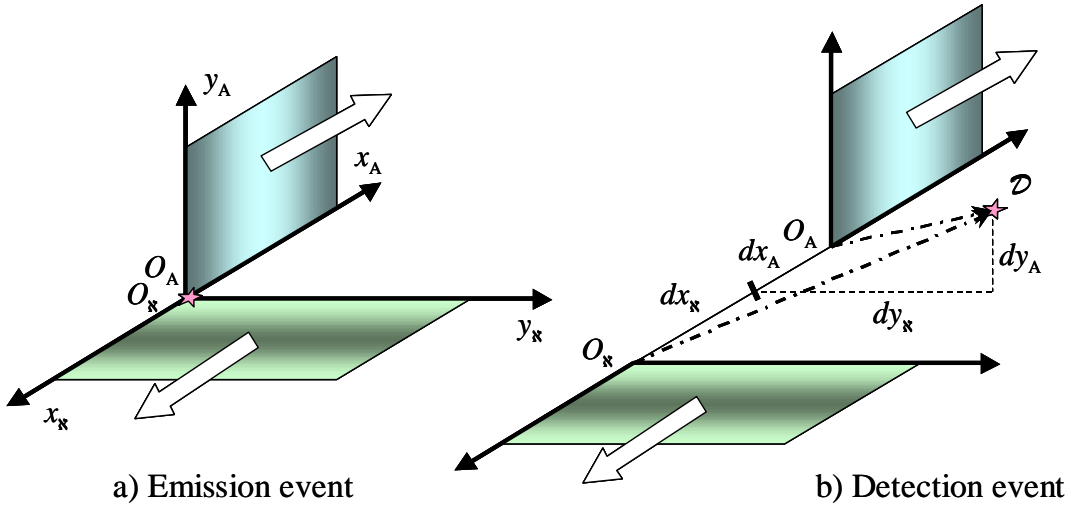


Fig. 7 Two near events: a) the emission of a light signal at \mathcal{O} , just as O_A passes by O_K , and b) the detection at \mathcal{D} .

A four-dimensional k_{AK} -frame is formed with the relative spaces of a pair of planes, each endowed with a pair of Cartesian coordinates, as in Fig. 7a. (The diagrams in the figure illustrate an experiment to be described later on.) The A-body of the binate frame is the three-dimensional relative space of the plane with the (x_A, y_A) coordinates, and similarly for the K-body, it is the relative space of the plane that carries the (x_K, y_K) coordinates. When at rest in each other's relative space, the planes are at right angle; thus $y_A \perp y_K$, and both x_A and x_K are normal to the $y_A y_K$ -plane (in the Euclidean sense).

For the two bodies to form a binate frame, they should slide freely, without changing their space orientation, on a track represented by the $x_A x_K$ -line. Then their relative motion should be calibrated to k_{AK} using light signals sent along the $x_A x_K$ -line, as in Sec. 2.2. An event is labeled with the coordinates of the coincidence of places from the two relative spaces. For example, \mathcal{D} in Fig. 7b denotes the event with coordinates

$(dx_A, dx_{\mathfrak{K}}, dy_A, dy_{\mathfrak{K}})$ that happened at a place near O_A on the A-body, and at a place near $O_{\mathfrak{K}}$ on the \mathfrak{K} -body. As illustrated, the two places coincide at \mathcal{D} , and thus

$$\overline{O_A O_{\mathfrak{K}}} = (-dx_A - dx_{\mathfrak{K}})|_{\mathcal{D}}.$$

Say a light signal is emitted at \mathcal{O} , just as O_A meets $O_{\mathfrak{K}}$, and is detected at a near event \mathcal{D} . The lines $O_A \mathcal{D}$ and $O_{\mathfrak{K}} \mathcal{D}$ drawn in Fig. 7b are the traces of the light ray as it propagates through the relative spaces of the reference planes. The trace through the A-body is not in the $x_A y_A$ -plane, but we could jointly rotate the reference planes around the $x_A x_{\mathfrak{K}}$ -line and bring this trace in the rotated $x_{\bar{A}} y_{\bar{A}}$ -plane. After the rotation, the new coordinates of the detection event \mathcal{D} are $(dx_{\bar{A}}, dx_{\bar{\mathfrak{K}}}, dy_{\bar{A}}, 0)$. These meet (3.2) and thus we have $\left(\frac{2k_{A\mathfrak{K}}}{1-k_{A\mathfrak{K}}^2}\right)^2 \left(dx_{\bar{A}}^2 + \frac{1+k_{A\mathfrak{K}}^2}{k_{A\mathfrak{K}}} dx_{\bar{A}} dx_{\bar{\mathfrak{K}}} + dx_{\bar{\mathfrak{K}}}^2\right) - dy_{\bar{A}}^2 = 0$. The planes are now rotated back, so as to return them to the original set-up. Since $dy_{\bar{A}}^2 = dy_A^2 + dy_{\mathfrak{K}}^2$ is the event's distance to the $x_A x_{\mathfrak{K}}$ -line, substitution in the above equation yields:

$$\left(\frac{2k_{A\mathfrak{K}}}{1-k_{A\mathfrak{K}}^2}\right)^2 \left(dx_A^2 + \frac{1+k_{A\mathfrak{K}}^2}{k_{A\mathfrak{K}}} dx_A dx_{\mathfrak{K}} + dx_{\mathfrak{K}}^2\right) - dy_A^2 - dy_{\mathfrak{K}}^2 = 0. \quad (4.1)$$

From similar considerations applied to the separation (3.13) between near events along the path of a particle:

$$ds^2 = \left(\frac{2k_{A\mathfrak{K}}}{1-k_{A\mathfrak{K}}^2}\right)^2 \left(dx_A^2 + \frac{1+k_{A\mathfrak{K}}^2}{k_{A\mathfrak{K}}} dx_A dx_{\mathfrak{K}} + dx_{\mathfrak{K}}^2\right) - dy_A^2 - dy_{\mathfrak{K}}^2. \quad (4.2)$$

With (4.1) and (4.2) added to the tools already introduced in the earlier sections, we can now analyze the counterparts in this world of situations that were previously set in worlds of lower dimensionality. For example, in appendix B4 we analyzed the Sagnac effect in a two-dimensional set-up where the mirrors rotated in the $x_A y_A$ -plane of a $k_{A\mathfrak{K}}$ -frame. The three-dimensional counterpart has the mirrors rotating in the $y_A y_{\mathfrak{K}}$ -plane. Our analysis in appendix C1 is nevertheless like that of appendix B4 and leads, as expected, to the same prediction for the magnitude of the effect.

4.1 Electrodynamics

The mechanics of motion and propagation needs also an understanding of the phenomena and experiments involving electromagnetic fields. By their very nature, these fields are four-dimensional and the equations involved are covariant: the potential A^μ (in the Lorenz gauge condition $\partial_\mu A^\mu = 0$) is related to the current j^μ via the D'Alembertian:

$\partial_\mu \partial^\mu A^\sigma = 4\pi j^\sigma$ [24]. In a $k_{\text{A}\text{N}}$ -frame, $z^\mu \equiv (x_{\text{A}}, x_{\text{N}}, y_{\text{A}}, y_{\text{N}})$, the relation between the potential-components and the corresponding current-components becomes:

$$-\frac{\partial^2 A^\mu}{\partial x_{\text{A}}^2} + \left(\frac{1 + k_{\text{A}\text{N}}^2}{k_{\text{A}\text{N}}} \right) \frac{\partial^2 A^\mu}{\partial x_{\text{A}} \partial x_{\text{N}}} - \frac{\partial^2 A^\mu}{\partial x_{\text{N}}^2} - \frac{\partial^2 A^\mu}{\partial y_{\text{A}}^2} - \frac{\partial^2 A^\mu}{\partial y_{\text{N}}^2} = 4\pi j^\mu. \quad (4.3)$$

The homogenous D'Alembertian is the wave equation of the $k_{\text{A}\text{N}}$ -frame.

Calculations are similar to those used with the familiar spacetime approach, but the decomposition of the four-potential into a scalar potential and a three-vector potential is not meaningful in a binate frame. Appendix C2 presents the electromagnetic field of a plane wave, and appendix C3, the Liénard-Wiechert potential of a charged particle in uniform motion.

4.2 Dynamics of a charged particle in a given electromagnetic field

It is well appreciated that when the equations of motion of charged particles and the equations of the fields that they produce have to be simultaneously solved, calculations are most difficult. (See, for example, Schild's analysis [25] of the interaction between two charged particles in circular motion.) In contrast, finding the motion of a charged particle in a given electromagnetic field involves no more than solving Hamilton's equations. These obtain from an energy equation [16] whereby the potential A^μ acts continuously on the charged particle like an impulse of intensity A_μ per unit charge. Thus the *reduced* momentum of the charged particle, $(p_\mu - qA_\mu)$, participates in the energy equation like the momentum of the free particle presented in Sec. 2.5:

$$\frac{1}{2m} \left[(p_\mu - qA_\mu)(p^\mu - qA^\mu) - \mathbf{p}_0^2 \right] = 0. \quad (4.4)$$

Here, $\mathbf{p}_0 = \sqrt{p_\mu p^\mu} \Big|_{\zeta=0}$ is the particle's momentum as it enters the field and ζ is the path parameter of Hamilton's equations derived from the specified energy constraint:

$$mz'^\mu = p^\mu - qA^\mu \quad \text{and} \quad mp'_\mu = q(p_\nu - qA_\nu) \partial_\mu A^\nu. \quad (4.5)$$

The equations lead to $p'_\mu = mz''_\mu + qz'^\nu \partial_\nu A_\mu$, but also to $p'_\mu = qz'^\nu \partial_\mu A_\nu$. Equating the two expressions for p'_μ produces the differential equations for the coordinates:

$$mz''^\mu = qF^\mu{}_\nu z'^\nu, \quad (4.6)$$

where $F_{\mu\nu} \equiv \partial_\mu A_\nu - \partial_\nu A_\mu$ is the electromagnetic field tensor of the given potential and $F^\mu{}_\nu \equiv \eta^{\mu\sigma} F_{\sigma\nu}$ in a $k_{\text{A}\text{N}}$ -frame obtains with $\eta^{\mu\sigma}$ of (3.19).

Evidently, (4.6) is the binate-frame counterpart of the *Minkowski equation* [26] of a charged particle that is acted upon by the Lorentz force of an electromagnetic field. The distinction is that the derivatives in (4.6) are with respect to the path parameter ζ of Hamilton's equations rather than the relativistic 'proper time.'

The examples next show the calculations involved in finding the motion of a charged particle in a given field that is uniform and unchanged at all events.

Charged particle in an electric field: Consider a charged particle that enters an electromagnetic field with one pair of non-null 'electric' components $F_{12} = -F_{21} = E$ in the frame $x^\alpha = (ct_A, x_A, y_A, z_A)$ of some observer's lab. At and near the entry event, the lab and the relative space of the particle form a $k_{\text{A}\text{N}}$ -frame. Say the field is uniform over the $y_A y_{\text{N}}$ -plane of this binate frame and when O_{N} meets O_A , the particle located at O_A enters the field carrying a charge q . Thus the particle comes to the field with only one non-null coordinate: $x_{\text{N}} = -\frac{1-k_{\text{A}\text{N}}^2}{2k_{\text{A}\text{N}}}s$ from its previous motion. The relevant physical space is one-dimensional and two coordinates, $z^\mu = (x_A, x_{\text{N}})$, suffice for the analysis.

For the observer in the lab, the relevant coordinates of an event are $x^\alpha = (ct_A, x_A)$, where as shown in Sec. 2.6, we have $cdt_A = -\frac{1+k_{\text{A}\text{N}}^2}{1-k_{\text{A}\text{N}}^2}dx_A - \frac{2k_{\text{A}\text{N}}}{1-k_{\text{A}\text{N}}^2}dx_{\text{N}}$. The potential $A_\alpha = [-\frac{1}{2}Ex_A, \frac{1}{2}Ect_A]$ generates the above-mentioned field: $F_{\alpha\beta} = \begin{bmatrix} 0 & E \\ -E & 0 \end{bmatrix}$. This then converts to $A_\mu \equiv \frac{\partial x^\alpha}{\partial z^\mu} A_\alpha = \frac{2k_{\text{A}\text{N}}}{1-k_{\text{A}\text{N}}^2}[-\frac{1}{2}Ex_{\text{N}}, \frac{1}{2}Ex_A]$ and thus $F_{\mu\nu} = \frac{2k_{\text{A}\text{N}}}{1-k_{\text{A}\text{N}}^2} \begin{bmatrix} 0 & E \\ -E & 0 \end{bmatrix}$ is the field in the $k_{\text{A}\text{N}}$ -frame.

From (4.6), we get: $x_A'' = \left(-\frac{1+k_{\text{A}\text{N}}^2}{2k_{\text{A}\text{N}}}x_A' - x_{\text{N}}'\right)\bar{q}\bar{E}$ and $x_{\text{N}}'' = \left(x_A' + \frac{1+k_{\text{A}\text{N}}^2}{2k_{\text{A}\text{N}}}x_{\text{N}}'\right)\bar{q}\bar{E}$, where \bar{q} is the charge per unit mass; $\bar{E} = \frac{2k_{\text{A}\text{N}}}{1-k_{\text{A}\text{N}}^2}E$ is the effective field intensity; and the derivatives are all with respect to ζ , the parameter of Hamilton's equations. We get the following parametric description of the particle's motion:

$$\begin{cases} \frac{x_A}{\lambda} = \frac{\exp(s/\lambda) + \exp(-s/\lambda)}{2} - 1 \\ \frac{x_{\text{N}}}{\lambda} = -\left(\frac{\exp(s/\lambda) + k_{\text{A}\text{N}}^2 \exp(-s/\lambda)}{2k_{\text{A}\text{N}}} - \frac{1+k_{\text{A}\text{N}}^2}{2k_{\text{A}\text{N}}}\right) \end{cases}, \quad (4.7)$$

where $\lambda \equiv \frac{\mathbf{p}_0}{qE}$ is a characteristic length and $s = (\mathbf{p}_0/m)\zeta$ is the finite separation along the particle's path, from the initial event, $s = 0$, when the particle entered the field, to the current event.

The hyperbolic nature the motion would tend to indicate that the curvature of the particle's path is constant. Indeed, we get $\ddot{z}_\mu \dot{z}^\mu = -(qE/\mathbf{p}_0)^2$.

The covariant components of the particle's momentum obtain from the first set of Hamilton's equations (4.5): $p_\mu = m\dot{z}'_\mu + qA_\mu$. Calculations show that $p_\mu A^\mu = 0$ and thus $p_\mu p^\mu - \mathbf{p}_0^2 = -q^2 A_\mu A^\mu = \frac{1}{2}[\cosh(s/\lambda) - 1]$, a positive value regardless of the sign of qE . The momentum p_μ is often labelled 'canonical' (or 'generalized', as we call it) and in the case considered here, it differs from the relativistic (kinetic) momentum: $mc\dot{z}^\mu$. The latter corresponds to the reduced momentum $p_\mu - qA_\mu$, whose magnitude is constant though the two components eventually grow exponential, and have opposite signs.

Charged particle in a magnetic field: Classical considerations of the dynamics of a charged particle entering a constant magnetic field normal to the particle's velocity show that the path of the particle in the plane normal to the field becomes circular. To explore the differences, if any, between this dynamics and that of a particle constrained by a circular track, we first note that an energy equation of the form:

$$\frac{1}{2m}[(p_\mu - \lambda f_\mu)(p^\mu - \lambda f^\mu) - \mathbf{p}_0^2] = 0, \quad (4.8)$$

where λf_μ is an *impulse* vector, generates the uniform circular motion of Sec. 2.3 when $f_\mu = [y_A \quad 0 \quad -x_A \quad 0]$ and $\lambda = \frac{1 - k_{A\aleph}^2}{2k_{A\aleph}} \frac{\mathbf{p}_0}{2\rho}$. Note that the multipliers λ of (4.8) and λ of (3.21) are defined by their respective equation, and thus need not be equal. Indeed, we have: $\sqrt{m\lambda}_{(3.21)} = \lambda_{(4.8)}$.

The so obtained momentum vector is not the same as that of (3.24) because (4.8) produces the canonical rather than the usual momentum of classical mechanics: p_μ here is larger than p_μ of (3.24) by the impulse vector λf_μ .

A $k_{A\aleph}$ -frame, $z^\mu = (x_A, x_\aleph, y_A, y_\aleph)$, is adapted to the situation when, on one hand, the charged particle enters the field while carried by the \aleph -plane and, on the other hand, the field's potential, $A_\mu = \frac{1}{2}B[y_A \quad 0 \quad -x_A \quad 0]$, has non-null components only in the A-plane. In the frame $x^\alpha = (ct_A, x_A, y_A, z_A)$ of an observer at O_A , the potential generates a 'magnetic' field since its only non-null components are: $F_{32} = -F_{23} = B$.

We note that qA_μ of (4.4) equals λf_μ of (4.8) only when $\lambda = qB/2$. Equating the two expressions obtained for λ of (4.8) yields: $\rho = \frac{2k_{A\aleph}}{1 - k_{A\aleph}^2} \frac{\mathbf{p}_0}{qB}$, which is the predicted radius of the particle's path.

Classical mechanics shows that a particle of mass m and charge q that enters the magnetic field of the potential A_α with a speed v along the x_A -axis acquires a uniform circular motion of radius $\rho = \frac{mv}{qB}$ in the $x_A y_A$ -plane normal to the field. The charged particle is viewed by Special Relativity as having the speed $v = \beta_{A\aleph} c$ with respect to the observer at O_A . We then have $\beta_{A\aleph} = \frac{1 - k_{A\aleph}^2}{1 + k_{A\aleph}^2}$, from (2.1), and $\gamma_{A\aleph} = \frac{1 + k_{A\aleph}^2}{2k_{A\aleph}}$. In these terms, our result reads $\rho = \beta_{A\aleph} \gamma_{A\aleph} \left(\frac{\mathbf{p}_0}{qB} \right)$ whereas the Special Relativity prediction is $\rho = \beta_{A\aleph} \gamma_{A\aleph} \left(\frac{mc}{qB} \right)$. But we observed in Sec. 2.5 that $\sqrt{p_\mu p^\mu} = mc$ could be used for comparison purposes, and since mc is the relativistic magnitude of the momentum of the free particle as measured in its own frame prior to entering the field, the prediction here is the same as that obtained from the observer-frame approach of Special Relativity.

4.3 Foliation

In Sec. 4.1, we considered from a geometric perspective the set of coincidences of places from the relative spaces of two bodies in relative motion, without rotation. We concluded that (4.2) shows this set to have the structure of a four-dimensional manifold with the line element: $ds^2 = \eta_{\mu\nu} dz^\mu dz^\nu$, where $dz^\mu = (dx_A, dx_\aleph, dy_A, dy_\aleph)$ and $\eta_{\mu\nu}$ are the coefficients of the differentials in (4.2). The metric tensor $\eta_{\mu\nu}$ has the $(+, -, -, -)$ Lorentz signature.

The line element (4.2) is typical of a 2+2 foliation of the manifold of events. It identifies a two-parameter family of spacelike $y_A y_\aleph$ -planes, with a Euclidean metric in its canonical form, and a two-parameter family of timelike $x_A x_\aleph$ -planes, with a Lorentz metric in non-diagonal form. The two families of planes are $\eta_{\mu\nu}$ -orthogonal.

As far as we know, 2+2 foliations have not been used in Special Relativity, which is based on the 1+3 foliation realized by an observer frame. But in General Relativity, it is not unusual to split the spacetime into other than a family of spacelike hyper-surfaces and a congruence of timelike curves [27-28]. In terms familiar with such other splittings [29], we would describe as follows the character of the foliation realized with a binate frame: First, an initial 2D sub-manifold is given, for example, the plane of the y_A - and y_\aleph -axes illustrated in Fig. 7. This plane is then dragged in opposite directions by two timelike vectors, the arrowed segments along the x_A - and x_\aleph -axes. This dragging yields two 3D-hypersurfaces. These are the relative 3D spaces of the A - and \aleph -planes that form the $k_{A\aleph}$ -frame of Fig. 7. In simpler terms, the neighborhood of a considered event has a natural 2+2 foliation provided by the intersection of the physical spaces of any two material bodies whose relative motion is relevant to the situation under scrutiny.

The double timelike foliation affected so naturally by the binate frame is not usually considered among the three most important ones [29], yet it is the only one that yields a 2+2 physically meaningful splitting of the manifold of events and provides all the material support needed for measuring the coordinates of events without invoking conceptual elements foreign to the considered physical circumstances, such as a clock-synchronization procedure. We found no mention in prior publications of a reference system with similar attributes.

5 Conclusion: *observer-frame* or *binate-frame*, which is more valuable?

In this paper we introduced a new type of reference system and illustrated its usefulness by undertaking analyses of physical phenomena and experimental situations that require the joint consideration of motion and propagation. At appropriate points throughout the presentation, we compared our approach, which uses a binate-frame parameterization of events, with the spacetime approach of Special Relativity, which uses an observer-frame parameterization. But these comparisons were selective and topical. We would like to conclude the presentation with a much more structured comparison.

In what follows, we were guided by Hertz' "standpoints from which we must estimate the value of physical theories and the value of representations of physical theories" [30]. We understand that no comparison between one's own approach and the more established alternative could ever be unbiased. But by adopting the strict terms under which Hertz conducted his own examination of the "various representation of the principles of mechanics" we hope to convince the reader of our sincere desire to be highly objective in our assessment.

Hertz writes about the nature of things and our conceptual images of these. As he sees it, the conceptual elements, the images of our thoughts, should as a minimum satisfy the fundamental requirement that "the necessary consequences of the images in thought are always the images of the necessary consequences in nature of the things pictured." On these grounds, the binate-frame and the observer-frame approaches rate fairly equal since they both emerge from the same theoretical relations typical of a semi-Riemannian, flat four-dimensional manifold with a metric of Lorentz signature. As such, they are both capable of capturing in geometric terms the essence of physical phenomena.

Hertz distinguishes between permissible and inadmissible concepts — only the former, not the latter, are free from internal logical contradictions. Of the permissible concepts, those whose logical consequences are contradicted by experiments are clearly incorrect, and Hertz labels them as such. The logical consequences of the observer-frame coordinatization have been explored for more than a century already, and none so far has been contradicted by experiments. Since a change of parameterization cannot change any theoretical prediction, the binate-frame approach is just as unlikely to be refuted by some new experimental results as Special Relativity itself. We have to conclude that both the binate-frame and the observer-frame approaches involve only permissible concepts and are free from any internal contradictions.

Not all permissible and correct concepts are equally appropriate. Hertz chooses two characteristics by which to judge the various degrees of appropriateness: He writes "Of two images of the same object that is more appropriate which pictures more of the

essential relations of the object.” Thus a concept that enables us to understand more of the reality is characterized as more appropriate in the sense that it is more “distinct,” to use Hertz’ term. He also writes, “Of two images of equal distinctiveness the more appropriate is the one which contains ... the smaller number of superfluous or empty relations.” Thus a concept that requires (or leads to) fewer unnecessary relations is more appropriate in the sense that it is “simpler,” again, to use Hertz’ term.

In respect to distinctiveness, the binate-frame and the observer-frame approaches cannot show any difference since they are parameterizations of the same theory. But in respect to simplicity, the binate-frame approach is definitely superior. To wit: The observer-frame approach introduces a time-coordinate, and thus requires a procedure for the synchronization of distant clocks. (It is immaterial here whether the stipulated logico-physical constraints imposed on such a procedure makes it unique or not.) In turn, the time-coordinate imposes a total ordering between events. But between some events, this ordering is unphysical since changing the frame of reference could reverse it. At least between such events, a temporal ordering relation is superfluous. A binate-frame does not need a time-coordinate, and thus has no notion of distant simultaneity. The only ordering of events envisaged to exist in a binate frame is for the sequence of events along a ray of light or along the path of a particle. Such ordering is invariant under any and all changes of parameterization.

Logic alone determines whether a concept is permissible or not, and clearly such characterization can be made without ambiguity, once for all. But whether a concept is correct or not we could determine “only according to the state of our present experience, and permitting an appeal to later and riper experience,” as Hertz put it. Here again, the binate-frame approach seems superior. To wit: All the observed phenomena and all the experimental data so far recognize the essential symmetry between two inertial frames. As implemented here, this symmetry is direct and immediate — it is the symmetry of the binate-frame coordinates. In contrast, observer-frame considerations break this symmetry by viewing one of the frames in such a pair as ‘stationary,’ the other one as ‘moving’. Symmetry is restored as a matter of principle only, by asserting that the roles assigned to the two frames could be freely interchanged. But the modeling of the physical situation remains asymmetric. This ‘restoration principle’ thus refers only to the logical symmetry between two views of the same pair of frames; it does not respect the inherent physical symmetry between two inertial frames. Since all calculations based on observer-frame considerations, unlike those using a binate-frame, employ a model of paired inertial frames that is asymmetric and thus unphysical, the binate-frame seems superior. (This assessment would have to be reversed if ever an ‘absolute’ frame is found, since this would then expose a break of symmetry between inertial frames that is indeed physical rather than just arbitrarily assigned for the mathematical representation.)

The question of ‘appropriateness’ of a concept is recognized by Hertz as being a matter of what is contained in the “notations, definitions, abbreviations, and, in short, all that we can arbitrarily add or take away.” Appropriateness is clearly not unambiguously decidable. Support for one or another representation of a theory tends to go up and down over time, and furthermore “... the history of science is full of cases of resistance to equivalent formulations of well-known theories in a different geometric language (such as Lagrange’s use of generalized coordinates, or the vectorial formulation of Maxwell’s equations), some of which are hard to understand for any present-day scientist, while

other still linger on.” [31] Observer-frame concepts have clear advantage in this respect because they have been around for a long time and so their ‘appropriateness’ is taken for granted. In fact, the spacetime concept is so prevalent today that most physicists would actually “consider a theory to be fundamental only if it does make explicit use of this concept.” [32] But still, it should be of interest to understand what new or changed notions and interpretations emerge when instead of the usual 1+3 foliation of an observer frame, one uses the 2+2 foliation of a binate frame. That such a change of approach brings with it a substantial change of paradigm is evident from the entire presentation: we obtained a metric with Lorentz signature from considerations based on qualitative rather than quantitative aspects of light propagation; discussed relativistic kinematics without a notion of simultaneity of distant events; used no frame-dependent concepts; and applied the Hamiltonian dynamics in the (z^μ, p_μ) phase space without the four-vector p^μ being interpreted as having one ‘energy’ component and three ‘momentum’ components. Yet we always obtained the expected relativistic results. This would tend to indicate that the notions appropriate for the binate-frame approach have a high degree of merit, worthy of further research and exploration.

A Relativistic phenomena: one physical-space dimension

A1 Longitudinal optical Doppler effect

The optical Doppler effect refers to the observed difference between the wavelength of an emitted and received light signal when the source and the detector are in relative motion. For predicting the magnitude of the effect, we analyze a set-up whereby the emitter and the detector are placed on opposite rulers of the $k_{A\aleph}$ -frame in Fig. A1. The emitter is on the \aleph -ruler, at O_\aleph ; it sends a first light signal when it meets O_A , and a second one when it encounters a trigger placed at $x_A = -\lambda_e < 0$ on the A-ruler. The detector is located on the A-ruler, at $x_A = -L$; it puts a mark on the \aleph -ruler whenever it detects a light signal. In the illustrated set-up, the emitter and the detector approach each other.

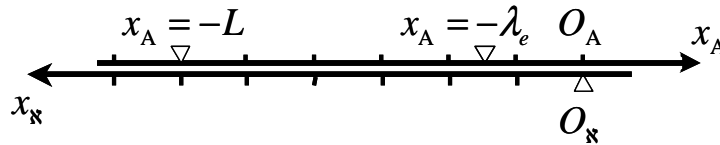


Fig. A1 The experimental set-up.

As specified, the coordinates of the two emission events are $(0,0)$ at \mathcal{E}_1 and $(-\lambda_e, 0)$ at \mathcal{E}_2 . Say \mathcal{D}_1 and \mathcal{D}_2 , respectively, are the events that detect the emitted signals. Each of these detections marks the place where it occurred on the \aleph -ruler. From (2.2), since the light signal is detected along $x_\aleph > 0$, we get $x_\aleph(\mathcal{D}_1) = k_{A\aleph}L$ and $x_\aleph(\mathcal{D}_2) = k_{A\aleph}(L - \lambda_e)$. The distance between these marks, $\lambda_d = x_\aleph(\mathcal{D}_1) - x_\aleph(\mathcal{D}_2) > 0$, obtains as $\lambda_d = k_{A\aleph}\lambda_e < \lambda_e$.

The relativistic ratio between the emitted and detected wavelengths of a light signal is known to be $\lambda_d/\lambda_e = \sqrt{(1-\beta_{\text{A}\text{N}})/(1+\beta_{\text{A}\text{N}})} < 1$, where $\beta_{\text{A}\text{N}}$ is the relative speed between the emitter and the detector, in light-speed units. The relativistic prediction and ours reflect the same physical reality since $k_{\text{A}\text{N}} = \sqrt{(1-\beta_{\text{A}\text{N}})/(1+\beta_{\text{A}\text{N}})}$, from (2.1).

A2 Lorentz-Fitzgerald contraction

An experiment with two rods moving in opposite directions, symmetric with respect to an observer, was envisaged by Einstein to show that no synchronized clocks are necessary to measure the Lorentz-Fitzgerald contraction [18]. That clocks are also not needed even to explain this contraction does not yet seem to have been noticed. We analyze this effect and predict its magnitude without using any clocks since the binate-frame approach needs no notion of distant simultaneity.

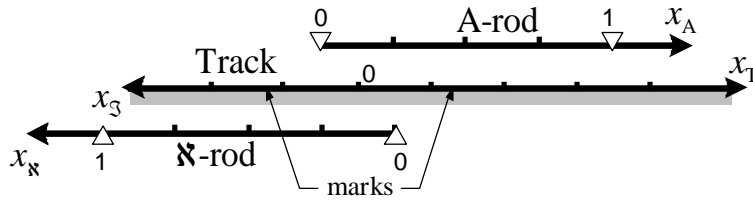


Fig. A2 Set-up of the experiment: the A-rod is between the illustrated sensors at $x_A = 0$ and $x_A = 1$; the \mathfrak{N} -rod is between $x_{\mathfrak{N}} = 0$ and $x_{\mathfrak{N}} = 1$.

Consider the set-up illustrated in Fig. A2. The distance between the two ends of each rod, when at rest on the track, is set to one unit length. The two rods are sent sliding freely on the track, from the opposite sides of it and towards each other. The motion of each rod is calibrated the same way with respect to the track: $k_{\text{A}\mathfrak{S}} = k_{\text{T}\mathfrak{N}} = k$. The rods are thus also calibrated with respect to each other, and from (2.3): $k_{\text{A}\mathfrak{N}} = k_{\text{A}\mathfrak{S}}k_{\text{T}\mathfrak{N}} = k^2$.

In their motion, the sensors at the ends of the rods pass by each other and mark the track. The two marks of our interest are those when the 0-end of one rod meets the 1-end of the other rod: say \mathcal{P} is the event with coordinates (0,1) and \mathcal{Z} is the one with coordinates (1,0). As discussed in Sec. 2.2, an event in a system of three rulers could be identified with any one of three pairs of coordinates: $(x_A, x_{\mathfrak{S}} = -x_T)$, or $(x_T = -x_{\mathfrak{S}}, x_{\mathfrak{K}})$, or $(x_A, x_{\mathfrak{K}})$. The three coordinates involved: x_A , $x_T = -x_{\mathfrak{S}}$, and $x_{\mathfrak{K}}$ are related through the integral form of the linear relation (2.4). Substituting the x_A - and $x_{\mathfrak{K}}$ -coordinates of \mathcal{P} and \mathcal{Z} in (2.4) yields the coordinates of the marks left on the track at the sensed events: $x_{\mathfrak{S}}(\mathcal{P})$ and $x_{\mathfrak{S}}(\mathcal{Z})$. From these, we get the predicted distance between the marks:

$$L = x_{\mathfrak{I}}(\mathcal{P}) - x_{\mathfrak{I}}(\mathcal{Z}) = \frac{2k_{\mathbb{A}\mathfrak{K}}}{1 + k_{\mathbb{A}\mathfrak{K}}} < 1.$$

Special Relativity's prediction for the relativistic contraction for rods of unit rest-length is $L = \gamma_{\text{A}\text{N}}^{-1}$, where $\gamma_{\text{A}\text{N}} = 1/\sqrt{1 - \beta_{\text{A}\text{N}}^2}$ and $\beta_{\text{A}\text{N}}$ denotes the (fractional) speed of each rod relative to the track. Since $k_{\text{A}\text{N}} = \sqrt{(1 - \beta_{\text{A}\text{N}})/(1 + \beta_{\text{A}\text{N}})}$ from (2.1), and thus $\frac{2k_{\text{A}\text{N}}}{1 + k_{\text{A}\text{N}}^2} = \sqrt{1 - \beta_{\text{A}\text{N}}^2}$, the prediction of Special Relativity is the same as ours.

A3 The decay of cosmic-ray mesons

It has been observed that only a fraction of the cosmic-ray mesons that enter the earth atmosphere survive to reach the ground. This is to be expected since experiments with mesons captured in a specialized detector show they decay over time. Since the decay is random, the classically formulated prediction is that $N = N_0 \exp(-t/T)$, where N_0 is the number of mesons at the start of some time interval of duration t and N is the number of mesons that survived at the end of this interval. Here, T is the experimentally determined remaining *average lifetime* (the constant of best exponential fit to the experimental curve) of the meson after its capture. However, when the duration t of the mesons flight through the atmosphere is calculated from the ratio of their traveled distance to their speed, as in classical mechanics, the predicted fraction of the surviving mesons is much smaller than the one observed.

In the above presentation of the observed phenomena, the rate of decay for the captured mesons is in terms of 'time interval' and 'duration.' These are observer-frame dependent notions. Instead, we use here $N = N_0 \exp(-s_c/S)$ where s_c is the separation along the path of a captured meson, from the initial event \mathcal{O} , when the N_0 count is taken, and until a current event \mathcal{E} , when the count N is taken; S is the *average lifespan* of the captured meson, that is, the constant of best fit to the experimentally determined curve that correlates N with s_c and N_0 . Since the above relation is in invariant terms (counts and separations), it is valid in all frames.

In what follows, we first model the physical situation using three binate frames. Then we show how the above exponential relation arises from experiments with captured mesons. Subsequently, we use this relation to explain the observed decay of mesons in flight. Finally, we compare our predictions with the recorded observations of the reported experiments that involve cosmic-ray mesons.

The model: Cosmic ray mesons are generated and freely fly toward the earth. As they pass by a detector located at the top of a mountain, some mesons are captured while others are allowed to continue in flight until they are detected at sea level. The relevant motion is between the captured mesons and those allowed to continue their flight.

We view the relative spaces of these mesons as the rulers of the $k_{\text{A}\text{N}}$ -frame. (The assumption is that the relative motion is uniform; other assumptions are possible, but unnecessary.) When rotated 90° clockwise, Fig. 3 of Sec. 2.2 illustrates the envisaged situation. The relative space of the free meson is the A-ruler, whose x_{A} -axis is toward the bottom of the mountain. The relative space of the captured meson is the N -ruler,

whose $x_{\mathbb{N}}$ -axis is pointing upward toward the sky. Each meson sits at the origin of the x -coordinate of its respective relative space.

To record the capture of mesons, as well as all subsequent events that happen at the top of the mountain, we employ a third ruler whose motion is downward vertical and calibrated to some $k_{\mathbb{T}\mathbb{N}}$ with respect to the mountain. The third ruler has two related x -coordinate: $x_{\mathbb{S}} = -x_{\mathbb{T}}$, as explained in Sec. 2.2, to enable it to form a further binate frame, the $k_{\mathbb{A}\mathbb{S}}$ -frame, with the meson in free flight. From (2.3), we have $k_{\mathbb{A}\mathbb{N}} = k_{\mathbb{A}\mathbb{S}}k_{\mathbb{T}\mathbb{N}}$.

The analysis of the decay of captured mesons: Say a specialized detector located at $O_{\mathbb{N}}$ is used to capture N_0 mesons with energies in a specified range. From our analysis of Sec. 2.3, since the detector with the captured mesons is at $O_{\mathbb{N}}$, the separation between any pair of near events along its path in the $k_{\mathbb{T}\mathbb{N}}$ -frame is $ds = -\frac{2k_{\mathbb{T}\mathbb{N}}}{1-k_{\mathbb{T}\mathbb{N}}^2} dx_{\mathbb{T}}$. Evidently,

this is also the separation along the path of a meson captured and held by the detector. We could thus integrate ds between the capture and decay of this meson.

The detector puts a mark on the third ruler at each meson-capturing event, as well as when it detects that the captured meson has decayed. Then the distance between marks left by the detector on the $x_{\mathbb{T}}$ -axis at such paired events could be used to calculate their

respective finite separations: $s_c = -\frac{2k_{\mathbb{T}\mathbb{N}}}{1-k_{\mathbb{T}\mathbb{N}}^2} (x_{\mathbb{T}}|_{\text{decay}} - x_{\mathbb{T}}|_{\text{capture}})$. Each pair of events, with

their respective separation, provides one count. The counts are added and plotted against their respective separations. The decays being random events, statistical analysis leads to the expectation that the plotted curve is exponential. The constant S of best fit to the curve is what we call here the *average lifespan* of the meson after capture. Hence, the earlier announced formula: $N = N_0 \exp(-s_c/S)$.

The analysis of the decay of the mesons in flight: Our first task is to show how the value of $k_{\mathbb{A}\mathbb{N}}$ that characterizes the motion of these mesons relative to the mountain could be found. For this, we use the relation (2.4) between the coordinates of an event that is recorded on three rules in relative motion. We place a second detector on the mountain, at $x_{\mathbb{N}} = -L$, a short distance from its top. The detector puts a mark on the $x_{\mathbb{T}}$ -axis when it detects a passing meson. Say for some meson in free flight, the mark is at $x_{\mathbb{T}} = \bar{L}$. Since

$x_{\mathbb{A}} = 0$ at this meson, the integral form of (2.4) yields: $\frac{\bar{L}}{k_{\mathbb{A}\mathbb{S}}^{-1} - k_{\mathbb{A}\mathbb{S}}} = \frac{L}{k_{\mathbb{A}\mathbb{N}}^{-1} - k_{\mathbb{A}\mathbb{N}}}$. With

$k_{\mathbb{A}\mathbb{N}} = k_{\mathbb{A}\mathbb{S}}k_{\mathbb{T}\mathbb{N}}$, from (2.3), we get $k_{\mathbb{A}\mathbb{N}} = \sqrt{\frac{k_{\mathbb{T}\mathbb{N}}L - \bar{L}}{k_{\mathbb{T}\mathbb{N}}^{-1}L - \bar{L}}}$ for this meson, since $k_{\mathbb{T}\mathbb{N}}$ is known

from the calibration of the third ruler.

Next, we calculate the separation s_f between the two relevant events along the path of the flying meson. These are (i) the event when the meson is counted at the top of the mountain, and (ii) the event when it is captured at the bottom of the mountain. Since

$x_{\text{K}} = 0$ at the top of the mountain and $x_{\text{K}} = -H$ at the bottom: $s_f = \frac{2k_{\text{AK}}}{1-k_{\text{AK}}^2} H$. Now the

prediction is that only a fraction of mesons, $N/N_0 = \exp(-s_f/S)$, survives the flight.

As defined here, S is an attribute of the meson, independent of the path of its motion between the counted events, N_0 and N . Then the value of S determined for the captured mesons could be used also for the mesons continuing their flight.

Comparing our prediction with recorded observations: For the comparison, we use the experimental data available from the investigation of Frisch and Smith [33], as presented by French [34]. Table 4-1 in [34] shows the number of mesons that survived a selected interval of time after their capture. The tabulated data exhibits an exponential dependency, with $T = 2.175 \mu\text{sec}$ as the constant of best fit. Conversion from T to the separation $S = cT$ between the capture and decay events yields $S \cong 650 \text{ m}$.

The described experiment measured the decay time of 568 mesons captured at the top of the mountain. These were mesons with speeds in the range $0.9950 < \beta_{\text{TK}} < 0.9954$, which we convert to $0.05 > k_{\text{TK}} > 0.048$ using (2.1). Within this k_{AK} -range, and for the mountain-height $H = 2 \text{ km}$, we get a separation-range for the free meson of about $210 \text{ m} > s_f > 190 \text{ m}$.

Everything is now in place for calculating the survival fraction of mesons. We find that $N/N_0 = \exp(-s_f/S)$ has a range of between 0.725 and 0.747. This yields the prediction that from the 568 mesons counted at mountaintop, only 410 to 425 would survive at sea level, well within the range of the experimentally recorded data.

It is perhaps of no small importance that the analysis in the binate frame requires none of the familiar explanations based on ‘time dilation’ and ‘length contraction’ [34].

A4 Fully inelastic collisions

Consider two free particles in relative motion, heading towards a fully inelastic collision. Eventually, the particles collide and coalesce into another free particle. Our model of the initial situation, just prior to the collision, consists of two particles located respectively at O_A and O_K , the origins of the coordinates of the rulers that form the k_{AK} -frame in Fig. 2. The analysis obtains the relation between the momentum of the coalesced particle, \hat{p}_μ , and the initial momentum of the colliding particles: \bar{p}_μ and $\bar{\bar{p}}_\mu$, respectively.

Prior to the collision event, the particles are free from external influences and thus according to Sec. 2.5:

$$\bar{p}_\mu = \left[-\frac{1+k_{\text{AK}}^2}{1-k_{\text{AK}}^2} \bar{\mathbf{p}} \quad -\frac{2k_{\text{AK}}}{1-k_{\text{AK}}^2} \bar{\mathbf{p}} \right], \quad \bar{\bar{p}}_\mu = \left[-\frac{2k_{\text{AK}}}{1-k_{\text{AK}}^2} \bar{\bar{\mathbf{p}}} \quad -\frac{1+k_{\text{AK}}^2}{1-k_{\text{AK}}^2} \bar{\bar{\mathbf{p}}} \right]. \quad (\text{A4.1})$$

We assume as usual that each momentum component of the coalesced particle is equal to the sum of the respective momentum components of the two colliding particles. Hence, in the specified $k_{\text{A}\text{N}}$ -frame, the momentum-components of the coalesced particle are:

$$\hat{p}_1 = -\frac{1+k_{\text{A}\text{N}}^2}{1-k_{\text{A}\text{N}}^2}\bar{\mathbf{p}} - \frac{2k_{\text{A}\text{N}}}{1-k_{\text{A}\text{N}}^2}\bar{\bar{\mathbf{p}}}, \quad \hat{p}_2 = -\frac{2k_{\text{A}\text{N}}}{1-k_{\text{A}\text{N}}^2}\bar{\mathbf{p}} - \frac{1+k_{\text{A}\text{N}}^2}{1-k_{\text{A}\text{N}}^2}\bar{\bar{\mathbf{p}}}. \quad (\text{A4.2})$$

Substitutions in $\hat{\mathbf{p}}^2 = \eta^{\mu\nu} \hat{p}_\mu \hat{p}_\nu = -\hat{p}_1^2 + \frac{1+k_{\text{A}\text{N}}^2}{k_{\text{A}\text{N}}} \hat{p}_1 \hat{p}_2 - \hat{p}_2^2$ lead to:

$$\hat{\mathbf{p}}^2 = (\bar{\mathbf{p}} + \bar{\bar{\mathbf{p}}})^2 + \left(\sqrt{k_{\text{A}\text{N}}^{-1}} - \sqrt{k_{\text{A}\text{N}}} \right)^2 \bar{\mathbf{p}} \bar{\bar{\mathbf{p}}}. \quad (\text{A4.3})$$

The relation is invariant since the magnitude of a momentum vector is an invariant scalar and $k_{\text{A}\text{N}}$ is an intrinsic measure of the relative motion between the incoming particles.

Note that $\hat{\mathbf{p}} > \bar{\mathbf{p}} + \bar{\bar{\mathbf{p}}}$ and thus the coalesced particle's momentum-magnitude is greater than the sum of the momentum-magnitudes of the colliding particles. A similar analysis would conclude that when a particle disintegrates, the resulting particles have momentum whose magnitudes add to less than the magnitude of the momentum of the disintegrating particle.

To verify the above predictions, we consider experiments that allow the tracking of the coalesced particle's motion. The analysis in Sec. 2.5 shows that the motion of a free particle is determined by $m z'^\mu = p^\mu$. Since $\hat{p}^\mu = \eta^{\mu\nu} \hat{p}_\nu$ is constant, a particle created at the event \mathcal{O} with coordinates (0,0) is expected to attend only events with coordinates

that meet the relation: $\frac{\hat{z}^1}{\hat{z}^2} = \frac{\hat{p}^1}{\hat{p}^2}$. But then we could measure the coordinates of an event

attended by the coalesced particle and calculate from (A4.2) the ratio of the momentum-magnitudes of the incoming particles. Since we are at liberty to assign a unit magnitude to the momentum of any one of the particles, we conclude that (in principle) experiments with colliding particles could be used to find the magnitude of the momentum of any free particle from the assigned unit momentum of some standard free particle.

With $k_{\text{A}\text{N}} = \sqrt{(1-\beta_{\text{A}\text{N}})/(1+\beta_{\text{A}\text{N}})}$, from (2.1), our result matches the relativistic prediction when, as explained in Sec. 2.5, we use $\sqrt{p_\mu p^\mu} = mc$ for the comparison.

A5 *Of moving clocks and light signals*

We envisaged the following experiment to illustrate the simplifications brought about by the binate-frame approach. The physical set-up is typical of situations where classical mechanics cannot be used because light propagates back and forth among moving bodies.

Consider two identical clocks, each placed on a long ruler strapped to a cart. The carts glide on a common track in opposite directions, not necessarily symmetrically with

respect to it. (The track plays no role in the experiment other than guiding the carts with the rulers; thus Fig. 2 rather than Fig. 3 appropriately describes the situation.) The clocks are initialized as they pass by each other, and each is set to emit a light signal toward the other at the same predetermined, symmetrically specified events. The light signals are emitted at the scheduled events and eventually meet. Each signal is then reflected back and detected by the clock that emitted it. The experiment ends after these two detections.

We arrange for a mark to be placed on both rulers at each significant event. Also, we further arrange for each clock to record its time when attending a significant event. These records are the data from the experiment. They are used to verify the predictions derived from two analyses of the envisaged experiment: a relativistic analysis with the observer-frame approach of Special Relativity and one with the binate-frame approach of this paper. A brief comparison of these approaches ends the appendix.

Observer-based approach: For an analysis based on the principles of Special Relativity, we specify the physical set-up in terms of the relative speed β between the two clocks and a scheduled proper time T , when each clock is to emit a light signal. One clock is viewed as ‘stationary’ and its frame, K , is parameterized with (x, t) ; the other clock is viewed as ‘moving’ and its frame, K' , is parameterized with (x', t') . Each clock is placed at the origin of its frame.

The physically significant events are denoted as follows: \mathcal{E}_1 and \mathcal{E}_2 are the events when the clocks in the K - and K' -frames, respectively, emit a light signal; \mathcal{R} is the event when the two signals meet and each is reflected back to its emitting clock; \mathcal{D}_1 and \mathcal{D}_2 are the events when the clocks in the K - and K' -frames each detects the light signal that was reflected back to its source.

The available information is sufficient to obtain from Lorentz transformations the coordinates of the emission events: $(x, t) = (0, T)$ and $(x', t') = (-\gamma\beta cT, \gamma T)$ at \mathcal{E}_1 ; and $(x, t) = (\gamma\beta cT, \gamma T)$ and $(x', t') = (0, T)$ at \mathcal{E}_2 . From the condition that the two signals

meet at the common event \mathcal{R} , we obtain its coordinates: $x = -x' = \left(\sqrt{\frac{1+\beta}{1-\beta}} - 1 \right) \frac{cT}{2}$ and

$t = t' = \left(\sqrt{\frac{1+\beta}{1-\beta}} + 1 \right) \frac{T}{2}$. Then once more from Lorentz transformations, we obtain the

prediction that the two clocks would read the same time when each detects the reflected signal. That is, the proper times on the clocks at the respective detections, \mathcal{D}_1 and \mathcal{D}_2 , are

expected to be the same: $t(\mathcal{D}_1) = t'(\mathcal{D}_2) = \sqrt{\frac{1+\beta}{1-\beta}} T$. These events are predicted to happen

at: $x'(\mathcal{D}_1) = -\frac{\beta cT}{1-\beta}$ in K' , and $x(\mathcal{D}_2) = -\frac{\beta cT}{1-\beta}$ in K . The symmetry of these predictions

is evident — it reflects the symmetry of the specified set-up for the experiment.

So much for calculations — the needed interpretations follow. First, we note that the set-up depends on the synchronicity convention since the speed of the ‘moving’ clock cannot be measured without first synchronizing the clocks of the ‘stationary’ frame. Then calculations based on Lorentz transformations imply the use of Einstein’s procedure for

clock synchronization. Hence, we could expect that some of the predictions might depend on this procedure, while other might not. In contrast, the data to be collected from the experiment does not depend on the stipulated clock synchronization. Also, we expect that when the two clocks detect the reflected signals, they would show the same proper time, since the two-way speed of light is convention-free. But short of running the experiment, or at least trying different synchronization procedures [3], it is not evident which other of the above predictions is free of synchronicity effects.

Binat-frame approach: Instead of employing observer-based frames and the Lorentz transformations, we could use the $k_{A\aleph}$ -frame formed by the rulers of the two clocks in relative motion. For this, we have to specify the physical set-up in term of the value $k_{A\aleph}$ used to calibrate this motion. The clocks, now denoted the A-clock and the \aleph -clock, are at the origin of the coordinates of the respective ruler. Each clock is set to emit a light signal when passing over a symmetrically specified predetermined location on the ruler of the other clock. This could be done with two devices placed at $x_A = -L$ and $x_{\aleph} = -L$, respectively. The devices would emit a light signal when a clock passes over them. The coordinates of the emission events \mathcal{E}_1 and \mathcal{E}_2 would then be $(0, -L)$ and $(-L, 0)$, respectively.

The coordinates (x_A, x_{\aleph}) of the event \mathcal{R} when emitted light signals meet obtain from (2.2): for the signal emitted at \mathcal{E}_1 , we get $k_{A\aleph}(x_A - 0) + (x_{\aleph} + L) = 0$ and for the signal emitted at \mathcal{E}_2 , we get $(x_A + L) + k_{A\aleph}(x_{\aleph} - 0) = 0$. The two relations are met only when $x_A = x_{\aleph} = -L/(1 + k_{A\aleph})$. Thus the coordinates of \mathcal{R} respect the symmetry of the situation.

The coordinates of the detections \mathcal{D}_1 and \mathcal{D}_2 also observe (2.2). That is, we have $\left(0 + \frac{L}{1 + k_{A\aleph}}\right) + k_{A\aleph}\left(x_{\aleph} + \frac{L}{1 + k_{A\aleph}}\right) = 0$ for the reflected signal detected at \mathcal{D}_1 ; this yields $x_{\aleph} = -k_{A\aleph}^{-1}L$. Then we have $k_{A\aleph}\left(x_A + \frac{L}{1 + k_{A\aleph}}\right) + \left(0 + \frac{L}{1 + k_{A\aleph}}\right) = 0$ for the reflected signal detected at \mathcal{D}_2 . It yields $x_A = -k_{A\aleph}^{-1}L$, and the symmetry is once again evident.

All the binat-frame results are free of synchronization effects. Thus we expect all our predictions to fall within the range of experimentally collected data.

The observed correlation between the average lifespan of a meson and the finite separation between the events along its path could be invoked to predict the ‘proper time’ readings of a clock from the separation along its path. But since clocks are not used with the binat-frame approach, we refrain from making any predictions of the times recorded at the significant events by the clocks in the experiment. Nevertheless, we invoke this correlation for comparing the binat-frame predictions with those based on the observer-frame approach. The most interesting aspect of this comparison comes from how the specified parameter T used with the observer-based approach of Special Relativity relates to the specified parameter L of the binat-frame approach.

Comparing the two approaches: With the observer-frame approach, the relation between L and T is not based on classical mechanics. That is, $L \neq vT$ because the

distance L is measured in the frame of the ‘stationary’ clock while the elapsed time T is measured on the ‘moving’ clock: the measurements have to come from the same frame. One gets $L = v(\gamma T)$, as calculated in the frame of the ‘stationary’ clock while accounting for time dilation, or $(\gamma^{-1}L) = vT$, as calculated in the frame of the ‘moving’ clock while accounting for length contraction. Evidently, both lead to the same relation: $L = \beta\gamma cT$.

With the binate-frame approach too, the relation between L and T cannot be based on classical mechanics, but now this is because v cannot be specified since the binate-frame approach has no notion of ‘time’. Instead, we extrapolate to the clocks of the experiment the (already mentioned) correlation between the average lifespan of a meson and the finite separation between the capture and decay events along its path.

The clocks are located at the origin of the respective coordinates on their rulers and are initialized at their encounter. Each emits a light signal after a finite displacement of magnitude L along the ruler of the other clock. From Sec. 2.3, the finite separation S between the initialization and emission is $S = \frac{2k_{\text{A}\text{N}}}{1-k_{\text{A}\text{N}}^2}L$. The expectation is that the time T shown on each clock-face at the emission is correlated with this finite separation. Thus the results of the two approaches could be compared when $cT = \frac{2k_{\text{A}\text{N}}}{1-k_{\text{A}\text{N}}^2}L$.

The conversion factor $k_{\text{A}\text{N}} = \sqrt{(1-\beta)/(1+\beta)}$, from (2.1), provides the further means by which the predictions of the two approaches could be compared. Substitutions show that both approaches predict symmetric locations for the marks left on the rulers by the clocks at the emission events. Both yield the same location for the marks left on the rulers when the emitted signals meet and are reflected back to their respective emitting clock: each mark is at the distance $\frac{1}{1+k_{\text{A}\text{N}}}L = \frac{1}{2}\left(\sqrt{\frac{1+\beta}{1-\beta}} - 1\right)cT$ from the clock of the respective ruler. Finally, both approaches predict the same location for the marks left on the rulers at the detection events: each mark is at the distance $k_{\text{A}\text{N}}^{-1}L = \frac{\beta}{1-\beta}cT$ from the appropriate clock.

As a general rule, a relativistic result free of synchrony dependency necessarily matches the respective binate-frame prediction.

B Relativistic phenomena: two physical-space dimensions

B1 Transverse optical Doppler effect

A transverse Doppler effect for light signals is observed in situations when the emitter and the detector are in relative motion and this motion is not along the line that separates them. The wavelength of the detected signal then differs from that of the emitted signal and the named effect refers to this difference. To predict the magnitude of the effect, we

consider the detector and the emitter as being in a $k_{A\aleph}$ -frame, $z^\mu = (x_A, x_\aleph, y_A)$, adapted to their relative motion, that is, each retains its location in the opposite planes of the frame. Say the detector is at $x_A = -L$ and $y_A = H$ in the A-plane, and the emitter is at O_\aleph in the \aleph -plane. As the emitter and the detector approach each other, though not along the line between them, two light signals are generated. Subsequently, these signals are detected and the detector marks the location of the detection events in the \aleph -plane.

The first signal is emitted from O_\aleph as it passes over O_A , at the event \mathcal{E}_1 with coordinates $(0, 0, 0)$; the signal is detected shortly thereafter at \mathcal{D}_1 with coordinates $(-L, -H \cot \alpha_{\aleph 1}, H)$. These events are shown in Fig. B1. The second signal is emitted at \mathcal{E}_2 , when O_\aleph passes over a trigger located at $x_A = -\lambda_e$ and $y_A = 0$ in the A-plane. The coordinates of \mathcal{E}_2 are $(-\lambda_e, 0, 0)$. The emitted signal is detected at \mathcal{D}_2 with coordinates $(-L + \lambda_e, -H \cot \alpha_{\aleph 2}, H)$. The emission and detection events of the second signal are not illustrated since the diagrams are similar to those of Fig. B1.

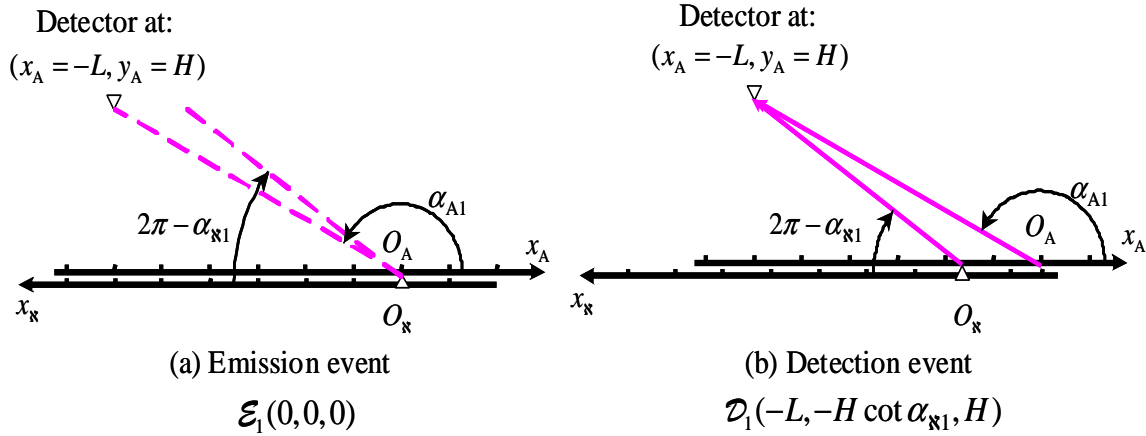


Fig. B1 a) Emission of the first signal: the dotted lines show the eventual traces of the light signal in the reference planes. b) Detection of the emitted signal: the solid lines are the actual traces.

The ray of the first signal traces the line $y_A = x_A \tan \alpha_{A1}$ in the A-plane and the line $y_\aleph = x_\aleph \tan \alpha_{\aleph 1}$ in the \aleph -plane. The angular elevation α_{A1} is known from the location of the detector in the A-plane: $\cot \alpha_{A1} = -L/H$. The ray of the second signal traces the lines: $y_A = (x_A + \lambda_e) \tan \alpha_{A2}$ and $y_\aleph = x_\aleph \tan \alpha_{\aleph 2}$ while $\cot \alpha_{A2} = (-L + \lambda_e)/H$. The angular elevations α_\aleph of the two signals are determined from (3.3), which requires that $\cot(\frac{1}{2} \alpha_A) \cot(\frac{1}{2} \alpha_\aleph) = -k_{A\aleph}$ be met by the $(\alpha_A, \alpha_\aleph)$ -pairs of the first signal and of the second signal, respectively.

The difference between the x_\aleph -coordinates of the two detections calculated with the so determined angular elevations is $\lambda_d = x_{\aleph 1} - x_{\aleph 2} = H (\cot \alpha_{\aleph 1} - \cot \alpha_{\aleph 2})$.

Alternatively, one could work with (3.2b) rather than (3.3). Thus the coordinate $x_{\mathfrak{N}1}$ of the first detection and $x_{\mathfrak{N}2}$ of the second should meet:

$$H^2 = \frac{k_{\text{A}\mathfrak{N}}}{(1-k_{\text{A}\mathfrak{N}})^2}(-L+x_{\mathfrak{N}1})^2 - \frac{k_{\text{A}\mathfrak{N}}}{(1+k_{\text{A}\mathfrak{N}})^2}(-L-x_{\mathfrak{N}1})^2, \text{ and} \quad (\text{B1.1})$$

$$H^2 = \frac{k_{\text{A}\mathfrak{N}}}{(1-k_{\text{A}\mathfrak{N}})^2}(-L+\lambda_e+x_{\mathfrak{N}2})^2 - \frac{k_{\text{A}\mathfrak{N}}}{(1+k_{\text{A}\mathfrak{N}})^2}(-L+\lambda_e-x_{\mathfrak{N}2})^2. \quad (\text{B1.2})$$

These are easily solved for $x_{\mathfrak{N}1}$ and $x_{\mathfrak{N}2}$, and then we get the explicit result:

$$\lambda_d = \frac{1+k_{\text{A}\mathfrak{N}}^2}{2k_{\text{A}\mathfrak{N}}} \lambda_e - \frac{1-k_{\text{A}\mathfrak{N}}^2}{2k_{\text{A}\mathfrak{N}}} \left(\sqrt{L^2+H^2} - \sqrt{(L-\lambda_e)^2+H^2} \right). \quad (\text{B1.3})$$

This in turn yields:

$$\left. \frac{d\lambda_d}{d\lambda_e} \right|_{\lambda_e=0} = \frac{1+k_{\text{A}\mathfrak{N}}^2}{2k_{\text{A}\mathfrak{N}}} - \frac{1-k_{\text{A}\mathfrak{N}}^2}{2k_{\text{A}\mathfrak{N}}} \frac{L/H}{\sqrt{1+(L/H)^2}}. \quad (\text{B1.4})$$

The prediction from relativistic calculations is usually presented only as the first order approximation: $\lambda_d/\lambda_e = \gamma[1-\beta \cos \theta]$ for $\lambda_e/\sqrt{L^2+H^2} \ll 1$, where θ is the angle that the emission direction makes with the direction of the motion between the source and the detector. This matches our prediction (B1.4), since $\theta = \pi - \alpha_{\text{A}1}$ as measured in Fig. B1 and $k_{\text{A}\mathfrak{N}} = \sqrt{(1-\beta_{\text{A}\mathfrak{N}})/(1+\beta_{\text{A}\mathfrak{N}})}$, from (2.1).

B2 Bradley's annual stellar-aberration

Annual stellar-aberration is the phenomenon by which light received on earth from a distant star appears to come from slightly different directions when measured on different seasons in the course of a year. The distance between a star and the earth is very much greater (at least 10,000 fold) than the length of the axes of the earth trajectory around the sun. Thus changes in the earth orbital location around the sun are negligible. The relevant factor is the change in the earth's direction of motion between the seasonal observations: in one season, the earth moves towards the emitted ray of light from the star, six month later, it moves away from the emitted ray. This change of direction of the relative motion between the star and the earth causes the observed annual aberration, as noted already in 1914, by Herassimovitch [35].

The kinematics of the situation is analyzed in a $k_{\text{A}\mathfrak{N}}$ -frame (see Fig. B2) whose A - and \mathfrak{N} -planes are the spatial extensions of the earth in September (when it is moving like O_{A} , away from the emitted ray) and in March (when it is moving like $O_{\mathfrak{N}}$, towards

the emitted ray), respectively. The extensions reach to the star and beyond; they include the line of the relative motion between the earth in March and in September.

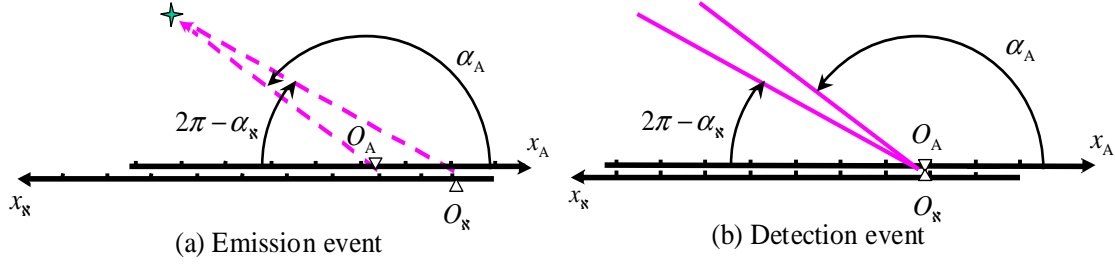


Fig. B2 (*not to scale*) Traces of the light ray from the star: the line to O_A is the trace of the September observation, while the line to O_K is the trace of the March observation.

Light is emitted from the star. The dotted lines in Fig. B2(a) show the directions of the emitted rays that eventually reach the earth. The actual traces of these rays are the solid lines in Fig. B2(b). The angular elevations of the two traces, α_A and α_K , are measured as illustrated. The ray emitted in September traces the solid line in Fig. B2(b), from the star to the earth at O_A . The ray emitted in March traces the line from the star to the earth at O_K . Although the two traces happen at different seasons, they are brought together for the analysis on the same diagrams in Fig. B2. By (3.3), we have: $\cot(\frac{1}{2}\alpha_A)\cot(\frac{1}{2}\alpha_K) = -k_{AK}$, and the difference $[\alpha_A - (\alpha_K - \pi)]$ is the angle of annual aberration.

Herassimovitch [35] obtained the relation: $\tan(\frac{1}{2}\alpha) = \sqrt{(c+v)/(c-v)} \tan(\frac{1}{2}\alpha')$, where α' is our α_A , and α is our $\alpha_K - \pi$. This is the usual relativistic result, though expressed in terms of *tangents*. It is also the same prediction as ours when considering that $k_{AK} = \sqrt{(1+\beta_{AK})/(1-\beta_{AK})}$, from (2.1), and $\beta_{AK} \equiv v/c$.

B3 Michelson-Morley null-effect

A Michelson-Morley type of experiment is performed with an apparatus whose elements essential for our kinematical analysis are illustrated diagrammatically in Fig. B3. The two arms of the apparatus hold the mirrors M_1 and M_2 . The arms are attached to a common vertex at O_A , on the A-plane of a k_{AK} -frame. Each series of test-runs is performed with the arms at a fixed inclination. The inclination is changed between the runs; alternatively, one could slowly rotate together the two arms around O_A in the A-plane.

A light signal is initiated at the encounter of O_A and O_K . The event is shown in Fig. B3. Eventually, the mirrors M_1 and M_2 each detects a ray from the emitted light, and each reflects the detected ray toward O_A . When detecting a reflected ray, at the events \mathcal{D}_1 and \mathcal{D}_2 , respectively, O_A puts a mark on the x_K -axis. The distance between the two marks is the data collected from the experiment.

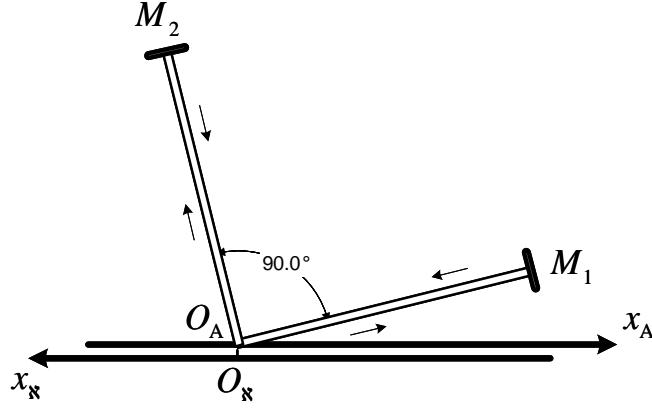


Fig. B3 Diagram of Michelson-Morley's experiment with only the essential elements of the apparatus and the x -coordinates of the A - and \mathfrak{K} -planes.

Consider the ray propagating from O_A to M_1 . The y_A -coordinate of the detection by the mirror M_1 obtains from (3.2):

$$y_A^2 = \left(\frac{2k_{A\mathfrak{K}}}{1-k_{A\mathfrak{K}}^2} \right)^2 \left[x_A^2 + \frac{1+k_{A\mathfrak{K}}^2}{k_{A\mathfrak{K}}} x_A x_{\mathfrak{K}} + x_{\mathfrak{K}}^2 \right]. \quad (\text{B3.1})$$

Furthermore, $\sqrt{x_A^2 + y_A^2} = L_1$, where L_1 denotes the length of the arm with the M_1 mirror. We substitute for y_A in terms of L_1 and solve the resulting equation for the coordinate $x_{\mathfrak{K}}$ of the detection, which is also the coordinates of the reflection event \mathfrak{R}_1 , since M_1 reflects the signal as soon as it detects it:

$$x_{\mathfrak{K}} = -\frac{1+k_{A\mathfrak{K}}^2}{2k_{A\mathfrak{K}}} x_A - \frac{1-k_{A\mathfrak{K}}^2}{2k_{A\mathfrak{K}}} L_1. \quad (\text{B3.2})$$

(A second solution yields the coordinate $x_{\mathfrak{K}}$ wherefrom M_1 could have sent a light signal that would have been subsequently detected by O_A just as it passes over $O_{\mathfrak{K}}$.)

Consider now the ray reflected from M_1 to O_A . The coordinates of the mark put by O_A at the detection event \mathfrak{D}_1 meet the appropriate form of (3.2):

$$\Delta y_A^2 = \left(\frac{2k_{A\mathfrak{K}}}{1-k_{A\mathfrak{K}}^2} \right)^2 \left[\Delta x_A^2 + \frac{1+k_{A\mathfrak{K}}^2}{k_{A\mathfrak{K}}} \Delta x_A \Delta x_{\mathfrak{K}} + \Delta x_{\mathfrak{K}}^2 \right]. \quad (\text{B3.3})$$

Here, Δx_A , $\Delta x_{\mathfrak{K}}$ and Δy_A are the differences between the respective coordinates of the reflection and detection events, \mathcal{R}_1 and \mathcal{D}_1 . The returned signal from M_1 is detected at $x_A = 0$, and evidently $\sqrt{\Delta x_A^2 + \Delta y_A^2} = L_1$. We get the difference $\Delta x_{\mathfrak{K}}$ from (B3.3):

$$\Delta x_{\mathfrak{K}} = -\frac{1+k_{A\mathfrak{K}}^2}{2k_{A\mathfrak{K}}} \Delta x_A - \frac{1-k_{A\mathfrak{K}}^2}{2k_{A\mathfrak{K}}} L_1. \quad (\text{B3.4})$$

By adding (B3.2) and (B3.4), we find that the coordinate in the \mathfrak{K} -plane of the mark left by O_A at \mathcal{D}_1 is $x_{\mathfrak{K}} = (k_{A\mathfrak{K}}^{-1} - k_{A\mathfrak{K}})L_1$.

The remarkable feature of the above result is that it depends on L_1 , which is the length of arm that holds the M_1 -mirror, but not on the angle that this arm makes with the x_A -axis. Similar calculations show that the returned ray from the M_2 mirror is detected by O_A at $x_{\mathfrak{K}} = (k_{A\mathfrak{K}}^{-1} - k_{A\mathfrak{K}})L_2$ in the \mathfrak{K} -plane, where L_2 is the length of the arm that holds this mirror. This result too depends only on the length of the arm that holds the mirror, not on its inclination.

The Michelson-Morley interferometer has arms of nominal equal length L . Thus the two returned rays would be detected together at the event with coordinates: $x_A = 0$ and $x_{\mathfrak{K}} = (k_{A\mathfrak{K}}^{-1} - k_{A\mathfrak{K}})L$. Were we to use an interferometer, we would not be observing any fringes other than perhaps those caused by some minute differences between the (nominally equal) lengths of the arms. And of course, changing the angle of the apparatus would cause no shift of the observed fringes. With an apparatus of unequal arm-lengths, the two rays would be detected at different events but the distance between the detection marks in the \mathfrak{K} -plane would remain unchanged at all orientations of the apparatus. Thus also in this case no fringe shift would be observed.

Our conclusions here match those first obtained with Lorentz transformations. But with the binate-frame approach, we found it unnecessary to involve considerations based on changing the reference frame.

B4 The Sagnac effect

It is observed that when two light signals counter-propagate around a closed path, they simultaneously complete a full loop around this path only when the apparatus does not rotate. The analysis in this section concerns a platform with mirrors that rotates counter-clockwise (see Fig. B4). At a specified event, the mirror \mathbf{M}_1 emits two light signals that circulate around the platform in opposite directions, as reflected by the other mirrors. The reflected signals are eventually detected back at \mathbf{M}_1 . The signal circulating clockwise is detected first, followed after a short delay by the signal circulating counter-clockwise. The difference between the angles of the platform's rotation at the detection events is the Sagnac effect. We predict its magnitude from an analysis that uses the kinematical relations for the uniform circular motion of a particle and a ring, as presented in Sec. 3.3.

The right-hand side of Fig. B4 shows four mirrors that rotate around O_A in the A-plane of a $k_{A\aleph}$ -frame adapted (see Sec. 3.3) to the platform's rotation. The mirrors are symmetrically placed on an imaginary ring of radius equal to the length of the arms with the mirrors. On this ring, the angular elevation $\alpha = 0$ is assigned to the arm of \mathbf{M}_1 . Then the arm of \mathbf{M}_2 is at the angular elevation $\alpha = \pi/2$, and so forth for the other mirrors.

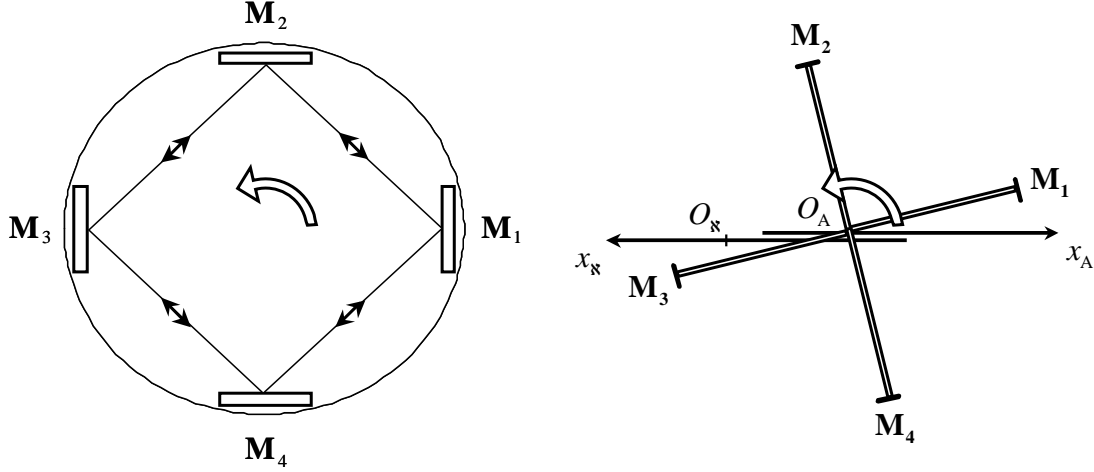


Fig. B4 The platform with the four mirrors (left side); the diagram of the situation in the $k_{A\aleph}$ -frame used for the analysis (right side).

Since the imagined ring rotates uniformly around O_A , the analysis in Sec. 3.3 applies.

Thus \mathbf{M}_1 moves according to: $x_A = \rho \cos \theta$ and $y_A = \rho \sin \theta$ around O_A , and from

(3.15), we have $x_{\aleph} = -\frac{1+k_{A\aleph}^2}{2k_{A\aleph}} \rho (\theta + \cos \theta - 1)$. Similarly, \mathbf{M}_2 moves around O_A

according to: $x_A = \rho \cos(\alpha + \theta)$ and $y_A = \rho \sin(\alpha + \theta)$, while from (3.17), we have

$x_{\aleph} = -\frac{1+k_{A\aleph}^2}{2k_{A\aleph}} \rho [\theta + \cos(\alpha + \theta) - 1]$. The ring's rotation angle θ is measured counter-clockwise from the x_A -axis.

A light signal is emitted from \mathbf{M}_1 as it crosses the x_A -axis and meets O_{\aleph} , at the event with coordinates $(\rho, 0, 0)$. The signal is detected by \mathbf{M}_2 at a rotation angle θ_d . Coordinate differences between the emission and detection are: $\Delta x_A = \rho \cos(\alpha + \theta_d) - \rho$,

$\Delta y_A = \rho \sin(\alpha + \theta_d)$ and $\Delta x_{\aleph} = -\frac{1+k_{A\aleph}^2}{2k_{A\aleph}} \rho [\theta_d + \cos(\alpha + \theta_d) - 1]$. These should meet the appropriate form of (3.2):

$$\left(\frac{2k_{A\aleph}^2}{1-k_{A\aleph}^2} \right)^2 (\Delta x_A^2 + \frac{1+k_{A\aleph}^2}{k_{A\aleph}} \Delta x_{\aleph} \Delta x_A + \Delta x_{\aleph}^2) - \Delta y_A^2 = 0. \quad (\text{B4.1})$$

Substitutions eventually lead to an equation for θ_d that has to be solved numerically:

$$\frac{\theta_d}{2} = \frac{1 - k_{\text{AN}}^2}{1 + k_{\text{AN}}^2} \sin\left(\frac{\alpha + \theta_d}{2}\right). \quad (\text{B4.2})$$

Let $\theta_d = \theta_+$ meet (B4.2). The analyses of the other three legs of the counter-clockwise propagating signal, $\mathbf{M}_2 \rightarrow \mathbf{M}_3 \rightarrow \mathbf{M}_4 \rightarrow \mathbf{M}_1$, yield exactly the same equation for the rotation angle on each leg of the circuit, as expected from the circular symmetry of the situation. Thus the signal emitted from \mathbf{M}_1 and circulating counter-clockwise would be detected back at \mathbf{M}_1 just as the mirror completes a rotation of magnitude $4\theta_+$. Similar analysis for the signal circulating clockwise yields:

$$\frac{\theta_d}{2} = \frac{1 - k_{\text{AN}}^2}{1 + k_{\text{AN}}^2} \sin\left(\frac{\alpha - \theta_d}{2}\right). \quad (\text{B4.3})$$

Let $\theta_d = \theta_-$ meet (B4.3). Thus the signal circulating clockwise would be detected back at \mathbf{M}_1 just as this mirror completes a $4\theta_-$ rotation.

Note that since (B4.2) and (B4.3) differ, $\theta_+ \neq \theta_-$. The non-null difference between the rotation angles when the two signals are detected depends on the angle α between the mirrors. For a setup of N mirrors symmetrically placed around the circle, we have $\alpha_N = \frac{2\pi}{N}$. Thus an arc of magnitude $\Delta\theta_N = N(\theta_{N+} - \theta_{N-})$ separates the events when \mathbf{M}_1 , the mirror that emitted the counter-propagating signals, detects the reflected signals after each completed a full circuit. The angles θ_{N+} and θ_{N-} meet respectively (B4.2) and (B4.3), with α replaced by α_N . We proceed to compare the predictions from our binate-frame analysis with those derived from classical mechanics considerations and those obtained with relativistic calculations.

Analysis by classical mechanics: The usual argument runs as follows: Suppose the mirrors and the light signal leave a trace of their path through the A-plane. The trace of the signal from the event when it was emitted by \mathbf{M}_1 to the event when it was detected by

\mathbf{M}_2 is a chord that spans an arc of magnitude $\alpha_N + \theta_+$; its length is $2\rho \sin\left(\frac{\alpha_N + \theta_{N+}}{2}\right)$.

In the time interval it took the light to trace this chord, the mirror \mathbf{M}_2 traces an arc of magnitude $\rho\theta_{N+}$. Thus the ratio of the two lengths should be equal to the ratio $\beta_\theta = v_\theta/c$

between the mirror's peripheral speed and the speed of light: $\frac{\theta_{N+}}{2} = \beta_\theta \sin\left(\frac{\alpha_N + \theta_{N+}}{2}\right)$. In

contrast, the trace of the light signal from \mathbf{M}_N to the event when it meets \mathbf{M}_1 is a chord that spans an arc of magnitude $\alpha_N - \theta_{N-}$, and thus $\frac{\theta_{N-}}{2} = \beta_\theta \sin\left(\frac{\alpha_N - \theta_{N-}}{2}\right)$.

Evidently, classical mechanics and the binate-frame analysis lead to the same conclusion when β_θ equals $\frac{1-k_{A\aleph}^2}{1+k_{A\aleph}^2}$. This is indeed the case, since the $k_{A\aleph}$ -frame of the analysis is adapted to the mirrors' motion. Thus at $\theta = 90^\circ$, the mirror \mathbf{M}_1 moves with respect to the A-plane just as the \aleph -plane and $\beta_{A\aleph} = \frac{1-k_{A\aleph}^2}{1+k_{A\aleph}^2}$, from (2.1), is indeed the relative speed between the planes of the adapted $k_{A\aleph}$ -frame.

Comparison with the relativistic prediction: With a large number of mirrors, α_N is a small angle, and when the mirrors rotate slowly, θ_{N+} and θ_{N-} are small angles too. Hence, we could replace each *sinus* function in (B4.2) and (B4.3) with the angle itself, to obtain: $\theta_{N+} = \frac{1-k_{A\aleph}^2}{1+k_{A\aleph}^2}(\alpha_N + \theta_{N+})$ and $\theta_{N-} = \frac{1-k_{A\aleph}^2}{1+k_{A\aleph}^2}(\alpha_N - \theta_{N-})$, which in turn yields:

$\Delta\theta_N = N(\theta_{N+} - \theta_{N-}) = 2N\alpha_N \left(\frac{1-k_{A\aleph}^2}{2k_{A\aleph}} \right)^2$. In the limit case, when the light signals are forced to propagate circularly, it leads to:

$$\Delta\theta_\infty = \lim_{N \rightarrow \infty} \Delta\theta_N = 4\pi \left(\frac{1-k_{A\aleph}^2}{2k_{A\aleph}} \right)^2. \quad (\text{B4.4})$$

This is the prediction from our binate frame analysis that we wish to compare next with the result of relativistic calculations.

Special Relativity presents the magnitude of the Sagnac effect in terms of a fringe shift or a time delay between the detections. For the comparison, we use the time-delay presentation: $\Delta t = \frac{4\omega A}{c^2 - \omega^2 \rho^2}$, where $\omega = v_\theta / \rho$ is the angular velocity of the platform and A is the area enclosed by the light-path circuit. For a set-up of N mirrors, the circuit is a N -sided polygon inscribed in a circle of radius ρ . Its area is $A = \frac{N}{2} \rho^2 \sin\left(\frac{2\pi}{N}\right)$.

Substitutions then yield $\Delta\theta_N \equiv \omega \Delta t = \frac{2N\beta_\theta^2}{1-\beta_\theta^2} \sin\left(\frac{2\pi}{N}\right)$. In the limit, as $N \rightarrow \infty$, we obtain

the prediction applicable to a circular circuit: $\Delta\theta_N \rightarrow \Delta\theta_\infty = \frac{4\pi\beta_\theta^2}{1-\beta_\theta^2}$. Thus the relativistic

approach and ours yield the same prediction when β_θ equals $\frac{1-k_{A\aleph}^2}{1+k_{A\aleph}^2}$. To show that this is the case even from a relativist point of view, we reason as follows.

For an observer located at O_A , the times of Einstein synchronized clocks of the A-plane holding the centre of rotation obtain from: $cdt_A = -\frac{1+k_{A\aleph}^2}{1-k_{A\aleph}^2}dx_A - \frac{2k_{A\aleph}}{1-k_{A\aleph}^2}dx_{\aleph}$, as in (2.6a). For the considered circular motion, substitutions and subsequent calculations yield: $cdt_A = \frac{1+k_{A\aleph}^2}{1-k_{A\aleph}^2}\rho d\theta$. By definition, $\omega = \frac{d\theta}{dt_A}$ is the platform's angular velocity and $\beta_\theta = \frac{\omega\rho}{c}$. These yield $\beta_\theta = \frac{1-k_{A\aleph}^2}{1+k_{A\aleph}^2}$, as expected.

B5 Elastic Scattering

On the basis of Newtonian mechanics, an elastic collision of a moving particle with an identical particle at rest in the laboratory results in the two particles either interchanging their motion and rest states or, in the case of scattering, moving in directions that make a right angle. But in experiments with high-speed particles colliding with a particle at rest in the laboratory, the measured angle was found to be somewhat less than 90° .

For the analysis of this high-speed phenomenon, we model the physical situation before the collision by considering two identical particles, \bar{P} and \hat{P} , located at O_A and O_{\aleph} , respectively, in the $k_{A\aleph}$ -frame of Fig. B5(i). Without prejudice, their momentum is viewed as being of unit magnitude. After the collision, the particles trace their passage in the reference planes. These traces are shown in Fig. B5(ii). The particle \bar{P} traces the line $O_A\bar{P}$ in the A-plane and the line $O_{\aleph}\bar{P}$ in the \aleph -plane; the particle \hat{P} traces the line $O_A\hat{P}$ in the A-plane and the line $O_{\aleph}\hat{P}$ in the \aleph -plane. The illustration is for the case when the symmetry between the motions of the particles prior to the collision is maintained after it. (This is not the only possible outcome of fully elastic collision experiments: calculations below show the situation to be physically under-determined.)

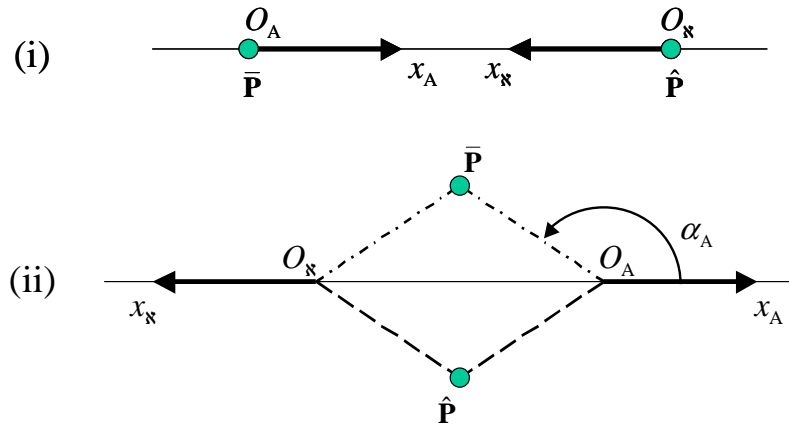


Fig. B5 (i) The two particles before the collision event. (ii) The particles after the collision event, together with the marked traces in the reference planes.

Before the collision, the particles are free from external influences; hence, the dynamical considerations and the results of Sec. 2.5 apply. It is convenient to use the contravariant momentum components so obtained:

$$\bar{p}^\mu|_{in} = \begin{bmatrix} 0 \\ -\frac{1-k_{A\aleph}^2}{2k_{A\aleph}} \\ 0 \end{bmatrix} \quad \text{and} \quad \hat{p}^\mu|_{in} = \begin{bmatrix} -\frac{1-k_{A\aleph}^2}{2k_{A\aleph}} \\ 0 \\ 0 \end{bmatrix}. \quad (\text{B5.1})$$

The particles are again free after the collision but the momenta are unknown. We denote them \bar{p}^μ and \hat{p}^μ , without the self-explanatory subscript $|_{out}$. The six components involved are not independent since the magnitude of each momentum retains its initial unit value in an elastic collision, and thus:

$$\left(\frac{2k_{A\aleph}}{1-k_{A\aleph}^2}\right)^2 \left[(\bar{p}^1)^2 + \frac{1+k_{A\aleph}^2}{k_{A\aleph}} \bar{p}^1 \bar{p}^2 + (\bar{p}^2)^2 \right] - (\bar{p}^3)^2 = 1 \quad \text{and} \quad (\text{B5.2})$$

$$\left(\frac{2k_{A\aleph}}{1-k_{A\aleph}^2}\right)^2 \left[(\hat{p}^1)^2 + \frac{1+k_{A\aleph}^2}{k_{A\aleph}} \hat{p}^1 \hat{p}^2 + (\hat{p}^2)^2 \right] - (\hat{p}^3)^2 = 1.$$

The outcome of the collision is to be predicted from the balance of momentum. This requires that the momentum-components of the outgoing particles meet:

$$-\frac{1-k_{A\aleph}^2}{2k_{A\aleph}} = \bar{p}^1 + \hat{p}^1, \quad -\frac{1-k_{A\aleph}^2}{2k_{A\aleph}} = \bar{p}^2 + \hat{p}^2, \quad 0 = \bar{p}^3 + \hat{p}^3. \quad (\text{B5.3})$$

Since only five equations, (B5.2) and (B5.3), are available but there are six unknowns (the momentum-components of the outgoing particles), the situation is physically under-determined. This explains the observed scattering of the particles. Among the possible solutions, there are those that retain the symmetry of the incoming particles. The nature of such solutions is what we explore next.

Let the trace of the scattered particle \bar{P} in the A -plane make the angle α_A with the x_A -axis. Then $d\bar{z}^3 = d\bar{z}^1 \tan \alpha_A$ and we also have $\bar{p}^3 = \bar{p}^1 \tan \alpha_A$, since $m \bar{z}'^\mu = p^\mu$ is one of Hamilton's equations of motion for the free particle. The set of the five equations complemented with the relation between \bar{p}^1 and \bar{p}^3 is now complete, but its solution depends the selected value of α_A . Thus we deal here with a one-parameter family of

solutions, the parameter being α_A . Among the solutions, the one with $\tan \alpha_A = \frac{2\sqrt{k_{A\aleph}}}{1+k_{A\aleph}}$

preserves the symmetry between the particles. Calculations for the corresponding value of α_A lead to the following momenta:

$$\bar{p}^1 = \hat{p}^1 = -\frac{1-k_{A\aleph}^2}{4k_{A\aleph}}, \quad \bar{p}^2 = \hat{p}^2 = -\frac{1-k_{A\aleph}^2}{4k_{A\aleph}}, \quad \text{and} \quad \bar{p}^3 = \hat{p}^3 = \frac{1-k_{A\aleph}}{2\sqrt{k_{A\aleph}}}. \quad (\text{B5.4})$$

Since $\tan \alpha_A < 1$ for the symmetric solution, $\alpha_{\aleph} = \alpha_A < 45^\circ$, that is, the directions of particles' motion in Fig. B5 make an angle less than 90° .

In terms of the angles used here, the prediction of Special Relativity [36] is that $\tan \alpha_A \tan \alpha_{\aleph} = 2/(\gamma_{A\aleph} + 1)$, where $\gamma_{A\aleph} = 1/\sqrt{1-\beta_{A\aleph}^2}$ and $\beta_{A\aleph}$ is the relative speed of the incoming particles. Thus for the symmetric solution: $\tan \alpha_A = \tan \alpha_{\aleph} = \sqrt{2/(\gamma_{A\aleph} + 1)}$. The relativistic prediction for the scatter angle matches ours when considering that we have $\beta_{A\aleph} = \frac{1-k_{A\aleph}^2}{1+k_{A\aleph}^2}$, from (2.1).

C Relativistic phenomena: three physical-space dimensions

C1 The Sagnac effect revisited

We revisit the analysis of the Sagnac effect that we undertook in appendix B4, but we now select a $k_{A\aleph}$ -frame, $z^\mu = (x_A, x_{\aleph}, y_A, y_{\aleph})$, whereby the mirrors rotate in the $y_A y_{\aleph}$ -plane, as illustrated in Fig. C1. (In B4, the rotation was in the $x_A y_A$ -plane.)

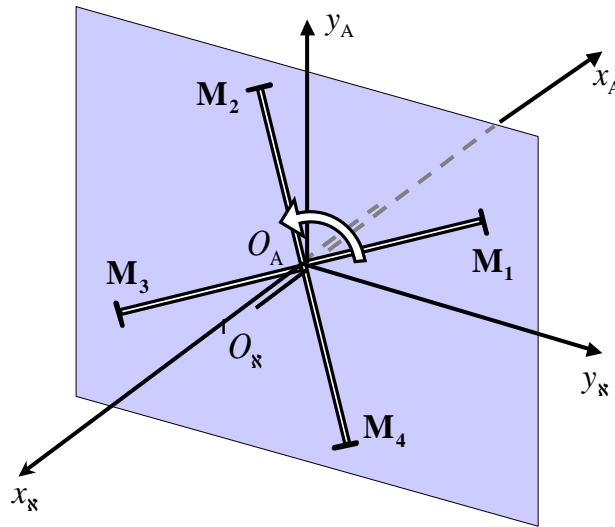


Fig. C1 The cross with mirrors rotates around O_A in the plane $y_A y_{\aleph}$.

The mirrors rotate uniformly around O_A , at a distance from it equal to the length ρ of the arms that hold them. The rotation angle θ is measured counter-clockwise from the $y_{\mathbb{K}}$ -axis. The \mathbf{M}_1 mirror moves according to: $x_A = 0$, $y_A = \rho \sin \theta$, $y_{\mathbb{K}} = \rho \cos \theta$, and the yet to be determined $x_{\mathbb{K}} = x_{\mathbb{K}}(\theta)$. The uniform rotation starts with \mathbf{M}_1 at $(0, 0, 0, \rho)$.

The selected frame is not adapted to the rotation of the mirrors since these cannot ever be at rest with respect to one or the other of the frame's reference planes. Yet, when proceeding as in Sec. 3.3, we arrive at the same prediction for the magnitude of the effect as in appendix B4.

We first substitute the known coordinates in (4.2) and get a differential equation for $\frac{dx_{\mathbb{K}}}{d\theta}$. Integration yields $x_{\mathbb{K}} = -\frac{1-k_{\mathbb{A}\mathbb{K}}^2}{2k_{\mathbb{A}\mathbb{K}}} \theta \sqrt{\left(\frac{ds}{d\theta}\right)^2 + \rho^2}$, since $\frac{ds}{d\theta}$ is constant in uniform rotation. The rate of change of the separation along the path of a particle in uniform rotation was shown (see Sec. 3.3) to be $\frac{ds}{d\theta} = \frac{2k_{\mathbb{A}\mathbb{K}}}{1-k_{\mathbb{A}\mathbb{K}}^2} \rho$ for the adapted $k_{\mathbb{A}\mathbb{K}}$ -

frame. But since the separation ds is invariant, so is its rate of change $\frac{ds}{d\theta}$. Thus when the frame selected for the current calculations is calibrated to the same $k_{\mathbb{A}\mathbb{K}}$ as the adapted frame, the above $ds/d\theta$ could be substitute in $x_{\mathbb{K}}$ to get: $x_{\mathbb{K}} = -\frac{1+k_{\mathbb{A}\mathbb{K}}^2}{2k_{\mathbb{A}\mathbb{K}}} \rho \theta$.

The motion of the mirror \mathbf{M}_2 is similar to that of the mirror \mathbf{M}_1 . Thus $x_A = 0$, $x_{\mathbb{K}} = -\frac{1+k_{\mathbb{A}\mathbb{K}}^2}{2k_{\mathbb{A}\mathbb{K}}} \rho \theta$, $y_A = \rho \sin(\alpha + \theta)$, and $y_{\mathbb{K}} = \rho \cos(\alpha + \theta)$, where $\alpha = \pi/2$ is the angle between the mirrors.

A light signal emitted from \mathbf{M}_1 at $(0, 0, 0, \rho)$ is detected by \mathbf{M}_2 at some angle of rotation θ_d . The coordinate differences between the emission and detection events:

$$\Delta x_A = 0, \Delta x_{\mathbb{K}} = -\frac{1+k_{\mathbb{A}\mathbb{K}}^2}{2k_{\mathbb{A}\mathbb{K}}} \rho \theta_d, \Delta y_A = \rho \sin(\alpha + \theta_d), \text{ and } \Delta y_{\mathbb{K}} = \rho [\cos(\alpha + \theta_d) - 1]$$

should meet (4.1). This leads to:

$$\left(\frac{2k_{\mathbb{A}\mathbb{K}}}{1-k_{\mathbb{A}\mathbb{K}}^2}\right)^2 (\Delta x_A^2 + \frac{1+k_{\mathbb{A}\mathbb{K}}^2}{k_{\mathbb{A}\mathbb{K}}} \Delta x_{\mathbb{K}} \Delta x_A + \Delta x_{\mathbb{K}}^2) - \Delta y_A^2 - \Delta y_{\mathbb{K}}^2 = 0. \quad (\text{C1-1})$$

Substitutions lead to: $\frac{\theta_d}{2} = \frac{1-k_{\mathbb{A}\mathbb{K}}^2}{1+k_{\mathbb{A}\mathbb{K}}^2} \sin(\frac{\alpha + \theta_d}{2})$, which is the same predictions as the one earlier obtained in (B4.2).

C2 Plane electromagnetic waves

In the absence of a current, the D'Alembertian (4.3) for the potential is null and admits plane waves among its solutions. For instance, the potential $A^\mu = C^\mu(u^\nu)e^{-i\varphi}$, where $\varphi(z^\mu) \equiv u_\sigma z^\sigma$, meets $\partial_\mu \partial^\mu A^\nu = 0$ for any constant null vector u^μ , and meets the Lorenz condition $\partial_\mu A^\mu = 0$ when $C_\mu u^\mu = 0$, that is, when the *amplitude* vector C^μ is orthogonal to the *wave* vector u^μ .

Suppose we have $C_1 = C_2 = 0$ in the $k_{\text{A}\text{N}}$ -frame, $z^\mu = (x_{\text{A}}, x_{\text{N}}, y_{\text{A}}, y_{\text{N}})$, and the wave vector has only two non-null components, $u^1 = 1$ and $u^2 = -k_{\text{A}\text{N}}^{-1}$, both in the $x_{\text{A}}x_{\text{N}}$ -plane. We get $u_\mu z^\mu = -\frac{2}{1-k_{\text{A}\text{N}}^2}(x_{\text{A}} + k_{\text{A}\text{N}}x_{\text{N}})$. This is a plane wave whose potential has just two non-null components, A^3 and A^4 , both in the $y_{\text{A}}y_{\text{N}}$ -plane and with constant amplitudes. The wave could be said to propagate along the light ray: $x_{\text{A}} + k_{\text{A}\text{N}}x_{\text{N}} = 0$.

Similar considerations show that we get $u_\mu z^\mu = -\frac{2k_{\text{A}\text{N}}}{1-k_{\text{A}\text{N}}^2}(k_{\text{A}\text{N}}x_{\text{A}} + x_{\text{N}})$ when the non-zero components of the wave vector are $u^1 = -1$ and $u^2 = k_{\text{A}\text{N}}$. The potential of this plane wave has, as before, only two components, A^3 and A^4 , in the $y_{\text{A}}y_{\text{N}}$ -plane and with constant amplitudes. But now the wave propagates along the light ray: $k_{\text{A}\text{N}}x_{\text{A}} + x_{\text{N}} = 0$.

C3 The field of a charged particle

A charged particle whose parametric equations of motion are $\bar{z}^\mu = \bar{z}^\mu(s)$ in a $k_{\text{A}\text{N}}$ -frame, $z^\mu = (x_{\text{A}}, x_{\text{N}}, y_{\text{A}}, y_{\text{N}})$, produces an electromagnetic field. The field potential obtains from Liénard-Wiechert formula [24], where q is the particle's charge:

$$A^\mu(z^\sigma) = \frac{q \dot{\bar{z}}^\mu(s_0)}{\dot{\bar{z}}_\nu(s_0) [\bar{z}^\nu - \bar{z}^\nu(s_0)]}, \text{ where } [z_\mu - \bar{z}_\mu(s_0)] [\bar{z}^\mu - \bar{z}^\mu(s_0)] = 0. \quad (\text{C3.1})$$

Say the charged particle is located at O_{A} . The particle's motion (see Sec. 2.3) has then one non-null coordinate: $\bar{z}^2 = -\frac{1-k_{\text{A}\text{N}}^2}{2k_{\text{A}\text{N}}}s$, where s is the finite separation along the path of the particle.

Our considerations of the field start with $s = -\infty$ at the event $\mathcal{P}(0, \infty, 0, 0)$. The calculations are routine, resembling those used with the observer-based approach. We find that the null vector $z^\mu - \bar{z}^\mu(s_0)$ has the following components:

$$z^2 - \bar{z}^2(s_0) = -\frac{1+k_{\text{A}\text{N}}^2}{2k_{\text{A}\text{N}}} z^1 \pm \frac{1-k_{\text{A}\text{N}}^2}{2k_{\text{A}\text{N}}} r_{\text{A}} \quad \text{and} \quad z^\mu - \bar{z}^\mu(s_0) = z^\mu \quad \text{for } \mu \neq 2. \quad (\text{C3.2})$$

Here $r_{\text{A}} = \sqrt{(z^1)^2 + (z^3)^2 + (z^4)^2}$ and s_0 is the finite separation for which the first equation (C3.2) holds true. There are two solutions for s_0 , that is, there are two events along the particle's path that meet the required condition. The particle attends first the solution obtained with the minus sign for the coefficient of r_{A} in R^2 . This solution leads to the so-called retarded-potential, and is the one selected for examination here.

Substitutions yield $A_\mu = -\frac{2k_{\text{A}\text{N}}}{1-k_{\text{A}\text{N}}^2} \frac{q}{r_{\text{A}}} \begin{bmatrix} \frac{1+k_{\text{A}\text{N}}^2}{2k_{\text{A}\text{N}}} & 1 & 0 & 0 \end{bmatrix}$. The corresponding field, $F_{\mu\nu} = \partial_\mu A_\nu - \partial_\nu A_\mu$, has the following non-zero components: $-F_{12} = F_{21} = \frac{2k_{\text{A}\text{N}}}{1-k_{\text{A}\text{N}}^2} \frac{q}{r_{\text{A}}^3} z^1$, $F_{13} = -F_{31} = \frac{1+k_{\text{A}\text{N}}^2}{1-k_{\text{A}\text{N}}^2} \frac{q}{r_{\text{A}}^3} z^3$, $F_{14} = -F_{41} = \frac{1+k_{\text{A}\text{N}}^2}{1-k_{\text{A}\text{N}}^2} \frac{q}{r_{\text{A}}^3} z^4$, $F_{23} = -F_{32} = \frac{2k_{\text{A}\text{N}}}{1-k_{\text{A}\text{N}}^2} \frac{q}{r_{\text{A}}^3} z^3$, and $F_{24} = -F_{42} = \frac{2k_{\text{A}\text{N}}}{1-k_{\text{A}\text{N}}^2} \frac{q}{r_{\text{A}}^3} z^4$.

It is of some interest to examine the field as measured in the relative space of the A-plane. This is the inertial frame $x^\alpha = (ct_{\text{A}}, x_{\text{A}}, y_{\text{A}}, z_{\text{A}})$ of the observer at O_{A} , where the charged particle is located. The time-coordinate of this frame relates to x_{A} and x_{N} of the

$k_{\text{A}\text{N}}$ -frame as in (2.6): $cdt_{\text{A}} = -\frac{1+k_{\text{A}\text{N}}^2}{1-k_{\text{A}\text{N}}^2} dx_{\text{A}} - \frac{2k_{\text{A}\text{N}}}{1-k_{\text{A}\text{N}}^2} dx_{\text{N}}$, while dx_{A} and dy_{A} are left

unchanged and $dz_{\text{A}} = dy_{\text{N}}$. The field in the observer's frame, $F_{\alpha\beta} = \frac{\partial x^\mu}{\partial x^\alpha} \frac{\partial x^\nu}{\partial x^\beta} F_{\mu\nu}$, emerges

with only non-null electric components: $F_{21} = -F_{12} = \frac{q}{r^3} x_{\text{A}}$, $F_{31} = -F_{13} = \frac{q}{r^3} y_{\text{A}}$, and

$F_{41} = -F_{14} = \frac{q}{r^3} z_{\text{A}}$. This is the expected Coulomb field of a charged particle at rest.

References

1. Synge J.L.: *Relativity: The Special Theory* (North-Holland, Amsterdam, 1965) Preface.
2. J. Ehlers: Foundations of Special Relativity Theory, Lect. Notes Phys. **702**, 35-44 (2006).
3. C. Lämmerzahl: Special Relativity and Lorentz Invariance, Ann. Phys. (Leipzig) **14**, 71-102 (2005).
4. C.M. Will: Special Relativity: A Centenary Perspective, Prog. Math. Phys. **47**, 33-58 (2006).

5. P. Wolf, S. Bize, M.E. Tobar, F. Chapelet, A. Clairon, A.N. Luiten, and G. Santarelli: Recent experimental tests of Special Relativity, *Lect. Notes Phys.* **702**, 451-478 (2006).
6. E.D. Greaves, A.M. Rodriguez, and J. Ruiz-Camacho: A one-way speed of light experiment, *Am. J. Phys.* **77**, 894-896 (2009).
7. J. Finkelstein: Comment on “A one-way speed of light experiment”, *Am. J. Phys.* **78**, 877 (2010).
8. C.M. Will: Clock synchronization and isotropy of the one-way speed of light, *Phys. Rev. D* **45**, 403-411 (1992).
9. A.S. Eddington: *The Mathematical Theory of Relativity* (University Press, Cambridge, 1923) footnote on p. 29.
10. C. Iyer and G.M. Prabhu: A constructive formulation of the one-way speed of light, *Am. J. Phys.* **78**, 195-203 (2010).
11. M.L. Ruggiero: Relative space: space measurements on a rotating platform, *Eur. J. Phys.* **24**, 563-573 (2003).
12. F.A.E. Pirani and A. Schild: Conformal geometry and the interpretation of the Weyl tensor, in: B. Hoffman (ed.), *Perspective in Geometry and Relativity* (Indiana Univ. Press, Bloomington and London, 1966), pp. 291-309.
13. J. Ehlers, F.A.E. Pirani, and A. Schild: The geometry of free fall and light propagation, in: O’Raifeartaigh (ed.), *General Relativity, Papers in Honor of J.L. Synge* (Clarendon, Oxford, 1972) pp. 63-84.
14. G. Schay, Jr.: On relativistic one-particle dynamics, *Il Nuovo Cimento*, **26** Supplement 3, 291-304 (1962).
15. A.O. Barut: *Electrodynamics and Classical Theory of Fields and Particles* (MacMillan, New York, 1964) p. 60.
16. J.L. Synge: Classical Dynamics, in: S. Flügge (ed.), *Principles of Classical Mechanics and Field Theory*, *Encyclopedia of Physics*, **III/1**, (Springer-Verlag, Berlin, 1961) p. 111.
17. J.L. Synge: What is Einstein’s Theory of Gravitation?, in: B. Hoffmann (ed.), *Perspective in Geometry and Relativity* (Indiana Univ. Press, Bloomington and London, 1966) pp. 7-15.
18. A.I. Miller: *Albert Einstein’s Special Theory of Relativity: Emergence (1905) and Early Interpretations (1905-1911)* (Springer-Verlag, New York, 1998) p. 238.
19. J.L. Synge: *Relativity: The Special Theory* (North-Holland, Amsterdam, 1965) pp. 24-26.
20. M. Friedman: *Foundations of Space-Time Theories* (Princeton University Press, New Jersey, 1983).
21. R. Torretti: *Relativity and Geometry* (Dover Publications, New York, 1996).
22. R. DiSalle: Space and Time: Inertial Frames, *Stanford Encyclopaedia of Philosophy*, <http://plato.stanford.edu/entries/spacetime-iframe/>, last accessed on 15 Feb 2011.
23. A.P. French: *Special Relativity* (Norton, New York, 1968) p. 114.
24. J. Franklin: *Classical Electromagnetism* (Addison Wesley, San Francisco, 2005) p. 425.
25. A. Schild: Electromagnetic two-body problem, *Phys. Rev.* **131**, 2762-2766 (1963).

26. B. Thidé: *Electromagnetic Field Theory*, 2nd Edition, p. 158, electronic text, <http://www.plasma.uu.se/CED/Book>, last accessed on 15 Feb 2011.
27. R.K. Sachs: On the characteristic initial value problem in gravitational theory, *J. Math. Phys.* **3**, 908-914 (1962).
28. J.H. Yoon: Kaluza-Klein formalism of general spacetimes, *Phys. Lett. B*, **451**, 296-302 (1999).
29. R.A. D’Inverno: DSS 2+2, *Boston Studies in the Philosophy of Science* **234**, 317-347 (2003).
30. H. Hertz: *The Principles of Mechanics Presented in a New Form* (Dover, Mineola, N.Y., 2003) Introduction.
31. P. Havas: Simultaneity, Conventionalism, General Covariance, and the Special Theory of Relativity, *Gen. Rel. Grav.* **19**, 435-453 (1987).
32. J.L. Anderson: *Principles of Relativity Physics* (Academic Press, New York, 1967) p. 3.
33. D.H. Frisch and J.H. Smith: Measurement of relativistic time dilation using μ -mesons, *Am. J. Phys.* **31**, 342-355 (1963).
34. A.P. French: *Special Relativity* (Norton, New York, 1968) p. 103.
35. M.B. Herassimovitch: Sur la nouvelle théorie de l’aberration, *Bulletin astronomique, Serie I*, **31**, 385-402 (1914).
36. C. Møller: *The Theory of Relativity* (Oxford University Press, London, 1955) p. 87.